Formulation of Water Insoluble Drugs for Ocular Delivery

By

Haley Ruth Shelley

A dissertation submitted to the Graduate Faculty of
Auburn University
In partial fulfillment of the
requirements for the Degree of
Doctor of Philosophy

Auburn, Alabama
August 4, 2018

Keywords: Hydroxypropyl-beta-cyclodextrin, Ocular, Ophthalmic,
Drug delivery, Nepafenac, Difluprednate

Approved by:

Jayachandra Babu Ramapuram, Chair, Professor of Drug Discovery and Development
Robert D. Arnold, Associate Professor of Drug Discovery and Development
Daniel L. Parsons, Professor of Drug Discovery and Development
William R. Ravis, Professor of Drug Discovery and Development
Elizabeth Lipke, Associate Professor of Chemical Engineering

Abstract

Cyclodextrins are unique cyclic molecules with a hydrophobic interior and hydrophilic exterior that can be used to solubilize, stabilize and enhance targetability of the encapsulated molecules. Chapter 1 will discuss uses of CDs as it applies to nanoparticle-based drug carriers.

Ocular drug delivery is a challenging field due to the large number of ocular barriers. Therefore, producing a new ophthalmic formulation requires consideration when it comes to the administration route, dosage form and site of action. Chapter 2 will cover the basics of ophthalmic formulation development.

Nepafenac is a common NSAID commercially available as a suspension, Nevanac®, due to the poor water solubility. Hydroxypropyl-beta-cyclodextrin (HPBCD) was complexed with nepafenac to increase the water solubility and transcorneal permeation of the drug. The complex in the liquid and solid state was confirmed. Perfusion studies using whole porcine eyes proved the solution had a significantly higher drug distribution and corneal retention compared to Nevanac®.

The HPBCD-nepafenac complex was formulated into an ion-activated *in-situ* gel to improve residence time in the eye, using sodium alginate. A sodium alginate concentration of 0.3% revealed the largest increase in viscosity following the addition of simulated tear fluid, allowing for the formulation of a nepafenac *in-situ* gel system for comparison with Nevanac®. Perfusion studies revealed an increased retention of nepafenac on the sclera when using the in-situ gel system, due to the gel formation in the presence of calcium ions.

Difluprednate is a corticosteroid used to treat anterior ocular inflammation. Due to the poor solubility of difluprednate, it is only available as an emulsion, Durezol®. Difluprednate was complexed with HPBCD to produce a positive-relationship complexation, meaning more than one cyclodextrin is needed to solubilize difluprednate. The solution exhibited higher ocular distribution, corneal permeation and retention compared to Durezol®.

Difluprednate loaded in poly(lactic-co-glycolic acid) (PLGA) based microneedles for delivery to the posterior segment of the eye. The patches contained a PAA backing that rapidly dissolved upon instillation in the eye; leaving the microneedles embedded in the sclera for sustained drug release. Microneedles containing PLGA of varying molecular weights and lactide content were compared in release, failure force, and permeation studies.

Acknowledgements

I would first like to thank my wonderful graduate committee: Dr. Jay Ramapuram, Dr. Robert Arnold, Dr. William Ravis, Dr. Daniel Parsons and Dr. Elizabeth Lipke; all of whom have provided me with the guidance, advice and skills needed to pursue this degree. Each one of these individuals has taught me about research, critical thinking and the ability to navigate life while pursuing my doctoral degree. Furthermore, I would like to express my deepest appreciation for my major professor, Dr. Jay Ramapuram, who helped me become the confident, independent, strong scientist that I am today; without you this degree would not be possible.

I would also like to thank my amazing DDD department and HSOP family. I have made so many special friends throughout the years, and each one has changed me for the better. There are too many to name, because everyone I pass in the hall/stairwell makes me smile for their own unique reason. The memories I have made in this Pharmily will last me a lifetime.

My friends and family have certainly helped me during this incredible journey and have supported me in continuing my education past my bachelor's degree. Last but certainly not least, I would like to thank my incredible husband, Ben Shelley. He has always supported me in every dream that I have ever considered pursuing. That type of unconditional love and support is rare and I am grateful to have found it for myself. Ben frequently helped me prepare samples, run experiments and fix machines and I am very thankful to have such a supportive husband by my side.

Table of Contents

List of Figures

List of Tables

Chapter 1. Role of Cyclodextrins in Nanoparticle Based Drug Delivery Systems

In part: Abarca, E. M., Cuming, R., Duran, S., & Ramapuram, J. (2015). Development of an ex-vivo trans-corneal permeation model in horses: Epithelial barrier evaluation. *Investigative Ophthalmology & Visual Science, 56*(7).

1.1 Abstract

Cyclodextrins (CDs) are cyclic oligosaccharides with unique hydrophobic interior surface. Three parent CDs, α-CD, β-CD, and γ-CD, are further chemically modified primarily to make them suited for parenteral administration and these are used for many pharmaceutical applications. CDs offer distinctive advantages due to their unique ability to form inclusion complexes with a variety of organic and inorganic lipophilic molecules. This attribute is promising for a wide range of fields such as drug delivery, cancer therapy, gene delivery, and biosensing. In recent years, CDs have become more commonly used as functional materials in nanoparticle (NP) based drug delivery. The properties of NPs can be advantageously modified by the inclusion of CDs or their derivatives. CD conjugated NPs (CD-NPs) have many benefits such as improved drug solubility, serve as drug carriers to specific locations such as cancer cells, which reduces toxicity to normal cells. Additionally, CDs can overcome the limitations of NPs such as low encapsulation efficiency and drug loading. This review will discuss the various uses of CDs as it applies to nanoparticle-based drug carriers. Specifically how CDs enhance the characteristics of polymeric, magnetic, lipid, metallic and mesoporous NPs are discussed.

1.2 Introduction

Cyclodextrins (CDs) are a group of unique compounds composed of rings of sugar molecules, α-1, 4-linked α-D-glucopyranose, making them cyclic oligosaccharides (Figure 1.1). French scientist Villiers first discovered CDs in 1891 when he noticed that starch produces a crystalline substance after the digestion by *Bacillus amylobacter* (Zafar, Fessi, & Elaissari, 2014). Amylases and glycosyl transferase, successfully break a turn in the starch helix and fuse the two ends of the fragment, thereby creating a cyclic molecule, the non-reducing CD (Saenger, 1980). The three natural parent CDs produced from the starch digestion are α-CD, β-CD, and γ-CD, consisting of 6, 7, and 8 glycopyranose units, respectively(Simoes, Rey-Rico, Concheiro, & Alvarez-Lorenzo, 2015) .The CD interior is lined with carbons and ethereal oxygen of the glucose residues, while the exterior is lined with hydroxyl groups (Thorsteinn Loftsson, 2005). Therefore, the parent CD molecules are amphiphilic structures containing a hydrophobic core and a hydrophilic shell. Additionally, the parent CDs have a homogenous crystalline structure and are non-hygroscopic (Zafar et al., 2014). However, the parent CDs have limited aqueous solubility; therefore, a plethora of derivatives have been developed. The hydroxyl groups of the parent CD are functionalized to obtain more hydrophilic, hydrophobic, or ionizable derivatives. Common processes used to synthesize CD derivatives are amination, etherification, and esterification of the primary face and secondary face hydroxyl groups (Zafar et al., 2014). Cyclodextrin derivatives and their applications have been extensively published in the recent years(Brewster & Loftsson, 2007; Krzak, Swiech, Majdecki, & Bilewicz, 2017; Loftsson & Duchene, 2007).

Cyclodextrins offer distinctive advantages due to their unique ability to form inclusion complexes with a variety of organic and inorganic lipophilic molecules (Arima, Hayashi, Higashi, & Motoyama, 2015). This attribute is promising for a wide range of nanotechnology fields such as drug delivery, cancer therapy, gene delivery, and biosensing. CDs are beneficial in drug delivery because the

bucket shaped cavity protects the drug from degradation and irritation is reduced at the administration site. The weak bonds of the inclusion complex allow the drug to become temporarily lodged in the CD cavity, yielding improved solubility and bioavailability (Arima et al., 2015). Cyclodextrins have also been useful for oral drug delivery due to the sweet taste and taste masking properties. Additionally, the inclusion complex prevents drug-drug or drug-excipient interactions (Thorsteinn Loftsson, 2005). Cyclodextrins are useful in cancer therapy because they increase the loading capacity and encapsulation efficiency of tumor-targeting NP delivery systems (Bina Gidwani, 2015). Gene delivery uses CDs to assist in the destabilization of biological membranes, because CDs bind and remove the cholesterol in the membrane making the cell membranes more permeable. Additionally, CDs can stabilize a biological molecule for delivery by protecting them from non-specific interactions (Carmen Ortiz Mellet, 2010). For biosensing applications, CDs help immobilize the target molecule onto the electrode by increasing sensitivity and selectivity (Holzinger, Bouffier, Vilialonga, & Cosnier, 2009). Table 1 lists US Food and Drug Administration (FDA) approved CDs and their individual uses in dosage forms for various routes of administration.

The inclusion process between CD and the 'guest' molecule occurs when the CD expels enthalpy rich water molecules from its hydrophobic core due to competition from the lipophilic guest molecule. Chemical bonds are neither created nor destroyed during the complexation. The inclusion complex occurs via electrostatic and non-covalent interactions such as hydrogen bonding, van der Waals forces as well as release of ring strain, especially in α-CD (Zafar et al., 2014). The physicochemical properties of the complex differ from that of the host and guest molecule alone. Potential guest molecules can be small molecular weight drugs (usually less than 500 Daltons), hydrophobic amino acid structures, enzymes and siRNA (Diez, Villalonga, Villalonga, & Pingarron, 2012; Ding et al., 2015; Gooding et al., 2015). The guest molecules are

caged and protected from oxygen, water, heat, and radiation; thereby preventing degradation of the guest molecule.

Cyclodextrins are generally considered safe for oral administration because they are not absorbed across gastrointestinal tract and are eliminated in feces. The few CDs that do get absorbed are rapidly eliminated from the body and are excreted in the urine unmetabolized (Loftsson, Jarho, Masson, & Jarvinen, 2005). A study revealed that after intravenous administration, 100% of a given dose of CD was recovered in the human urine after 6-12 hours (Stella & He, 2008). Natural CDs are toxic when administered intravenously. For instance, α-CD causes aggregates and β-CD causes nephrotoxicity when given via parenteral route; therefore, these CDs are not used for injections (Stella & He, 2008). Additionally, if the kidneys are already damaged, large amounts of CDs accumulate leading to vacuolation of the proximal tubular epithelium. The vacuolation will reverse itself once the CD treatment is removed (Stella & He, 2008). Furthermore, some CDs (β-CD and HP-β-CD) form insoluble complexes with cholesterol in the blood and collect in the kidneys leading to nephrotoxicity. Therefore, for specific biological applications care must be taken when deciding which CDs to use.

In recent years, CDs have become more commonly used as functional materials in NP based drug delivery. Nanoparticles (NPs) have many benefits such as targeting drug carriers to specific locations, such as cancer cells, which reduces toxicity to normal cells. Additionally, CDs can overcome the limitations of NPs such as low encapsulation efficiency and drug loading. Nanoparticles aided by CDs yield a novel drug delivery system with the benefits of both components: the CDs offer improved water solubility and drug loading while the NPs provide targeted drug delivery. Furthermore, some of the complexes created in CD-assisted NPs are considered non-conventional complexes because the CDs will act as surfactants or result in aggregation (Loftsson, Masson, & Brewster, 2004). Together these aforementioned elements

have resulted in a large variety of CD-linked NPs such as lipid, magnetic, gold, and polymeric NPs.

A literature search on “cyclodextrins” and “nanoparticles” resulted in over 1000 articles using the PubMed database, which included various types of NPs in the gene or drug delivery and biosensing. Among the many are a few recent review articles that discuss CDs and their applications, specifically on the formulation of NPs (Arima et al., 2015; Bina Gidwani, 2015; Lakkakula & Krause, 2014; Sherje, Dravyakar, Kadam, & Jadhav, 2017; Zafar et al., 2014). The scope of this article is to expand the focus of CD linked NPs and their applications in chemotherapeutics, drug delivery, gene delivery, and biosensing. This article will also focus on reviewing the role of CDs in designing the specific types of NPs such as magnetic, polymeric, lipid-based NPs. In addition, this article will also explore newer types of CD NPs such as mesoporous, gold and silver NP. Table 2 lists general types of nonionic, anionic, and cationic CDs and their applications in various types of NPs.

1.3 Application of CDs in Magnetic Nanoparticles

Magnetic nanoparticles (MNPs) have become more common in biomedical applications due to advantageous properties such as: narrow size distribution, high colloidal stability, low toxicity, and high specific surface area (Ahmed, Laino, Calzon, & Garcia, 2014; Subathra Sinniah, 2015). Magnetic NPs also exhibit superparamagnetism: they are easily magnetized when an external magnetic field is applied and they revert back to a demagnetized nature once the magnetic field is removed. This valuable property makes these NPs easy for magnetic separation, removal and recovery. Such magnetic property enables the NPs to localize at the targeted site within the human body in response to the externally applied magnetic field. However, MNPs tend to agglomerate due to small size and high surface free energy, leading to lack of tissue distribution and intracellular targeting upon administration. Additionally, bare magnetic NPs are easily

oxidized leading to demagnetization. Therefore, silica is generally added to the surface of the NP to maintain the stability of magnetic NPs. Cyclodextrins are commonly linked to the silica-coated surface of the MNP via linkers, such as 3-aminopropyltriethoxysilane (APTS). This conjugation allows the CD to function as a carrier for drugs, proteins, and cell targeting ligands on the surface of the MNPs. Furthermore, to prevent premature drug release into non-target regions, such as blood and extracellular space, some magnetic nanoparticles are equipped with stimuli-sensitive drug release. Stimuli responsive factors include pH, light, enzymes, temperature, competitive binding and redox (Rastegari, Karbalaei-Heidari, Zeinali, & Sheardown, 2017). For instance, certain linkers are cleavable once the MNPs are in the cancer cell microenviroment (H. Kim et al., 2010) . The most common use of functionalized magnetic CD NPs is for hydrophobic anti-cancer drug delivery. However, MNPs have been applied to other applications such as solid-phase extraction (Ansari, Habibi-Rezaei, Salahshour-Kordestani, Movahedi, & Poursasan, 2015) and biosensing materials (Gooding et al., 2015).

Magnetic NPs have been developed for the delivery of 5-fluorouracil (5-FU), which is used to treat different cancers (breast, stomach, colon, and lung) and has detrimental effects on normal cells, as it is not targeted specifically for the tumor cells. Anirudhan et al. (Anirudhan, Divya, & Nima, 2015) produced magnetic hydrogels by the chemical precipitation method for the controlled delivery of 5-FU. β-CD was grafted with maleic anhydride to create a new CD derivative, maleated CD (MACD), which consisted of unique properties: increased water solubility, pH sensitivity, and lowered toxicity. This system was tested on breast cancer cells and the results suggested that the cytotoxicity was significantly higher as compared to 5-FU alone (control). The CD-MNP delivery system also displayed lower toxic side effects to normal cells. Lv et al. (Lv, Zhao, Cheng, & Zhao, 2014) fabricated a pH-dependent 5-FU delivery system consisting of magnetic colloidal nanocrystals decorated with β-CD polymer brushes (polymers tethered to a surface). The β-CD magnetic nanocrystals, averaging 230 nm in diameter, yielded a 32% higher 5-FU adsorption

capacity as compared to CD-free magnetic nanocrystals. Similarly, Ding et al. (Ding et al., 2015) created a MNP (Fe_3O_4) hydrogel for the delivery of 5-FU by crosslinking carboxymethyl-β-CD (CM-β-CD) with chitosan via emulsion chemical crosslinking method. The anionic CM-β-CD has a high aqueous solubility and low toxicity, while the cationic chitosan provides the MNP with mucoadhesive properties. The hydrogel yielded 97.6% encapsulation efficiency due to the negative charged CM-β-CD having strong electrostatic interactions with the positively charged 5-FU. Furthermore, unlike previous examples, Ding's tumor-targeting drug delivery system provided dual mechanisms of drug release: diffusion of drug molecules and degradation of polymer chitosan matrix, giving a desirable controlled released mechanism.

Recently, all-trans retinoic acid (ATRA) has been studied in the treatment of various types of cancers (Institute, 2016). Banerjee et al. (Banerjee & Chen, 2010) devised Fe_3O_4 MNPs coated with gum arabic grafted with HP-β-CD for the delivery of ATRA. The resultant NPs had a mean diameter of 17 nm and exhibited a significantly higher capability for ATRA loading than those without HP-β-CD. Badruddoza et al.(Badruddoza et al., 2013) constructed a silica coated Fe_3O_4 MNP cross-linked with CM-β-CD for the delivery of ATRA. These MNPs had mean diameter of 11 nm and contained two functionalities that Banerjee's (Banerjee & Chen, 2010) MNPs lacked: fluorescence labeling by FITC and a common cancer-targeting ligand, folic acid (Figure 1.2) (Badruddoza et al., 2013). Where APTS was used to conjugate the CM-β-CD, folic acid, and FITC to the MNP surface. The amount of ATRA absorbed to Banerjee's MNPs as well as the release profiles were comparable to dual-functionalized MNPs developed by Badruddoza; however, the latter MNPs offer the advantage of targetability to cancer cells. Cytotoxicity studies showed that the drug-loaded functionalized MNPs increased cellular uptake and successfully targeted tumor cells due to folic acid receptor binding.

Cyclodextrin-MNPs are also used for solid-phase extraction techniques, because the target molecule can complex with the CD and the MNPs can be removed using a magnet and reused with the same efficiency. One specific example is the solid-phase extraction of a common cancer biomarker 5-hydroyindole-3-acetic acid (5-HIAA) from urine using Fe_3O_4-APTS-CD complex (Ahmed et al., 2014). 5-HIAA forms a strong complex with mono-6-deoxy-6(p-tolylsufonyl)-β-CD (Ts-β-CD) allowing for easy identification and extraction. Similarly, Shamekhi grafted β-CD on 3-mercaptopropyltrimethoxy silane modified Fe_3O_4 nanoparticle for the sorption and extraction of sertraline hydrochloride, Zoloft, from human biological fluids (Shamekhi, Ahmad Panahi, Alaei, & Moniri, 2017). Abdolmohammad-Zadeh et al.(Abdolmohammad-Zadeh & Talleb, 2015) achieved an extremely high recovery of gemfibrozil from pharmaceutical wastewater and human serum, by grafting β-CD onto a graphene oxide/Fe_3O_4 nano-hybrid (Abdolmohammad-Zadeh & Talleb, 2015).

A unique solid-phase extraction technique using CM-β-CD conjugated MNPs to prevent glycation of proteins was reported (Ansari et al., 2015). CM-β-CD was conjugated to Fe_3O_4 NPs using tetraethyl orthosilicate. The particle size of CM-β-CD-MNPs was about 20 nm, which is slightly bigger than that of bare MNPs. Thioflavin was used to measure the amount of amyloid formation in the presence and absence of CM-β-CD with the MNP. The amount of thioflavin was significantly lower in the presence of CM-β-CD proving that CD protects the proteins and prevents amyloid formation. Therefore, the strong complexation capabilities of CDs make them optimal for extraction of a plethora of compounds in a variety of environments.

MNPs combined with CDs have also been utilized for biosensing applications, since they are capable of capturing the target molecule more effectively while exhibiting the same amount of superparamagnetism. A variety of methods have been used to create CD-MNPs for biosensing, some more complex than others. A biosensor based on mono-6-formyl-β-CD coated MNPs to

detect catechol and xanthine was reported (Diez et al., 2012). In this case, the magnetic core (Fe_3O_4) was coated with APTS and then mono-6-formyl-β-CD was attached. $NaBH_3CN$ was introduced to the system to reduce the CDs to CD-substituted secondary derivatives. These MNPs are then attached to an electrode. Next, the CDs form complexes with two adamantane-modified enzymes, tyrosine and xanthine oxidase, which are used to detect catechol and xanthine. These CD-MNP electrodes showed 10 and 6 times higher sensitivity and a lower detection limit when compared to the original tyrosine and xanthine biosensors. Similarly, Xie et al. (Xie, Zhang, Yuan, Chai, & Yuan, 2015) designed an electrochemical biosensing electrode to detect prostate specific antigens with high sensitivity and good conductivity. The MNPs contained the β-CD-ferrocene complex, which were used to transduce peptide cleavage events into electrochemical signals.

Sinniah et al. [18] constructed MNPs coated with β-CD functionalized-ionic liquid (Fe_3O_4-β-CD-IL) attached to glass carbon electrodes for the detection of Bisphenol A (BPA). The ionic liquids decreased aggregation and provided a stabilized protective shell for the MNPs. Finally, Duan et al. (H. M. Duan et al., 2015) avoided using conventional electrodes and instead they fabricated surface molecular imprint polymers from the polymerization of β-CD, chitosan, and graphene oxide to capture bovine serum albumin. This chemiluminescence biosensor provided high sensitivity and near perfect recovery.

1.4 Application of CDs in Polymeric CD Nanoparticles

Polymeric NPs (PNPs) are highly versatile, as various functionalities decorated on the NP surface can determine when and where the NP disassembles in the body. For instance, functionalities can be added to control the response of the PNPs to pH, temperature, light, magnetic fields, and oxidative, reductive, and enzymatic conditions (Elsabahy & Wooley, 2012). Polymeric NPs are both biocompatible and biodegradable, so the fate of the PNPs in biological system is not a

concern. Examples of natural and synthetic polymers used in the PNPs are: chitosan, polyethylene glycol (PEG), poly lactic acid) (PLA), and poly (lactic-co-glycolic acid) (PLGA) (Conte et al., 2015; Fulop, Saokham, & Loftsson, 2014; Ruiz-Esparza et al., 2014). By varying the polymer composition, the particle size, surface charge, the drug release can be altered.

Conjugation of CDs with PNPs allow the PNPs to successfully deliver poorly soluble drugs by encapsulating the drugs in the hydrophobic cyclodextrin core. The PNPs have CDs forming the outer shell, while the core of the PNP is a synthetic or natural polymer. Therefore, the drugs can be loaded in the core of the PNP or it can be complexed with the CD in the outer shell. Other PNPs simply have a cross linked matrix consisting of polymers and CDs (Fulop et al., 2014). The CD loaded PNPs are used for intravenous dual-drug delivery or siRNA delivery to the tumor sites.

1.4.1 Chitosan-CD Nanoparticles

Chitosan is a common polysaccharide obtained from shrimp shells. This polymer is cationic in nature and can be conjugated with CDs to provide NPs with high drug loading, mucoadhesive properties and targeting capabilities. Zhang et al. (N. Zhang et al., 2010) designed acid-resistant PNPs containing cationic-β-CD (CP-β-CD) and chitosan for the slow-release oral delivery of insulin. Three variations of CP-β-CDs were formulated with the following ratios of β-CD/epichlorohydrin/choline chloride: 1/15/4, 1/15/6, and 1/15/10, with particle sizes of 146, 338 and 165 nm, respectively. The cationic charge of the CP-β-CD protected the insulin from degradation within the stomach's gastric fluids, which in turn allowed for a higher release of insulin (40%) compared to insulin alone (18%) in the intestinal fluids. In a similar study this formulation was altered by using a chitosan derivative, trimethyl chitosan (TMC), because TMC is soluble at higher pH values and penetrates enterocytes, which produced a particle size of 150.82 ± 21 nm(Mansourpour et al., 2015). In both scenarios, the cationic β-CD was modified using a quaternary ammonium group; yielding better drug-CD complexation and leaving the CD unable

to bind to cholesterol. Additionally, alginates were added to both formulations to create a gel-like matrix when the formulation comes in contact with Ca^{2+} ions as well in an acidic pH; therefore, the drug molecule can be carried through the stomach protected from acid degradation and then can be released later in the intestine. The cumulative intestinal release of insulin showed that TMC NPs had a 38% lower release than the chitosan CP-β-CD-NPs. Caco2 cell permeability studies performed showed higher permeability by TMC NPs, most likely due to the positive charge of the NPs. Release studies in simulated gastric and intestinal medium revealed that the chitosan derivative had a 27% higher release in the intestine compared to the original chitosan/β-CD mixture, making the TMC β-CD NPs more acceptable for oral insulin delivery. In another study, a low molecular weight chitosan was used to increase the water solubility of hydrocortisone (Fulop et al., 2014). Ionotropic gelation technique was used to prepare a PNP matrix consisting of SBE-β-CD (anionic) cross-linked with chitosan (cationic), which had approximately 3-times higher release rate when compared to hydrocortisone alone.

1.4.2 PEG-CD Nanoparticles

NPs are commonly PEGylated to increase circulation time or to enhance permeation across biological membranes. Such properties of PEG could be enhanced when paired with CDs. CDs have immunogenicity and multiple chemical equivalent binding sites for attachment of functional groups, making them ideal for gene delivery (Guo, Ogier, Desgranges, Darcy, & O'Driscoll, 2012). For instance, PEGylated CDs are commonly used for the delivery of siRNA. Godhino et al (Godinho et al., 2014) determined that an increase in PEG length as well as PEG molecular weight led to an increase in stability of PEGylated CDs used for siRNA delivery. Similarly, PEGylated cyclodextrin (CD) nanoparticles tagged with a CNS-targeting peptide, derived from the rabies virus glycoprotein (RVG), was formulated and characterized. The goal of the formulation was to protect siRNA from degradation, enhance cell uptake and gene silencing efficiency. Various

amphiphilic cyclodextrin derivatives such as SC12-CD-click-propylamine (CD1), SC12- CD-click-PEG500 (CD2), SC12-CD-click-PEG500-ethylamine (CD3) and SC12-CD-clickPEG500-RVG (CD4) were synthesized and co-formulated to form nanoparticles containing siRNA. The CD4.siRNA nanoparticles showed enhanced receptor specific cellular uptake compared to the untargeted nano-complexes (CD1-CD3) in human glioblastoma cells and achieved gene knockdown. This CD based nano-complex was suitable for systemic delivery of siRNA targeting brain cancer (Gooding et al., 2015).

1.4.3 PLA-CD Nanoparticles

Polylactic acid (PLA) is a safe biodegradable thermoplastic polymer and has been used extensively in NP formulations. A vast amount of research has been conducted on NPs, which consist of a PLA core and a CD shell, for the delivery of hydrophobic anticancer drugs. For instance, Wang et al. (T. Wang, Zhang, Liang, Liang, & Wu, 2011) formulated NPs containing PLA and 1, 2-dipalmitoyl-sn-glycero-3-phosphoethanolamine (DPPE) along with hydrophilic HP-β-CD to improve the encapsulation efficiency of doxorubicin. These PNPs had improved cytotoxicity and cellular uptake towards A549 cancer cells compared to that of free doxorubicin. Similarly, Miao et al. (Miao et al., 2012) used a similar system (PLA-DPPE-HP-β-CD) to deliver paclitaxel, but added an integrin-specific targeting peptide. The targeted NPs resulted in high loading capacity as well as a 4-times increase in tumor cell inhibition relative to paclitaxel-loaded NPs. Fagui et al. (El Fagui, Wintgens, Gaillet, Dubot, & Amiel, 2014) formulated a PLA core NP with a layered shell of alternating cationic and anionic β-CD (Figure 1.3) for the controlled intravenous delivery of benzophenone. Increasing the number of alternating β-CD layers resulted in a more sustained release PNP system.

1.4.4 PLGA-CD Nanoparticles

Poly(lactic acid and glycolic acid) (PLGA) is another safe biodegradable polymer, in which the lactic acid and glycolic acid content can be varied for degradation at a certain time (Mura, Maestrelli, Cecchi, Bragagni, & Almeida, 2010). PLGA-CD NPs are commonly used for the delivery of poorly water-soluble drugs. Furthermore, like PLA NPs, some PLGA-CD NPs consist of a PLGA core and a CD shell, which allows for the delivery of two different drugs to the targeted site. For instance, Ruiz-Esparza et al. (Ruiz-Esparza et al., 2014) created a sequence-specific dual drug release system for model drugs: rhodamine and Bodipy®, common fluorophores. The nested PNP consists of a PLGA core that contains rhodamine, while the shell is composed of quaternary ammonium β-cyclodextrin (QA-β-CD) complexed with Bodipy®, with a size of 142 nm. The various forces holding the QA-β-CD shell and PLGA core together are thought to be Van der Waals, ionic and molecular interactions and are responsible for the profound stability of the PNP. The release of Bodipy® was governed by the detachment of the QA-β-CD shell from the polymeric core, once the polymeric core is exposed the rhodamine slowly begins to release from the high viscosity PLGA. As expected and desired, Bodipy® was released at a 2.5 times greater rate when compared to rhodamine, since Bodipy was located in the CD nanoparticle shell and rhodamine was located in the PLGA core. These CD-PNPs showed high internalization rates in breast cancer cells, due to the positive charge of the QA-β-CD shell. In another study, the PLGA-CD NPs containing oxaprozin-methyl-β-CD complex were formulated for enhanced drug penetration in the inflamed tissues (Mura et al., 2010). The methyl-β-CD oxaprozin NPs demonstrated 84% higher oxaprozin release than oxaprozin-NPs. Similarly, the HP-β-CD-docetaxel and heptaarganine were loaded in PLGA NPs (Bu, Zhu, Ma, & Shen, 2015). The oral bioavailability of docetaxel-CD-heptaarganine NPs increased 9-times as compared to free docetaxel. Tao et al. (Tao et al., 2013) used PLGA-HP-β-CD NPs to enhance permeation of puerarin across the blood-brain barrier for the treatment of ischemic-reperfusion induced brain injury. The PLGA-HP-β-CD-puerarin NPs

significantly reduced the infarction volume as compared to puerarin alone after a three-day period, suggesting that the HP-β-CD aided in transporting puerarin across the blood-brain barrier.

Recently, it has been reported that CDs can prevent drug metabolism by cytochrome P450 3A (CYP3A) and the inhibitory effects of P-glycoprotein (P-gp) when combined with PNPs (Ishikawa, Yoshii, & Furuta, 2005). Zhang et al. (D. Zhang et al., 2015) examined poly (methyl vinyl ether-co-maleic anhydride)-graft-HP-β-CD amphiphilic copolymer (CD-PVM/MA) as a PNP oral carrier for tacrolimus, a low bioavailability drug. CD-PVM/MA was prepared by using 1-ethyl-3-(3-(dimethylamino) propyl) carbodiimide (EDC) as a coupling agent to link the PVM/MA to the backbone of the HP-β-CD. The size of the NPs obtained was 273.7 ± 13.3 nm. Fluorescence studies using coumarin-6 revealed that the PNPs are taken into the cell by two pathways: clathrin- and caveolae-mediated endocytosis. The former mechanism led the PNPs to blood capillaries via passive diffusion. The latter mechanism led to lymphatic absorption of the PNPs, which bypassed the first-pass effect, thereby increasing the bioavailability of tacrolimus by 20-times. In a similar study, HP-β-CD complexed with fisetin (a plant polyphenol) provided enhanced solubility and loading capacity into PLGA NPs; ~79% loading was achieved with the complexed drug compared to 47% with the native drug. The HP-β-CD also increased oral bioavailability and revealed 4 fold higher cytotoxicity compared to free fisetin, presumably due to the P450/P-gp inhibitory effects (Amrita Kadari, 2017).

Also, CDs can be added to PNP formulations to act as a skin permeation enhancer. For example, Conte et al. examined the distribution of Zinc (II) phthalocyanine (ZnPc) in the skin layers after being delivered by an amphiphilic diblock copolymer, polyethylene glycol-b-polycaprolactone (PEG-b-PCL), assisted by HP-β-CD (Conte et al., 2015). In this case, HP-β-CD was not attached to the PNPs but it was added to the PNP mixture to assist with transport and enhance skin penetration of the drug (Figure 1.4). Bare PNPs were only able to deliver the ZnPc to the stratum

corneum while the PNPs accompanied by HP-β-CD were able to penetrate deeper into the viable epidermis. Fluorescent imaging revealed that the HP-β-CD PNPs penetrated to deeper layers of skin, proving that HP-β-CD was able to alter the barrier characteristics of the skin layers in order to transport the drug molecules. However, no effects on the lipid composition of the skin could be found, meaning HP-β-CD only alters the skin's water activity to enhance solute penetration. Furthermore, García-González et al. found that β-CD adsorbed onto PLGA NPs avoids interactions with mucin, thereby increasing internalization into the nucleus and cytoplasm of the intestinal epithelial Caco-2 cells (Lorena García-González, 2015). The interaction between the NPs and Caco-2 cells revealed that NPs with β-CD had greater cell internalization, having higher concentrations in the cytoplasm and nucleus as compared to those without β-CD. The hydrophilic property and permeation enhancing activity of the β-CD-PLGA-NPs made them an effective drug delivery carrier for oral administration.

1.5 Lipid CD Nanoparticles

Lipid CD nanoparticles (L-CD-NPs) belong to one of the following categories: colloidal drug carriers, liposomes, nanoemulsions, solid lipid nanoparticles (SLN) or nanostructured lipid carriers (NLC). Liposomes consist of a lipid bilayer enclosing an aqueous core; where the core can store hydrophilic drugs and the shell can hold lipophilic drugs. Additionally, liposomes allow for easier penetration of a cell wall as the lipid bilayer mimics the cell wall; therefore, payloads can either be delivered to the cell membrane or the interior of the cell (Negi, Chattopadhyay, Sharma, & Ram, 2014). Nanoemulsions (typically oil-in-water type) offer ease of preparation and can be delivered through a variety of routes. SLNs are completely solid and consist of a single lipid layer encasing a solid lipid core, whereas NLCs are composed of both liquid and solid lipids yielding a less compact structure allowing for higher drug loading (Figure 1.5). Additionally, NLCs offer the ability to form micelles with bile salts in the intestine, thereby passing liver metabolism

(Lin et al., 2014). By introducing CDs into lipid NP systems, an increase in hydrophobic drug loading can be achieved within the aqueous components of the L-CD-NPs, while still maintaining the targetability of L-CD-NPs. The benefits of adding CDs to LNPs are specific for each type of LNPs.

1.5.1 Nanoemulsions

Nanoemulsions containing CDs, also known as Pickering nanoemulsions, are most commonly used for pharmaceutical and nutraceutical delivery. The CDs decrease the emulsion droplet size, by reducing the interfacial tension, thereby providing a more stable product compared to traditional nanoemulsions. For instance, a CD-nanoemulsion for the delivery of lutein showed that CD increased the stability, entrapment efficiency and partition coefficient of the lutein into the eye (sclera)(C. H. Liu et al., 2015). Similarly, the poor aqueous solubility and storage stability of Kenaf (Hibiscus Cannabinus L) oil was overcome by a Pickering nanoemulsion using β-CD (Cheong, Tan, Tan, & Nyam, 2016). In this system, β-CD served as a co-emulsifier with sodium caseinate and Tween 20. Gharibzahedi et al. (Gharibzahedi, Razavi, & Mousavi, 2015) designed a Pickering nanoemulsion with an optimum ratio of Tween 80: Span 20: HP-β-CD: sunflower oil, which produced the most stable nanoemulsion. The water insoluble anti-cancer drug, canthaxanthin (Dietzia natronolimnaea), was successfully solubilized by HP-β-CD and the amphiphilic drug complex was incorporated into Pickering nanoemulsion.

1.5.2 Liposomes

Traditional liposomes allow lipophilic drugs to be trapped in the lipophilic shell of the liposome; however, these drugs are rapidly released, thus it is more desirable to store the drugs in the aqueous core (Gharib, Greige-Gerges, Fourmentin, Charcosset, & Auezova, 2015). CD-liposomes make this possible since the CDs can encapsulate the lipophilic drug and store it in the aqueous core of the liposome, these systems are termed “drug-in-CD-in-liposome” (DCL) (J.

Chen et al., 2017). For example, a hydrogel consisting of an aceclofenac DCL system for topical skin delivery was prepared (particle size, ~131 nm). Compared to the current marketed formulation, the aceclofenac-CD loaded liposomes had enhanced skin bioavailability, molecule stability and permeation in mice (Sharma, 2011). Another approach is that the lipophilic drug could be stored in both the core and shell yielding a dual-encapsulation method. Soo et al. (Soo et al., 2016) loaded β-CD-resveratrol complexes into the hydrophilic core and resveratrol alone into the lipophilic shell, which led to a significant improvement in the drug release across a dialysis membrane (100% vs 40-60% for conventional formulation in 24 h), thus more drug was available to inhibit the growth of cancer cells. However, there is some concern as to whether or not the CDs will extract cholesterol from the liposomal wall leading to destabilization of the liposome. For instance, Piel et al. created a betamethasone-in-CD-in-liposome formulation and compared the effects on the liposomal structure by using different CDs such as HP-β-CD, β-CD, γ-CD, HP-γ-CD, Heptakis(2,6-di-O-methyl)- β-CD (Dimeb), heptakis(2,3,6-tri-O-methyl)- β-CD (Trimeb), methylated β-CD (Crysmeb), and randomly methylated β-CD (Rameb) to determine which CDs will remove cholesterol from the liposome causing destabilization of the NP (Piel et al., 2006). The results revealed that the betamethasone (BM) formed stable complexes with HP-β-CD, Crysmeb, HP-γ-CD and Rameb; this is due to the fact that the CD has a higher affinity for the drug compared to the cholesterol. Even though the CD formulations yielded a higher encapsulation efficiency, the BM-Rameb and BM-HP-γ-CD complex had the same release profile as the CD-free liposomal formulations. Even though CDs improve encapsulation they may not always yield a sufficient drug release depending on the formulation recipe. Joset et al (Arnaud Joset, 2015) performed studies using Rameb inside cholesterol doped dimyristoyl-phosphatidylcholine (DMPC) liposomes and found that Rameb had a high affinity for the cholesterol since no drug was present. Therefore, liposomal stabilization will depend on the type of CD and guest molecule. Finally, Ji et al. (Ji et al., 2016) used CDs to enhance the tumor targeting ability of the LNP on the outside of the

liposomal wall. The outside of the liposome consisted of pirfenidone-loaded β-CD linked with a cleavable peptide, along with Arg-Gly-Asp peptides to target pancreatic tumor cells while the inside of the liposome contained the chemotherapeutic, gemcitabine (Ji et al., 2016). This effective enzymatic pathway allowed for increased gemcitabine perfusion within pancreatic tumor tissue, 3 and 6 times higher when compared to the free pirfenidone and the control, along with a successful reduction in tumor fibrosis.

1.5.3 Solid Lipid Nanoparticles (SLNs)

SLNs are more stable in biological fluids compared to nanoemulsions and liposomes, and are typically made from fatty acids, waxes, mono-, di-, triglycerides and surfactants of biological origin, thus they are well tolerated and metabolized by the body (Baek, So, Shin, & Cho, 2012). Cyclodextrins can stabilize SLNs by taking the place of surfactants; however, only a few studies have been reported. Negi et al. prepared γ-CD-stearic acid inclusion complexes for their use in Lopinavir loaded SLNs (Negi et al., 2014). The γ-CD SLNs had higher drug loading and similar NP size (~212.5 nm) when compared to the CD-free drug-loaded SLNs (~180.6 nm). To eliminate the harmful effects of Cremophor EL in commercial paclitaxel formulations, Baek et al. used HP-β-CD to increase the cellular uptake of Cremophor EL-free paclitaxel-loaded SLNs in Caco-2 cells (Baek & Cho, 2013; Baek et al., 2012). The HP-β-CD modified SLNs had a 5 fold higher cytotoxicity, and a 12 fold higher drug concentration in lymph nodes when compared to the solution formulation. In a later study, Baek et al. encapsulated paclitaxel and verapamil, a common p-Gp inhibitor, into CDs to further improve the uptake into MCF-7/ADR resistant breast cancer cells. This formulation provided sustained release of both compounds as well as increased cellular uptake, and down-regulated p-Gp expression compared to the solution in MCF-7/ADR resistant breast cancer cells (Baek & Cho, 2015). Recently, Gidwani et al. (Gidwani & Vyas, 2017) complexed altretamine with epichlorohydrin-β-CD which was loaded into SLNs, comprising of Poloxamer-188 and soya

lecithin. This complexation led to enhanced solubility, resulting in 2.75 times higher oral bioavailability of altretamine compared to the free drug.

1.5.4 Nanostructured lipid carriers

When compared to SLNs, the imperfections in the NLC matrix yield higher drug loading, enhanced stability, and decreased chance of drug leakage (Muller, Radtke, & Wissing, 2002; Souto, Mehnert, & Muller, 2006). Drug-in-CD-in-NLCs are relatively new, but they have been used to improve the solubility of water insoluble drugs. Specifically, Lin et al. (Lin et al., 2014) used β-CD to solubilize and improve the oral bioavailability of vinpocetine. The CD-NLCs maintained consistently small particle size and high encapsulation efficiency while still providing a higher dissolution rate in varying pH values, compared to the suspension and CD-free NLCs. Similarly, Cirri et al. (M. Cirri 2016) created CD-NLCs by co-grinding Epichlorohydrin-β-CD and ketoprofen, which provided higher solubilizing action compared to Epichlorohydrin NLCs. The Epichlorohydrin β-CD NLCs had a 1.3-fold higher permeation rate through a lipophilic barrier compared to CD-free NLCs.

1.6 Gold and Silver CD Nanoparticles

Metallic NPs, such as gold and silver, are easily functionalized with ligands, antibodies and drugs; thus they have a wide variety of biological applications (Vicky. V Mody, 2010). Gold nanoparticles (AuNPs) and silver nanoparticles (AgNPs) have unique modifiable optical and electronic properties, which make them ideal for molecular imaging, drug/gene delivery, biosensors and therapeutic agents. Furthermore, AgNPs have antibacterial properties that make them desirable for drug delivery systems as they provide additional antimicrobial action. When combined with CDs, these metallic NPs can become more targeted and more effective. Gold and silver CD NPs are commonly produced by connecting CD to the metallic core using a linker, such as adamantane, which forms a strong stable complex with the CDs. Sometimes the CDs are added

by using CD-loaded macromolecules (CD-modified hyaluronic acid) (Y. Chen, Li, Yang, & Liu, 2015; Ha et al., 2013; Holzinger et al., 2009; N. Li et al., 2014). In some instances, the CDs can be capped directly on the surface of the metallic NP without the need for a linker (Gannimani et al., 2016; Premkumar & Geckeler, 2014). The CD molecules can then be functionalized or used to carry drugs, siRNA or targeting molecules (Figure 1.6).

The most common use of CD-AuNPs is for biosensor technology. A single-walled carbon nanotube framework was constructed with β-CD functionalized AuNPs attached to the surface, which encapsulated polymerized adamantane (Holzinger et al., 2009). The affinity between the polymerized adamantane and the β-CD functionalized AuNPs perfectly mimics the biological interactions of biotin and avidin. The high specific surface of the CD-AuNPs yielded a 3-factor increase in sensitivity and maximum current density with regards to glucose detection. Similarly, Manivannan (S. M. a. K. Kim, 2015) mimicked the interactions of biotin and avidin by embedding AuNPs in a sol-gel silicate matrix that was topped with β-CD functionalized reduced graphene oxide nanosheets. The AuNPs increased the interactions between CDs and the reduced graphene oxide as well as improved the durability and electrical communication by behaving as miniature electrodes. Additionally, the CDs-AuNPs led to improved chemical current, which yielded a stronger synergistic electrocatalytic effect in the case of the CD-AuNPs when compared to the electrodes without gold and CDs.

Another common use of CD-AuNPs is for the targeted delivery of cancer therapeutics because the AuNPs can be used to induce radiofrequency ablation leading to destruction of cancer cells (Patra, Bhattacharya, Mukhopadhyay, & Mukherjee, 2010; Sierpe et al., 2015). Furthermore, the AuNPs allow for easier imaging of cancer cells. Wang et al. (Y. Wang, Li, Jin, & Ji, 2016) formulated β-CD AuNPs loaded with ferrocene which formed aggregates once inside the cell, the aggregation was triggered by intracellular glutathione. The aggregates increased in size leading

to a proportional rise in AuNPs photothermal properties allowing the aggregates to cause apoptosis when exposed to near-infrared irradiation. Typically, AuNP linked CDs are more effective as anticancer therapeutics when combined with other anticancer active molecules. For instance, Bakar et al (Bakar, Caglayan, Onur, Nebioglu, & Palabiyik, 2015) decreased breast cancer cell (MCF-7) proliferation by complexing various ligands (pinoresinol, lariciresinol, and secoisolariciresinol) with thiolated-β-CD and decorating them on the surface of AuNPs. Common anticancer drugs such as doxorubicin, paclitaxel, and docetaxel were incorporated into the CD-AuNPs and targeted to cancer cells via receptor-mediated endocytosis by a RGD peptide (W. H. Chen et al., 2015). Cell line studies revealed that the DOX-β-CD-AuNPs increased the uptake and cell cytotoxicity of U87 cancer cells while decreasing the damage done to the COS7 normal cells. Similarly, AuNPs decorated with PEG and poly (N-isopropylacrylamide) attached via complexation between β-CD and adamantane groups (Ha et al., 2013). When these AuNPs were exposed to a low temperature, the CD-AuNPs disassemble leading to release of the doxorubicin. These CD-AuNPs can transport the doxorubicin directly to the cancer cell nucleus, providing a unique release mechanism compared to liposomes and polymersomes. Chen et al. (Y. Chen et al., 2015) delivered paclitaxel to cancer cells by using biotin-modified CD-AuNPs (particle size, ~189 nm) as targeting moieties. The β-CD was linked using adamantane, which was weakened when exposed to acidic environment of the cancer cells, leading to an increase in drug release in cancer cells and a decrease in normal cells. Comparably, Yan et al. (Yan, 2014) constructed AuNPs decorated with sulfhydrylation-modified β-CD and positively-charged PEG for the delivery of paclitaxel. This delivery system can effectively kill cancer cells with P-gp multidrug resistance. Similarly, a dual delivery nanoplatform of docetaxel and siRNA using gold nanorods coated with polyethylenimine-grafted β-CD was reported (D. G. Wang et al., 2016). When near-infrared laser irradiation (NIR) was applied to the CD-Au nanorod, the siRNA and docetaxel were released from the CD.

Like gold NPs, silver NPs display useful properties such as high functionalization and good catalytic activity, which make them ideal for biosensor applications. A sandwich-like α-fetoprotein (AFP) biosensor was designed by Gao et al(Gao et al., 2015) using β-CD functionalized silver as the mock enzyme with adamantine modified glucose oxidase attached on the bottom side, while the top side of the sandwich consisted of Fe-CD multiwall carbon nanotubes (Figure 1.7). The AFP would become sandwiched between the two layers, allowing for dual amplification of the electrochemical signals. In this study, β-CD functionalized silver was utilized as a mimic enzyme and a carrier, and β-CD based multiwalled carbon nanotubes were used as a platform.

A guanine and adenine biosensor utilized β-CD as the reducing agent between $AgNO_3$ and graphene oxide (Hui, Ma, Hou, Chen, & Yu, 2015). β-CD also served as a stabilizer for the AgNPs-graphene oxide, as a dispersant and provided a microenvironment, which yielded an accelerated absorption of guanine and adenine leading to faster electrocatalysis. Similarly, Qu et al. (Qu et al., 2015) produced a more complex nanoparticle: AgNPs-graphene oxide using β-CD as the reducing agent, while CM-β-CD was used to complex and immobilize ferrocenecarboxylic acid for glucose biosensing. This allowed for the creation of a novel dual-path electron transfer mechanism, which lead to a more rapid biosensor. Overall, CD-AgNP biosensors allowed for a wider linear range, 1.7-fold increase in sensitivity, and a 2.8-fold decrease in the detection limit.

Jose et al. (George, Kuriakose, George, & Mathew, 2011) utilized β-CD to increase the antibacterial/antifungal properties of silver without the addition of a drug. Likewise, Gannimani (Gannimani et al., 2016) combined the antibacterial properties of silver NPs with the hydrophobic drug carrier abilities of CD to form supramolecules that improved the antibacterial efficacy of chloramphenicol. A study comparing chloramphenicol with the three different parent CDs showed that γ-CD had the strongest interaction and anti-bacterial activity. Similarly, Gaurav et al. used β-CD to solubilize clotrimazole which was then attached to albumin stabilized AgNPs, while the

albumin served to reduce the interaction between the AgNPs and the CD-clotrimazole complex (Gaurav et al., 2015). These hybrid NPs had a synergistic effect against candida yeast cells. Jaiswal et al. (Jaiswal, Bhattacharya, McHale, & Duffy, 2015) found that in addition to the enhanced biofilm inhibition, the cytotoxicity of AgNPs in human HaCat skin cells was eliminated due to the protective capping of β-CD. To specifically target cancerous cells while continuing to avoid uptake in healthy cells, Zhai et al. (Zhai et al., 2017) modified the surface of β-CD-capped AgNPs using para-aminothiophenol and folic acid. Therefore, CDs can be used to increase the water solubility of drugs paired with AgNPs as well as diminish and possibly abolish cytotoxicity of healthy cells and enhance the anti-bacterial activity of AgNPs (T. Wang, Li, & Lin, 2013).

1.7 Mesoporous CD Nanoparticles

Mesoporous silica NPs (MSNs) linked with CDs are employed in imaging and cancer therapeutic delivery. MSNs have many advantages such as large surface area, good chemical and mechanical stability, and can be modified for controlled-release by tailoring the pore size of the mesostructure (D. Wang & Wu, 2016). Additionally, MSNs can be programmed for controlled release by modulating voltage, pH, enzymes, redox reactions and light (Bai et al., 2015; T. Wang, Sun, Wang, Zhou, & Fu, 2015). MSNs can be combined with CDs to create snap-top nanocarriers (Ambrogio et al., 2010). The drug is carried within the MSN pores, which are capped by CDs complexed with a gatekeeper. A cycloreversion allows the CD complex to dissociate from the MSN surface, allowing for the drug to escape.

CD linked MSNs are utilized in the controlled delivery of anti-cancer drugs such as doxorubicin (DOX). Tumor specific enzyme-responsive MSNs were formulated using α-CD as the gatekeeper to release DOX when in contact with the designated tumor enzyme (Cheng et al., 2015). This allowed for an “off-on” system, which reduced normal cell toxicity in vitro and increased tumor cell apoptosis and growth inhibition. Another internal biological signal release mechanism is acidic

pH-activated MSNs, since the microenvironment of the tumor is more acidic than normal tissues. Chen et al. functionalized MSNs with β-CD gatekeepers and used 3-carboxy-5-nitrophenylboronic acid to initiate pH-dependent release of the DOX from the MSNs (X. F. Chen, Yao, Wang, Chen, & Chen, 2015) . In addition, fluorescein was linked to β-CD to allow for molecular imaging, which suggests that MSNs could be administered as probes to track the drug delivery pathway. pH-dependent MSNs were formulated with β-CD and α-CD as gatekeepers and found that β-CD had the better pH-responsive behavior (Bai et al., 2015) . Wang et al. created monoferrocene-β-CD capped MSN with dual release mechanism, using voltage to release gemcitabine and pH to release the DOX (T. Wang et al., 2015). Similar internally-responsive release MSNs have been created by utilizing CDs and cancer therapeutics (Huang et al., 2016; Z. L. Li et al., 2015; J. J. Liu et al., 2016; Qiu et al., 2015).

In contrast to internally controlled MSNs, other researchers have focused on regulating the release of doxorubicin from MSNs via external stimuli such as redox potential (Luo et al., 2014; Zhu & Wang, 2016), NIR irradiation (S. Duan, Yang, Zhang, Zhao, & Xu, 2016) and temperature, although no research has been done using CDs in temperature responsive MSNs to date. For instance, NIR-light-responsive supramolecular valves were lodged in the core of MSNs capped with β-CD for the delivery of doxorubicin was reported (D. Wang & Wu, 2016). Similarly, Quin-Lin et al(Q. L. Li et al., 2017). combined β-CD with copper nanoparticles to serve as both gatekeeper and photothermal agent for the release of DOX. Finally, NIR-light-responsive MSNs with α-CDs as the gatekeepers were prepared and drug release experiments revealed that the α-CD successfully hindered the release of DOX in the absence of NIR (Figure 1.8) (Liru Cui, 2015).

1.8 Summary and Conclusions

This review has provided all of the unique characteristics of CDs and their role in nanoparticle-based drug delivery systems. The properties of nanocarriers can be advantageously modified by

the inclusion of parent CDs and their derivatives. The most important uses of CDs in the NPs are enhanced solubility and stability of drugs, improved targetability of NPs to tumor tissues, and increased drug loading capacity of the NPs. In particular, CDs were very useful for magnetic NPs in improving hydrophobic anti-cancer drug delivery, solid-phase extraction and biosensing materials. CDs were exploited with various polymeric NPs to improve the drug loading and targeting of anti-cancer drugs as well as siRNA delivery. Various lipid-based NPs (especially liposomes, SLNs, and NLCs) increased drug loading, targetability of cancer therapeutics and the NPs physical stability due to the addition of CDs. Gold and silver NPs linked CDs to the metallic surface for stabilized scaffolding of biosensors, targeting of cancer therapeutics, and increased antibacterial/antifungal characteristics of silver NPs. Finally, mesoporous NPs used CDs as gatekeepers over the porous NP core to provide a time-released or stimuli-dependent release drug delivery.

It is unknown if different CD derivatives behave differently when they are associated with the NPs in terms of drug loading, targetabilty or stability of the given system. Currently, the USFDA has only approved a few parent CDs (γ-CD for intravenous injection, β-CD for oral and topical delivery) and derivative CDs (HP-γ-CD for topical application, SBE-β-CD for injection, HP-β-CD for oral delivery and injection) as listed in Table 1. As more lipophilic drug compounds are discovered, CDs may very well become the next generation excipient to improve solubility of hydrophobic drugs in all routes and types of formulations, as they are safe and relatively non-irritating(Products, 2014). Currently, NPs are at the forefront of drug delivery; therefore, it can be expected that newly devised NPs will continue to take advantage of CDs to improve NP characteristics.

Conflict of Interest: Authors declare no personal or financial conflict of interest with any parties.

1.9 References

Abdolmohammad-Zadeh, H., & Talleb, Z. (2015). Magnetic solid phase extraction of gemfibrozil from human serum and pharmaceutical wastewater samples utilizing a beta-cyclodextrin grafted graphene oxide-magnetite nano-hybrid. *Talanta, 134*, 387-393. doi:10.1016/j.talanta.2014.11.054

Ahmed, G. H. G., Laino, R. B., Calzon, J. A. G., & Garcia, M. E. D. (2014). Magnetic nanoparticles grafted with beta-cyclodextrin for solid-phase extraction of 5-hydroxy-3-indole acetic acid. *Microchimica Acta, 181*(9-10), 941-948. doi:10.1007/s00604-014-1192-y

Ambrogio, M. W., Pecorelli, T. A., Patel, K., Khashab, N. M., Trabolsi, A., Khatib, H. A., . . . Stoddarrt, J. F. (2010). Snap-Top Nanocarriers. *Organic Letters, 12*(15), 3304-3307. doi:10.1021/ol101286a

Amrita Kadari, S. G., Hitesh Kulhari, Murali Mohan Bhandi, Roshan M. Borkar, Venketa Ramana Murthy Kolapalli, Ramakrishna Sistla (2017). Enhanced oral bioavailability and anticancer efficacy of fisetin by encapsulating as inclusion complex with HPβCD in polymeric nanoparticles. *Drug Delivery, 24*(1), 224-232.

Anirudhan, T. S., Divya, P. L., & Nima, J. (2015). Synthesis and characterization of silane coated magnetic nanoparticles/glycidylmethacrylate-grafted-maleated cyclodextrin composite hydrogel as a drug carrier for the controlled delivery of 5-fluorouracil. *Mater Sci Eng C Mater Biol Appl, 55*, 471-481. doi:10.1016/j.msec.2015.05.068

Ansari, M., Habibi-Rezaei, M., Salahshour-Kordestani, S., Movahedi, A. A. M., & Poursasan, N. (2015). Prevention of Serum Albumin Glycation/Fibrillation by beta-Cyclodextrin Functionalized Magnetic Nanoparticles. *Protein and Peptide Letters, 22*(7), 594-600.

Arima, H., Hayashi, Y., Higashi, T., & Motoyama, K. (2015). Recent advances in cyclodextrin delivery techniques. *Expert Opinion on Drug Delivery, 12*(9), 1425-1441. doi:10.1517/17425247.2015.1026893

Arnaud Joset, A. G., Maryse Hoebeke, Bernard Leyh. (2015). Small-angle Neutron Scattering investigation of cholesterol-doped DMPC liposomes interacting with Beta-cyclodextrin. *J Incl Phenom Macrocycl Chem, 84*, 153-161.

Badruddoza, A. Z. M., Rahman, M. T., Ghosh, S., Hossain, M. Z., Shi, J. Z., Hidajat, K., & Uddin, M. S. (2013). beta-Cyclodextrin conjugated magnetic, fluorescent silica core-shell nanoparticles for biomedical applications. *Carbohydrate Polymers, 95*(1), 449-457. doi:10.1016/j.carbpol.2013.02.046

Baek, J. S., & Cho, C. W. (2013). 2-Hydroxypropyl-beta-cyclodextrin-modified SLN of paclitaxel for overcoming p-glycoprotein function in multidrug-resistant breast cancer cells. *Journal of Pharmacy and Pharmacology, 65*(1), 72-78. doi:10.1111/j.2042-7158.2012.01578.x

Baek, J. S., & Cho, C. W. (2015). Controlled release and reversal of multidrug resistance by co-encapsulation of paclitaxel and verapamil in solid lipid nanoparticles. *International Journal of Pharmaceutics, 478*(2), 617-624. doi:10.1016/j.ijpharm.2014.12.018

Baek, J. S., So, J. W., Shin, S. C., & Cho, C. W. (2012). Solid lipid nanoparticles of paclitaxel strengthened by hydroxypropyl-beta-cyclodextrin as an oral delivery system. *International Journal of Molecular Medicine, 30*(4), 953-959. doi:10.3892/ijmm.2012.1086

Bai, L., Zhao, Q. F., Wang, J., Gao, Y. K., Sha, Z., Di, D. H., . . . Wang, S. L. (2015). Mechanism study on pH-responsive cyclodextrin capped mesoporous silica: effect of different stalk densities and the type of cyclodextrin. *Nanotechnology, 26*(16). doi:Artn 165704

10.1088/0957-4484/26/16/165704

Bakar, F., Caglayan, M. G., Onur, F., Nebioglu, S., & Palabiyik, I. M. (2015). Gold Nanoparticle-Lignan Complexes Inhibited MCF-7 Cell Proliferation in vitro: A Novel Conjugation for Cancer Therapy. *Anti-Cancer Agents in Medicinal Chemistry, 15*(3), 336-344.

Banerjee, S. S., & Chen, D. H. (2010). Grafting of 2-Hydroxypropyl-beta-Cyclodextrin on Gum Arabic-Modified Iron Oxide Nanoparticles as a Magnetic Carrier for Targeted Delivery of

Hydrophobic Anticancer Drug. *International Journal of Applied Ceramic Technology, 7*(1), 111-118. doi:10.1111/j.1744-7402.2008.02332.x

Bienvenu, C., Martinez, A., Blanco, J. L. J., Di Giorgio, C., Vierling, P., Mellet, C. O., . . . Fernandez, J. M. G. (2012). Polycationic amphiphilic cyclodextrins as gene vectors: effect of the macrocyclic ring size on the DNA complexing and delivery properties. *Organic & Biomolecular Chemistry, 10*(29), 5570-5581. doi:10.1039/c2ob25786f

Bina Gidwani, A. V. (2015). A Comprehensive Review on Cyclodextrin-Based Carriers for Delivery of Chemotherapeutic Cycotoxic Anticancer Drugs. *BioMed Research International, 2015*.

Brewster, M. E., & Loftsson, T. (2007). Cyclodextrins as pharmaceutical solubilizers. *Adv Drug Deliv Rev, 59*(7), 645-666.

Bu, X. Y., Zhu, T., Ma, Y. R., & Shen, Q. (2015). Co-administration with cell penetrating peptide enhances the oral bioavailability of docetaxel-loaded nanoparticles. *Drug Development and Industrial Pharmacy, 41*(5), 764-771. doi:10.3109/03639045.2014.902465

Carmen Ortiz Mellet, J. M. G. F., Juan M. Benito. (2010). Cyclodextrin-based gene delivery systems. *Chemical Society Reviews, 40*, 1586-1608.

Chen, J., Yao, J., Ma, Z., Peng, P., Lu, S., Hu, Y., . . . Yang, X. (2017). Delivery of fluorescent-labeled cyclodextrin by liposomes: role of transferrin modification and phosphatidylcholine composition. *J Liposome Res, 27*(1), 21-31. doi:10.3109/08982104.2016.1140184

Chen, W. H., Lei, Q., Luo, G. F., Jia, H. Z., Hong, S., Liu, Y. X., . . . Zhang, X. Z. (2015). Rational Design of Multifunctional Gold Nanoparticles via Host-Guest Interaction for Cancer-Targeted Therapy. *Acs Applied Materials & Interfaces, 7*(31), 17171-17180. doi:10.1021/acsami.5b04031

Chen, X. F., Yao, X. M., Wang, C. R., Chen, L., & Chen, X. S. (2015). Mesoporous silica nanoparticles capped with fluorescence-conjugated cyclodextrin for pH-activated

controlled drug delivery and imaging. *Microporous and Mesoporous Materials, 217*, 46-53. doi:10.1016/j.micromeso.2015.06.012

Chen, Y., Li, N., Yang, Y., & Liu, Y. (2015). A dual targeting cyclodextrin/gold nanoparticle conjugate as a scaffold for solubilization and delivery of paclitaxel. *Rsc Advances, 5*(12), 8938-8941. doi:10.1039/c4ra13135e

Cheng, Y. J., Luo, G. F., Zhu, J. Y., Xu, X. D., Zeng, X., Cheng, D. B., . . . He, F. (2015). Enzyme-Induced and Tumor-Targeted Drug Delivery System Based on Multifunctional Mesoporous Silica Nanoparticles. *Acs Applied Materials & Interfaces, 7*(17), 9078-9087. doi:10.1021/acsami.5b00752

Cheong, A. M., Tan, K. W., Tan, C. P., & Nyam, K. L. (2016). Kenaf (Hibiscus cannabinus L.) seed oil-in-water Pickering nanoemulsions stabilised by mixture of sodium caseinate, Tween 20 and beta-cyclodextrin. *Food Hydrocolloids, 52*, 934-941. doi:10.1016/j.foodhyd.2015.09.005

Conte, C., Costabile, G., d'Angelo, I., Pannico, M., Musto, P., Grassia, G., . . . Quaglia, F. (2015). Skin transport of PEGylated poly(epsilon-caprolactone) nanoparticles assisted by (2-hydroxypropyl)-beta-cyclodextrin. *Journal of Colloid and Interface Science, 454*, 112-120. doi:10.1016/j.jcis.2015.05.010

Diez, P., Villalonga, R., Villalonga, M. L., & Pingarron, J. M. (2012). Supramolecular immobilization of redox enzymes on cyclodextrin-coated magnetic nanoparticles for biosensing applications. *J Colloid Interface Sci, 386*(1), 181-188. doi:10.1016/j.jcis.2012.07.050

Ding, Y. L., Shen, S. Z., Sun, H. D., Sun, K. N., Liu, F. T., Qi, Y. S., & Yan, J. (2015). Design and construction of polymerized-chitosan coated Fe3O4 magnetic nanoparticles and its application for hydrophobic drug delivery. *Materials Science & Engineering C-Materials for Biological Applications, 48*, 487-498. doi:10.1016/j.msec.2014.12.036

Duan, H. M., Li, L. L., Wang, X. J., Wang, Y. H., Li, J. B., & Luo, C. N. (2015). beta-Cyclodextrin/chitosan-magnetic graphene oxide-surface molecularly imprinted polymer nanocomplex coupled with chemiluminescence biosensing of bovine serum albumin. *Rsc Advances, 5*(84), 68397-68403. doi:10.1039/c5ra11061k

Duan, S., Yang, Y., Zhang, C., Zhao, N., & Xu, F. J. (2016). NIR-Responsive Polycationic Gatekeeper-Cloaked Hetero-Nanoparticles for Multimodal Imaging-Guided Triple-Combination Therapy of Cancer. *Small*. doi:10.1002/smll.201603133

El Fagui, A., Wintgens, V., Gaillet, C., Dubot, P., & Amiel, C. (2014). Layer- by- Layer Coated PLA Nanoparticles with Oppositely Charged similar to- Cyclodextrin Polymer for Controlled Delivery of Lipophilic Molecules. *Macromolecular Chemistry and Physics, 215*(6), 555-565. doi:10.1002/macp.201300693

Elsabahy, M., & Wooley, K. L. (2012). Design of polymeric nanoparticles for biomedical delivery applications. *Chemical Society Reviews, 41*(7), 2545-2561. doi:10.1039/c2cs15327k

Fulop, Z., Saokham, P., & Loftsson, T. (2014). Sulfobutylether-beta-cyclodextrin/chitosan nano- and microparticles and their physicochemical characteristics. *Int J Pharm, 472*(1-2), 282-287. doi:10.1016/j.ijpharm.2014.06.039

Gannimani, R., Ramesh, M., Mtambo, S., Pillay, K., Soliman, M. E., & Govender, P. (2016). gamma-Cyclodextrin capped silver nanoparticles for molecular recognition and enhancement of antibacterial activity of chloramphenicol. *Journal of Inorganic Biochemistry, 157*, 15-24. doi:10.1016/j.jinorgbio.2016.01.008

Gao, J., Ma, H. M., Lv, X. H., Yan, T., Li, N., Cao, W., & Wei, Q. (2015). A novel electrochemical immunosensor using beta-cyclodextrins functionalized silver supported adamantine-modified glucose oxidase as labels for ultrasensitive detection of alpha-fetoprotein. *Analytica Chimica Acta, 893*, 49-56. doi:10.1016/j.aca.2015.08.052

Gaurav, C., Nikhil, G., Deepti, S., Kalra, S., Goutam, R., & Amit, G. K. (2015). Albumin stabilized silver nanoparticles-clotrimazole beta-cyclodextrin hybrid nanocomposite for enriched anti-fungal activity in normal and drug resistant Candida cells. *Rsc Advances, 5*(87), 71190-71202. doi:10.1039/c5ra08274a

George, C., Kuriakose, S., George, S., & Mathew, T. (2011). Antifungal activity of silver nanoparticle-encapsulated beta-cyclodextrin against human opportunistic pathogens. *Supramolecular Chemistry, 23*(8), 593-597. doi:10.1080/10610278.2011.575471

Gharib, R., Greige-Gerges, H., Fourmentin, S., Charcosset, C., & Auezova, L. (2015). Liposomes incorporating cyclodextrin-drug inclusion complexes: Current state of knowledge. *Carbohydrate Polymers, 129*, 175-186. doi:10.1016/j.carbpol.2015.04.048

Gharibzahedi, S. M. T., Razavi, S. H., & Mousavi, M. (2015). Optimal Development of a New Stable Nutraceutical Nanoemulsion Based on the Inclusion Complex of 2-Hydroxypropyl-beta-cyclodextrin with Canthaxanthin Accumulated by Dietzia natronolimnaea HS-1 Using Ultrasound-Assisted Emulsification. *Journal of Dispersion Science and Technology, 36*(5), 614-625. doi:10.1080/01932691.2014.921188

Gidwani, B., & Vyas, A. (2017). Pharmacokinetic study of solid-lipid-nanoparticles of altretamine complexed epichlorohydrin-beta-cyclodextrin for enhanced solubility and oral bioavailability. *International Journal of Biological Macromolecules, 101*, 24-31. doi:10.1016/j.ijbiomac.2017.03.047

Godinho, B. M. D. C., Ogier, J. R., Quinlan, A., Quincy, R., Griffin, B. T., Cryan, J. F., & O'Driscoll, C. M. (2014). PEGlyated cyclodextrins as novel siRNA nanosystems: Correlations between polyetyhlene glycol length and nanoparticle stability. *Int J Pharm*(473), 105-112.

Gooding, M., Malhotra, M., McCarthy, D. J., Godinho, B. M. D. C., Cryan, J. F., Darcy, R., & O'Driscoll, C. M. (2015). Synthesis and characterization of rabies virus glycoprotein-tagged amphiphilic cyclodextrins for siRNA delivery in human glioblastoma cells: In vitro

analysis. *European Journal of Pharmaceutical Sciences, 71*, 80-92. doi:10.1016/j.ejps.2015.02.007

Guo, J. F., Ogier, J. R., Desgranges, S., Darcy, R., & O'Driscoll, C. (2012). Anisamide-targeted cyclodextrin nanoparticles for siRNA delivery to prostate tumours in mice. *Biomaterials, 33*(31), 7775-7784. doi:10.1016/j.biomaterials.2012.07.012

Ha, W., Kang, Y., Peng, S. L., Ding, L. S., Zhang, S., & Li, B. J. (2013). Vesicular gold assemblies based on host-guest inclusion and its controllable release of doxorubicin. *Nanotechnology, 24*(49). doi:Artn 495103

10.1088/0957-4484/24/49/495103

Holzinger, M., Bouffier, L., Vilialonga, R., & Cosnier, S. (2009). Adamantane/beta-cyclodextrin affinity biosensors based on single-walled carbon nanotubes. *Biosensors & Bioelectronics, 24*(5), 1128-1134. doi:10.1016/j.bios.2008.06.029

Huang, P. L., Zeng, B. Z., Mai, Z. X., Deng, J. T., Fang, Y. P., Huang, W. H., . . . Zhou, W. Y. (2016). Novel drug delivery nanosystems based on out-inside bifunctionalized mesoporous silica yolk-shell magnetic nanostars used as nanocarriers for curcumin. *Journal of Materials Chemistry B, 4*(1), 46-56. doi:10.1039/c5tb02184g

Hui, Y. C., Ma, X. Y., Hou, X. Z., Chen, F., & Yu, J. (2015). Silver nanoparticles-beta-cyclodextrin-graphene nanocomposites based biosensor for guanine and adenine sensing. *Ionics, 21*(6), 1751-1759. doi:10.1007/s11581-014-1343-5

Institute, N. C. (2016). NCI Dictionary of Cancer Terms.

Ishikawa, M., Yoshii, H., & Furuta, T. (2005). Interaction of modified cyclodextrins with cytochrome P-450. *Biosci Biotechnol Biochem, 69*(1), 246-248.

Jaiswal, S., Bhattacharya, K., McHale, P., & Duffy, B. (2015). Dual effects of beta-cyclodextrin-stabilised silver nanoparticles: enhanced biofilm inhibition and reduced cytotoxicity. *Journal of Materials Science-Materials in Medicine, 26*(1). doi:ARTN 52

10.1007/s10856-014-5367-1

Ji, T., Li, S., Zhang, Y., Lang, J., Ding, Y., Zhao, X., . . . Nie, G. (2016). An MMP-2 Responsive Liposome Integrating Antifibrosis and Chemotherapeutic Drugs for Enhanced Drug Perfusion and Efficacy in Pancreatic Cancer. *ACS Appl Mater Interfaces, 8*(5), 3438-3445. doi:10.1021/acsami.5b11619

Kim, H., Kim, S., Park, C., Lee, H., Park, H. J., & Kim, C. (2010). Glutathione-Induced Intracellular Release of Guests from Mesoporous Silica Nanocontainers with Cyclodextrin Gatekeepers. *Advanced Materials, 22*(38), 4280-+. doi:10.1002/adma.201001417

Kim, S. M. a. K. (2015). Electrochemical Biosensor Utilizing Supramolecular Association of Enzyme Sol-Gel Matrix Embedded Gold Nanoparticles Support Reduced Graphene Oxide- cyclodextrin nanocomposite. *Electroanalysis, 28*, 1-10.

Krzak, A., Swiech, O., Majdecki, M., & Bilewicz, R. (2017). Complexing daunorubicin with beta-cyclodextrin derivative increases drug intercalation into DNA. *Electrochimica Acta, 247*, 139-148. doi:10.1016/j.electacta.2017.06.140

Kumar, L., Verma, S., Prasad, D. N., Bhardwaj, A., Vaidya, B., & Jain, A. K. (2015). Nanotechnology: a magic bullet for HIV AIDS treatment. *Artif Cells Nanomed Biotechnol, 43*(2), 71-86. doi:10.3109/21691401.2014.883400

Lakkakula, J. R., & Krause, R. W. M. (2014). A vision for cyclodextrin nanoparticles in drug delivery systems and pharmaceutical applications. *Nanomedicine, 9*(6), 877-894. doi:10.2217/Nnm.14.41

Li, N., Chen, Y., Zhang, Y. M., Yang, Y., Su, Y., Chen, J. T., & Liu, Y. (2014). Polysaccharide-Gold Nanocluster Supramolecular Conjugates as a Versatile Platform for the Targeted Delivery of Anticancer Drugs. *Scientific Reports, 4*. doi:ARTN 4164

10.1038/srep04164

Li, Q. L., Wang, D., Cui, Y., Fan, Z., Ren, L., Li, D., & Yu, J. (2017). AIEgen-Functionalized Mesoporous Silica Gated by Cyclodextrin-Modified CuS for Cell Imaging and Chemo-Photothermal Cancer Therapy. *ACS Appl Mater Interfaces*. doi:10.1021/acsami.7b14566

Li, Z. L., Clemens, D. L., Lee, B. Y., Dillon, B. J., Horwitz, M. A., & Zink, J. I. (2015). Mesoporous Silica Nanoparticles with pH-Sensitive Nanovalves for Delivery of Moxifloxacin Provide Improved Treatment of Lethal Pneumonic Tularemia. *Acs Nano, 9*(11), 10778-10789. doi:10.1021/acsnano.5b04306

Lin, C. C., Chen, F., Ye, T. T., Zhang, L. N., Zhang, W. J., Liu, D. D., . . . Pan, W. S. (2014). A novel oral delivery system consisting in "drug-in cyclodextrin-in nanostructured lipid carriers" for poorly water-soluble drug: Vinpocetine. *International Journal of Pharmaceutics, 465*(1-2), 90-96. doi:10.1016/j.ijpharm.2014.02.013

Liru Cui, F. Z., Oian Wang, Huiming Lin, Chunyu Yang, Ting Zhang, Ruihan Tong, Na An, Fengyu Cu. (2015). Nir light repsonsive core-shell nanocontainers for drug delivery. *Journal of Materials Chemistry B*(35), 7046-7054. doi:10.1039/C5TB00709G

Liu, C. H., Lai, K. Y., Wu, W. C., Chen, Y. J., Lee, W. S., & Hsu, C. Y. (2015). In Vitro Scleral Lutein Distribution by Cyclodextrin Containing Nanoemulsions. *Chemical & Pharmaceutical Bulletin, 63*(2), 59-67.

Liu, J. J., Luo, Z., Zhang, J. X., Luo, T. T., Zhou, J., Zhao, X. J., & Cai, K. Y. (2016). Hollow mesoporous silica nanoparticles facilitated drug delivery via cascade pH stimuli in tumor microenvironment for tumor therapy. *Biomaterials, 83*, 51-65. doi:10.1016/j.biomaterials.2016.01.008

Loftsson, T., & Duchene, D. (2007). Cyclodextrins and their pharmaceutical applications. *International Journal of Pharmaceutics, 329*(1-2), 1-11. doi:10.1016/j.ijpharm.2006.10.044

Loftsson, T., Jarho, P., Masson, M., & Jarvinen, T. (2005). Cyclodextrins in drug delivery. *Expert Opin Drug Deliv, 2*(2), 335-351. doi:10.1517/17425247.2.1.335

Loftsson, T., Masson, M., & Brewster, M. E. (2004). Self-association of cyclodextrins and cyclodextrin complexes. *Journal of Pharmaceutical Sciences, 93*(5), 1091-1099. doi:10.1002/jps.20047

Lorena García-González, L. Y.-M., Adriana Ganem. (2015). Effect of β-cyclodextrin on the internalization of nanoparticles into intestine epithelial cells. *European Journal of Pharmaceutics, 81*, 113-118.

Luo, Z., Hu, Y., Cai, K., Ding, X., Zhang, Q., Li, M., . . . Zhao, Y. (2014). Intracellular redox-activated anticancer drug delivery by functionalized hollow mesoporous silica nanoreservoirs with tumor specificity. *Biomaterials, 35*(27), 7951-7962. doi:10.1016/j.biomaterials.2014.05.058

Lv, S. N., Zhao, M. Q., Cheng, C. J., & Zhao, Z. G. (2014). beta-Cyclodextrin polymer brushes decorated magnetic colloidal nanocrystal clusters for the release of hydrophobic drugs. *Journal of Nanoparticle Research, 16*(5). doi:10.1007/s11051-014-2393-3

M. Cirri , M. B., N. Mennini, P. Mura. (2016). Development of a new delivery system consisting in ‘‘drug – in cyclodextrin – in nanostructured lipid carriers’’ for ketoprofen topical delivery. *European Journal of Pharmaceutics and Biopharmaceutics, 80*, 46-53.

Mansourpour, M., Mahjub, R., Amini, M., Ostad, S. N., Shamsa, E. S., Rafiee-Tehrani, M., & Dorkoosh, F. A. (2015). Development of acid-resistant alginate/trimethyl chitosan nanoparticles containing cationic beta-cyclodextrin polymers for insulin oral delivery. *AAPS PharmSciTech, 16*(4), 952-962. doi:10.1208/s12249-014-0282-9

Mavridis, I. M., & Yannakopoulou, K. (2015). Anionic cyclodextrins as versatile hosts for pharmaceutical nanotechnology: Synthesis, drug delivery, enantioselectivity, contrast agents for MRI. *International Journal of Pharmaceutics, 492*(1-2), 275-290. doi:10.1016/j.ijpharm.2015.06.004

Miao, Q. H., Li, S. P., Han, S. Y., Wang, Z., Wu, Y., & Nie, G. J. (2012). Construction of hydroxypropyl-beta-cyclodextrin copolymer nanoparticles and targeting delivery of paclitaxel. *Journal of Nanoparticle Research, 14*(8). doi:ARTN 1043

10.1007/s11051-012-1043-x

Muller, R. H., Radtke, M., & Wissing, S. A. (2002). Nanostructured lipid matrices for improved microencapsulation of drugs. *International Journal of Pharmaceutics, 242*(1-2), 121-128. doi:Pii S0378-5173(02)00180-1

Doi 10.1016/S0378-5173(02)00180-1

Mura, P., Maestrelli, F., Cecchi, M., Bragagni, M., & Almeida, A. (2010). Development of a new delivery system consisting in 'drug-in cyclodextrin-in PLGA nanoparticles'. *Journal of Microencapsulation, 27*(6), 479-486. doi:10.3109/02652040903515508

Negi, J. S., Chattopadhyay, P., Sharma, A. K., & Ram, V. (2014). Preparation of gamma cyclodextrin stabilized solid lipid nanoparticles (SLNS) using stearic acid-gamma-cyclodextrin inclusion complex. *Journal of Inclusion Phenomena and Macrocyclic Chemistry, 80*(3-4), 359-368. doi:10.1007/s10847-014-0415-5

Oh, N. M., Oh, K. T., & Lee, E. S. (2014). Development of pH-responsive poly(gamma-cyclodextrin) derivative nanoparticles. *Colloids and Surfaces B-Biointerfaces, 119*, 14-21. doi:10.1016/j.colsurfb.2014.04.017

Patra, C. R., Bhattacharya, R., Mukhopadhyay, D., & Mukherjee, P. (2010). Fabrication of gold nanoparticles for targeted therapy in pancreatic cancer. *Advanced Drug Delivery Reviews, 62*(3), 346-361. doi:10.1016/j.addr.2009.11.007

Piel, G., Piette, M., Barillaro, V., Castagne, D., Evrard, B., & Delattre, L. (2006). Betamethasone-in-cyclodextrin-in-liposome: The effect of cyclodextrins on encapsulation efficiency and

release kinetics. *International Journal of Pharmaceutics, 312*(1-2), 75-82. doi:10.1016/j.ijpharm.2005.12.044

Premkumar, T., & Geckeler, K. E. (2014). Facile synthesis of silver nanoparticles using unmodified cyclodextrin and their surface-enhanced Raman scattering activity. *New Journal of Chemistry, 38*(7), 2847-2855. doi:10.1039/c3nj01375h

Products, C. f. H. M. (2014). *Background review for cyclodextrins used as excipients*. Retrieved from London, UK:

Qiu, X. L., Li, Q. L., Zhou, Y., Jin, X. Y., Qi, A. D., & Yang, Y. W. (2015). Sugar and pH dual-responsive snap-top nanocarriers based on mesoporous silica-coated Fe3O4 magnetic nanoparticles for cargo delivery. *Chemical Communications, 51*(20), 4237-4240. doi:10.1039/c4cc10413g

Qu, F. J., Ma, X. Y., Hui, Y. C., Hou, X. Z., Yu, J., Zhang, Q. L., & Chen, F. (2015). Fabrication of Dual-Path Electron Transfer Electrode for Electrochemical Glucose Sensing. *Journal of the Electrochemical Society, 162*(1), B27-B35. doi:10.1149/2.0641501jes

Rastegari, B., Karbalaei-Heidari, H. R., Zeinali, S., & Sheardown, H. (2017). The enzyme-sensitive release of prodigiosin grafted beta-cyclodextrin and chitosan magnetic nanoparticles as an anticancer drug delivery system: Synthesis, characterization and cytotoxicity studies. *Colloids and Surfaces B-Biointerfaces, 158*, 589-601. doi:10.1016/j.colsurfb.2017.07.044

Ruiz-Esparza, G. U., Wu, S. H., Segura-Ibarra, V., Cara, F. E., Evans, K. W., Milosevic, M., . . . Blanco, E. (2014). Polymer Nanoparticles Encased in a Cyclodextrin Complex Shell for Potential Site-and Sequence-Specific Drug Release. *Advanced Functional Materials, 24*(30), 4753-4761. doi:10.1002/adfm.201400011

Saenger, W. (1980). Cyclodextrin Inclusion-Compounds in Research and Industry. *Angewandte Chemie-International Edition in English, 19*(5), 344-362. doi:DOI 10.1002/anie.198003441

Shamekhi, R., Ahmad Panahi, H., Alaei, H. S., & Moniri, E. (2017). Functionalized superparamagnetic nanoparticles with a polymer containing beta-cyclodextrin for the extraction of sertraline hydrochloride in biological samples. *J Sep Sci, 40*(18), 3690-3695. doi:10.1002/jssc.201700454

Sharma, R. T. a. Y. (2011). Pathogenesis of Dermatophytes. *Indian Journal of Dermatology, 56*(3).

Sherje, A. P., Dravyakar, B. R., Kadam, D., & Jadhav, M. (2017). Cyclodextrin-based nanosponges: A critical review. *Carbohydrate Polymers, 173*, 37-49. doi:10.1016/j.carbpol.2017.05.086

Shi, Q., Zhang, L., Liu, M. Y., Zhang, X. L., Zhang, X. J., Xu, X. Q., . . . Zhang, J. X. (2015). Reversion of multidrug resistance by a pH-responsive cyclodextrin-derived nanomedicine in drug resistant cancer cells. *Biomaterials, 67*, 169-182. doi:10.1016/j.biomaterials.2015.07.023

Sierpe, R., Lang, E., Jara, P., Guerrero, A. R., Chornik, B., Kogan, M. J., & Yutronic, N. (2015). Gold Nanoparticles Interacting with beta-Cyclodextrin-Phenylethylamine Inclusion Complex: A Ternary System for Photothermal Drug Release. *Acs Applied Materials & Interfaces, 7*(28), 15177-15188. doi:10.1021/acsami.5b00186

Simoes, S. M. N., Rey-Rico, A., Concheiro, A., & Alvarez-Lorenzo, C. (2015). Supramolecular cyclodextrin-based drug nanocarriers. *Chemical Communications, 51*(29), 6275-6289. doi:10.1039/c4cc10388b

Soo, E., Thakur, S., Qu, Z., Jambhrunkar, S., Parekh, H. S., & Popat, A. (2016). Enhancing delivery and cytotoxicity of resveratrol through a dual nanoencapsulation approach. *J Colloid Interface Sci, 462*, 368-374. doi:10.1016/j.jcis.2015.10.022

Souto, E. B., Mehnert, W., & Muller, R. H. (2006). Polymorphic behaviour of Compritol (R) 888 ATO as bulk lipid and as SLN and NLC. *Journal of Microencapsulation, 23*(4), 417-433. doi:10.1080/02652040600612439

Stella, V. J., & He, Q. (2008). Cyclodextrins. *Toxicol Pathol, 36*(1), 30-42. doi:10.1177/0192623307310945

Subathra Sinniah, S. M., Ninie S.A. Manan. (2015). Magnetite nanoparticles coated with Beta-Cyclodextrin functionalized-ionic liquid: synthesis and its preliminary investigation as a new sensing material. *Applied Surface Science, 357*, 543-550.

Tao, H. Q., Meng, Q. F., Li, M. H., Yu, H., Liu, M. F., Du, D., . . . Peng, H. S. (2013). HP-beta-CD-PLGA nanoparticles improve the penetration and bioavailability of puerarin and enhance the therapeutic effects on brain ischemia-reperfusion injury in rats. *Naunyn-Schmiedebergs Archives of Pharmacology, 386*(1), 61-70. doi:10.1007/s00210-012-0804-5

Thorsteinn Loftsson, P. J., Mar Masson, and Tomi Jarvinen. (2005). Cyclodextrins in Drug Delivery. *Expert Opinion on Drug Delivery*(2), 335-351.

Vicky. V Mody, R. S., Ajay Singh, Hardik R. Mody. (2010). Introduction to metallic nanoparticles. *Journal of Pharmacy and BioAllied Sciences*.

Villari, V., Mazzaglia, A., Darcy, R., O'Driscoll, C. M., & Micali, N. (2013). Nanostructures of cationic amphiphilic cyclodextrin complexes with DNA. *Biomacromolecules, 14*(3), 811-817. doi:10.1021/bm3018609

Wang, D., & Wu, S. (2016). Red-Light-Responsive Supramolecular Valves for Photocontrolled Drug Release from Mesoporous Nanoparticles. *Langmuir, 32*(2), 632-636. doi:10.1021/acs.langmuir.5b04399

Wang, D. G., Wang, T. T., Xu, Z. A., Yu, H. J., Feng, B., Zhang, J. Y., . . . Li, Y. P. (2016). Cooperative Treatment of Metastatic Breast Cancer Using Host-Guest Nanoplatform Coloaded with Docetaxel and siRNA. *Small, 12*(4), 488-498. doi:10.1002/smll.201502913

Wang, T., Li, B., & Lin, L. (2013). Preparation, Characterization, and Bacteriostasis of AgNP-Coated beta-CD Grafting Cellulose Beads. *Applied Biochemistry and Biotechnology, 169*(6), 1811-1821. doi:10.1007/s12010-013-0108-3

Wang, T., Sun, G. P., Wang, M. D., Zhou, B. J., & Fu, J. J. (2015). Voltage/pH-Driven Mechanized Silica Nanoparticles for the Multimodal Controlled Release of Drugs. *Acs Applied Materials & Interfaces, 7*(38), 21295-21304. doi:10.1021/acsami.5b05619

Wang, T., Zhang, C., Liang, X. J., Liang, W., & Wu, Y. (2011). Hydroxypropyl-beta-cyclodextrin copolymers and their nanoparticles as doxorubicin delivery system. *J Pharm Sci, 100*(3), 1067-1079. doi:10.1002/jps.22352

Wang, Y., Li, H., Jin, Q., & Ji, J. (2016). Intracellular host-guest assembly of gold nanoparticles triggered by glutathione. *Chemical Communications, 52*(3), 582-585. doi:10.1039/c5cc07195j

Xie, S. B., Zhang, J., Yuan, Y. L., Chai, Y. Q., & Yuan, R. (2015). An electrochemical peptide cleavage-based biosensor for prostate specific antigen detection via host-guest interaction between ferrocene and beta-cyclodextrin. *Chemical Communications, 51*(16), 3387-3390. doi:10.1039/c4cc10363g

Yan, B. L., Fei; Zhai, Shumei; Zhang, Bin. (2014). China Patent No. Faming Zhuanli Shenqing.

Zafar, N., Fessi, H., & Elaissari, A. (2014). Cyclodextrin containing biodegradable particles: from preparation to drug delivery applications. *Int J Pharm, 461*(1-2), 351-366. doi:10.1016/j.ijpharm.2013.12.004

Zhai, Z., Zhang, F., Chen, X., Zhong, J., Liu, G., Tian, Y., & Huang, Q. (2017). Uptake of silver nanoparticles by DHA-treated cancer cells examined by surface-enhanced Raman spectroscopy in a microfluidic chip. *Lab Chip, 17*(7), 1306-1313. doi:10.1039/c7lc00053g

Zhang, D., Pan, X., Wang, S., Zhai, Y., Guan, J., Fu, Q., . . . Sun, J. (2015). Multifunctional Poly(methyl vinyl ether-co-maleic anhydride)-graft-hydroxypropyl-beta-cyclodextrin Amphiphilic Copolymer as an Oral High-Performance Delivery Carrier of Tacrolimus. *Mol Pharm, 12*(7), 2337-2351. doi:10.1021/acs.molpharmaceut.5b00010

Zhang, N., Li, J. H., Jiang, W. F., Ren, C. H., Li, J. S., Xin, J. Y., & Li, K. (2010). Effective protection and controlled release of insulin by cationic beta-cyclodextrin polymers from alginate/chitosan nanoparticles. *International Journal of Pharmaceutics, 393*(1-2), 212-218. doi:10.1016/j.ijpharm.2010.04.006

Zhu, X., & Wang, C. Q. (2016). pH and redox-operated nanovalve for size-selective cargo delivery on hollow mesoporous silica spheres. *J Colloid Interface Sci, 480*, 39-48. doi:10.1016/j.jcis.2016.06.043

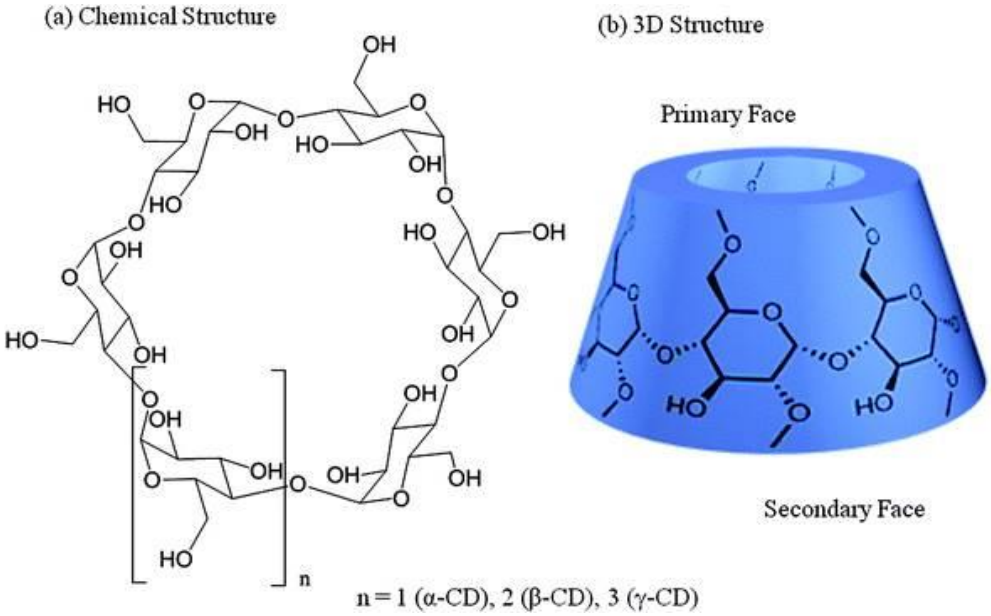

Figure 1.1: Chemical structure and 3D structure of cyclodextrin (CD). The CD interior is lined with carbons and ethereal oxygen of the glucose residues, while the exterior is lined with hydroxyl groups. Therefore, the CD molecules contain a hydrophobic core and a hydrophilic shell. Reproduced with permission from Zafar et al. (ZAFAR ET AL., 2014)

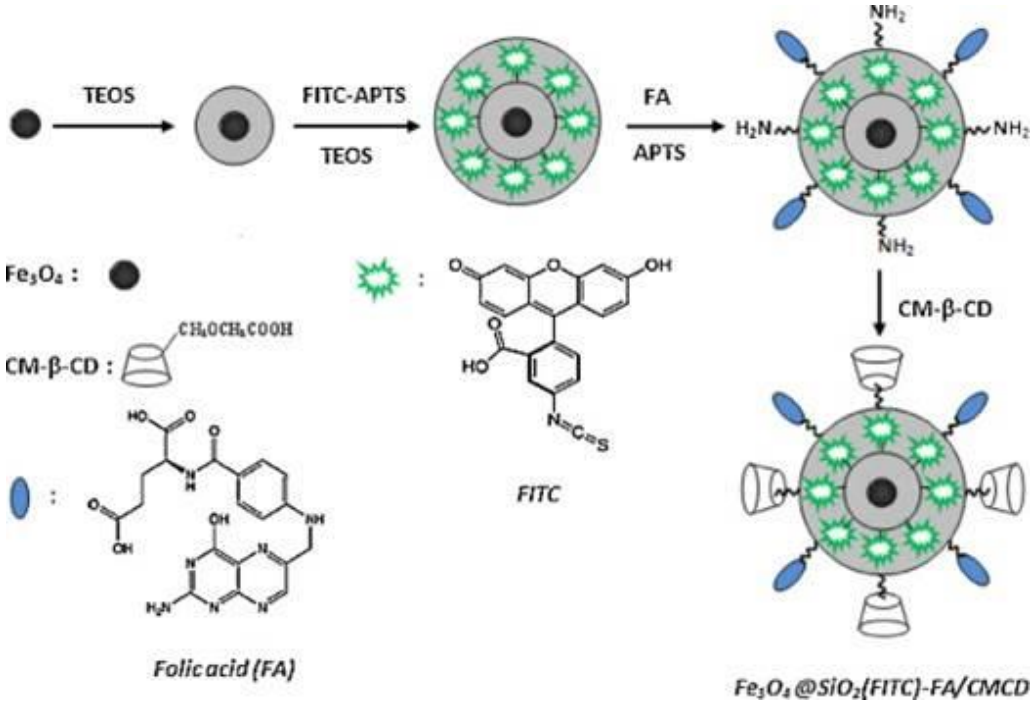

Figure 1.2: Structure of CM-β-CD conjugated fluorescein-doped magnetic silica nanoparticles. Fluorescence labeling by FITC and the addition of a common cancer-targeting ligand, folic acid. Reproduced with permission from Badruddoza et al. (29)

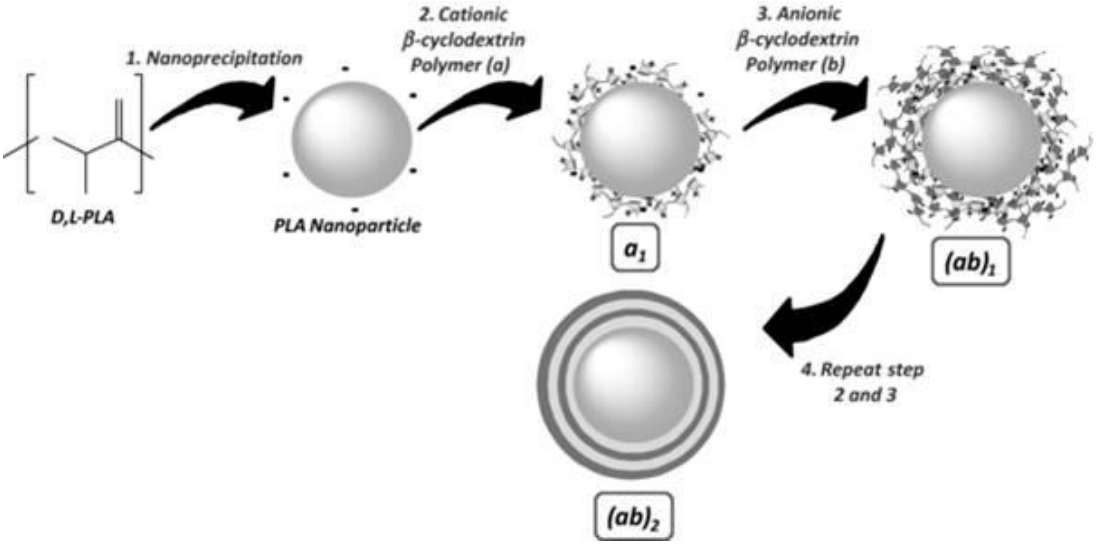

Figure 1.3: Schematic for the preparation of PLA core nanoparticles coated with alternating layers of cationic β-CD polymer (light grey, a) and anionic β-CD (dark grey, b) for the controlled intravenous delivery of benzophenone. Reproduced with permission from Fagui et al. (EL FAGUI ET AL., 2014)

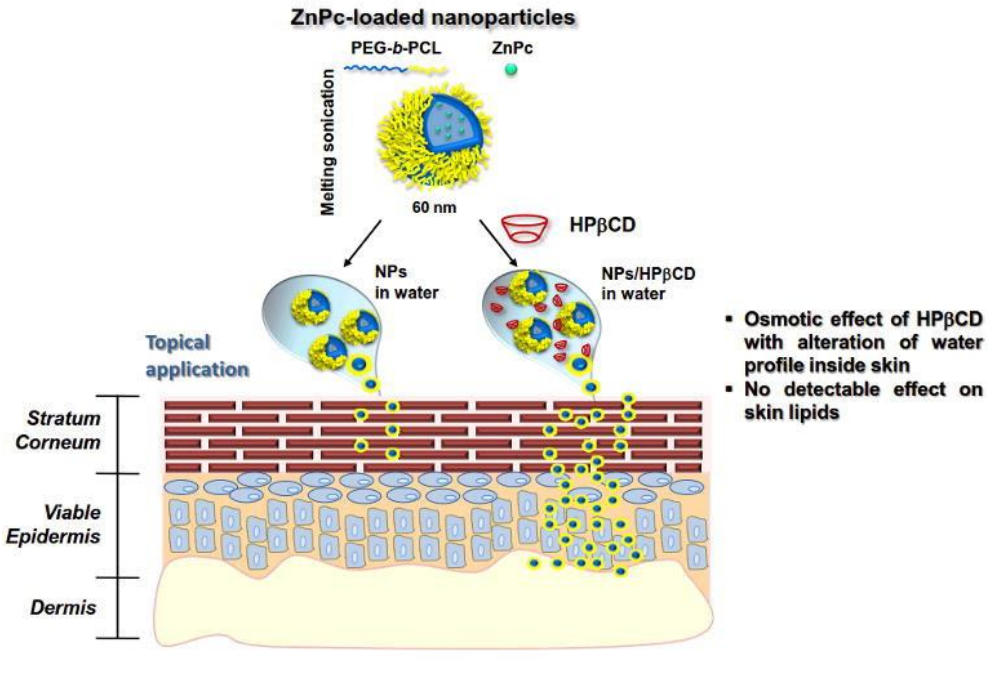

Figure 1.4: Skin transport of PEGlyated poly (ε-caprolactone) nanoparticles assisted by HP-β-CD, which serves as a permeation enhancer in this study. Reproduced with permission from Conte et al. (35).

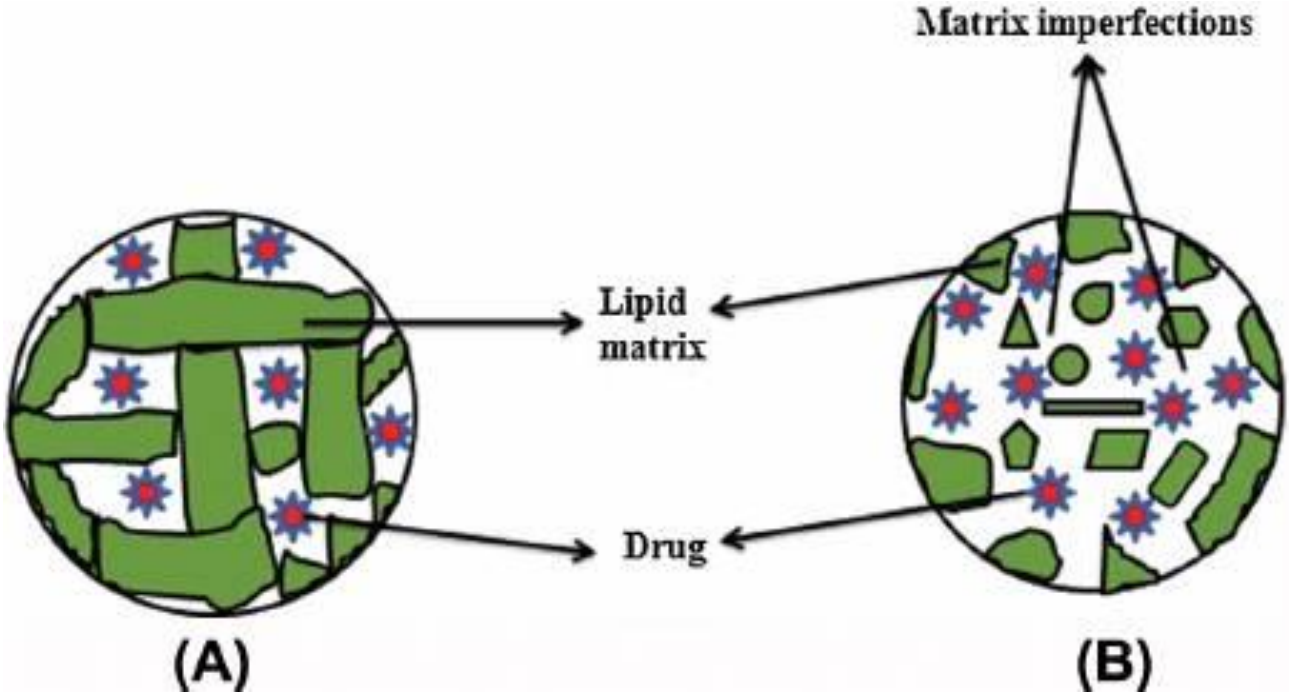

Figure 1.5: SLNs are completely solid and consist of a single lipid layer encasing a solid lipid core Nanostructured lipid carriers are comprised of both solid and liquid lipids providing a less compact structure for higher drug loading. Reproduced with permission from Kumar et al. (KUMAR ET AL., 2015)**.**

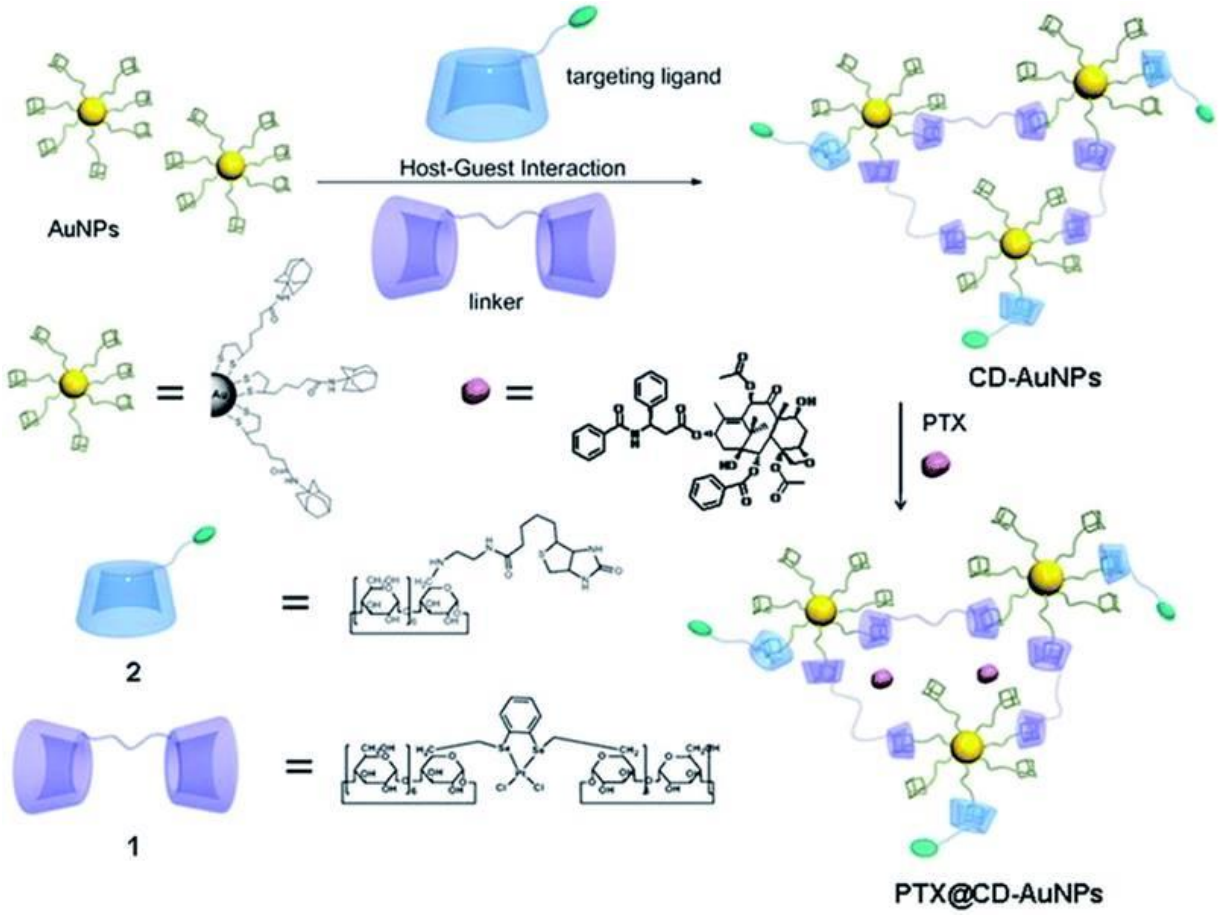

Figure 1.6: Chemical structures and construction of CD-AuNPs loaded with paclitaxel (PTX). AuNPs are targeted and linked with assistance from the host guest interactions of the CDs, and then PTX is loaded in the matrix of the CD-AuNPs. Reproduced with permission from Chen et al. (Y. CHEN ET AL., 2015)

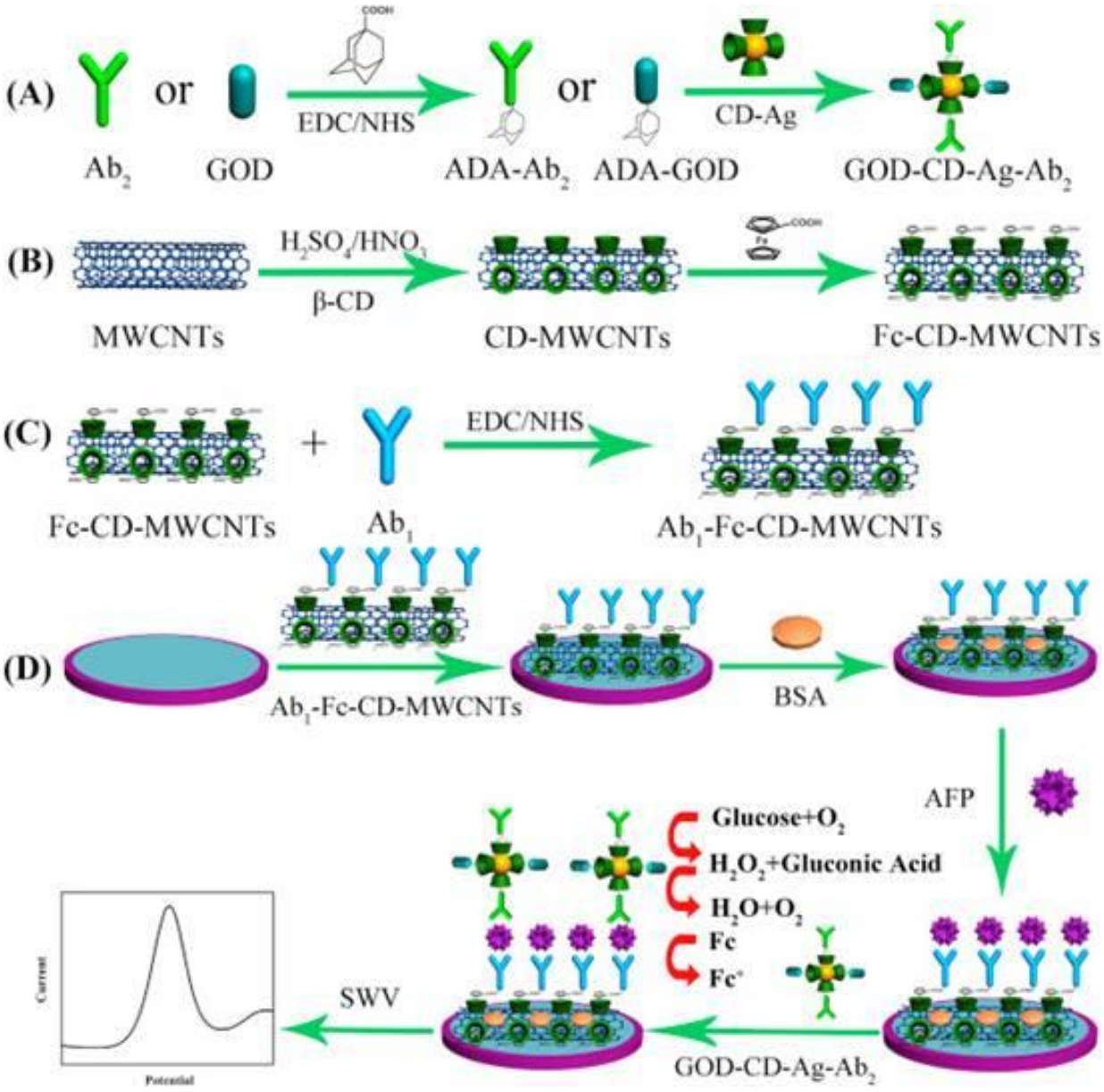

Figure 1.7: Fabrication of a sandwich-like α-fetoprotein (AFP) immunosensor using gold nanoparticles and β-CD functionalized silver as the mock enzyme. Adamantine modified glucose oxidase was attached to the bottom, while the top included Fe-CD multiwall carbon nanotubes. Reproduced with permission from Gao et al. (GAO ET AL., 2015)

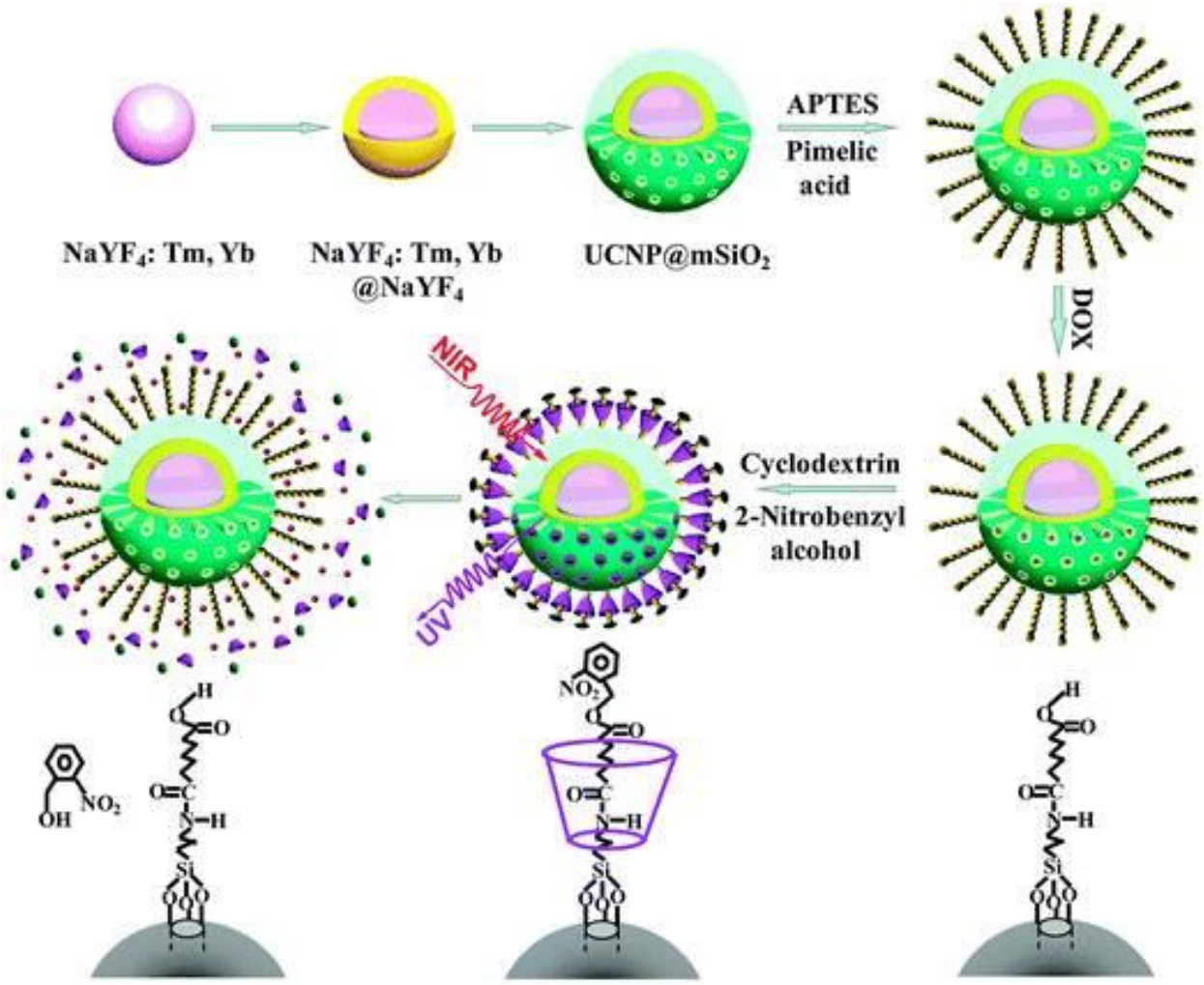

Figure 1.8: Schematic illustration of the mesoporous silica nanoparticles (MSN)-CDs synthesis and the controlled NIR-light-responsive release of dox process by the α-CD gatekeepers. Reproduced with permission from Cui et al. (LIRU CUI, 2015)

CD type	Route of administration and dosage form
α-CD	Powder for injection as solution
β -CD	Oral tablet, topical gel
γ-CD	Intravenous injection as solution
Sulfobutyl ether Na β-CD	Intravenous/intramuscular/subcutaneous injection as solution
Hydroxypropyl β-CD	Oral solution; orally disintegrating tablet; lyophilized powder for injection solution; intramuscular/intravenous injection as solution
Hydroxypropyl γ-CD	Topical Solution

Table 1.1: List of US-FDA approved CDs in various dosage forms

Type of CD	Types of Nanoparticles	Uses
Nonionic	pH sensitive NP: Acetylated α-CD(Shi et al., 2015)	Target MDR cancer cells
Nonionic	Fluorescent magnetic silica core-shell NP β-CD(Badruddoza et al., 2013)	Cancer-targeting ligand and imaging
Nonionic	Mono-6-formyl-β-CD attached to (3-aminopropyl)triethoxysilane-coated magnetic NP(Diez et al., 2012)	CD-coated NP for biosensing applications
Nonionic	β-CD gold NPs attached to single-walled carbon nanotubes(Holzinger et al., 2009)	Biosensing of Adamantane
Nonionic	Polycationic amphiphilic γ–CD(Bienvenu et al., 2012)	Gene Vector
Nonionic	pH responsive poly(γ–CD-DEAP) derivative(Oh, Oh, & Lee, 2014)	Antitumor drug delivery
Nonionic	Mono-6-deoxy-6(p-toylsulfonyl)-β-CD(Ahmed et al., 2014)	Solid-phase extraction of 5-HIAA from urine
Nonionic	PEGylated poly(ε-caprolactone) NP assisted by 2-HP-β-CD(Conte et al., 2015)	Skin transport of drug delivery system
Anionic	Chitosan (CS) cross-linked SBE-β-CD NP loaded with Ciproflaxin (Mavridis & Yannakopoulou, 2015)	Microbial protection for titanium implants
Anionic	CS cross-linked CM-β-CD magnetic NP(Ding et al., 2015)	Delivery of hydrophobic cancer drugs
Anionic	Gold- CM-β-CD NP(Mavridis & Yannakopoulou, 2015)	Stability of Antimicrobial gold nanoclusters
Cationic	Cationic β-CD polymers(Mansourpour et al., 2015)	Insulin delivery
Cationic	Co-formulation of neutral PEGylated CD with a cationic click chemistry CD(Gooding et al., 2015)	siRNA Delivery

Cationic	Heptakis-[2-(ω-amino-oligo-(ethylene glycol))-6-deoxy-6-hexadecylthio]- β-CD(Villari, Mazzaglia, Darcy, O'Driscoll, & Micali, 2013)	Therapeutic Gene Delivery

Table 1.2: Uses of CDs in various nanoparticle applications

Chapter 2: Introduction to Ophthalmic Drug Delivery

2.1 Abstract

The eye is approximately 98% water and is divided into two segments: the anterior segment and posterior segment. The anterior segment consists of the cornea, iris, lens, ciliary body, pupil and aqueous humor. The remaining two-thirds of the eye is the posterior segment: the vitreous humor, retina, choroid, sclera and the optic nerve. When producing new ophthalmic formulations, the route of administration and type of dosage form must be given careful consideration. Ocular drug delivery systems can be delivered via topical, injectable or systemic routes. Conventional dosage forms make up 90% of all commercial ophthalmic formulations, which include solutions, suspensions, emulsions, ointments, gels and ocular inserts. Each dosage form is presented with individual advantages and disadvantages that can be used to determine which dosage form is best for a specific drug and disease.

2.2 Introduction to the Eye

The ocular globe is composed of 98% water, 1.8% solid, 0.67% protein, 0.65% sugar, 0.66% NaCl, and the remaining is made up of sodium, ammonia and potassium. The eye consists of two sections: the front anterior section and the posterior segment (Figure 5.1). The anterior segment includes the cornea, aqueous humor, lens, pupil iris and the ciliary body. The cornea is the transparent tissue in the front of the eye that serves as a protective barrier to the anterior segment (Zinn & Mockel-Pohl, 1973). The lens, in combination with the cornea, assists in refracting and focusing the incoming light on the retina. The aqueous humor is 98% water and fills the spaces within the anterior segment providing nutrients to the surrounding tissues. Aqueous humor is constantly being produced by the ciliary body muscle, which also controls the lens shape. The iris is a thin circular tissue responsible for adjusting the diameter and size of the pupil. Irises are also responsible for the color seen in an individual's eyes. The pupil is the hole in the center of the iris, which enables light to strike the retina in the back of the eye. A number of conditions affect the anterior segment including some more common conditions such as dry eye, cataract, pterygium and conjunctivitis (College, 2018).

The posterior segment is the larger part of the eye consisting of two-thirds of the entire ocular globe. This segment contains the vitreous humor, retina, choroid, sclera and the optic nerve. The vitreous humor is a clear gel that fills spaces in between the retina and lens and makes up the majority of the eyeball. The three outer layers of the eye begin with the outermost layer, the sclera, commonly known as the white of the eye in humans. The sclera has the main responsibility of providing a protective outer layer. The innermost layer of the eye is the retina, which is where the optics of the eye create a focused image that is sent to the brain via electrical impulses. The second layer, in between the sclera and the retina, is the choroid which is composed of connective tissues. The individual structures of the posterior segment can develop a variety of conditions

such as: macular edema, glaucoma, age-related macular degeneration, diabetic retinopathy and uveitis.

2.3 Routes of Administration

One of the first things to consider in ophthalmic formulation development is the route of administration. The proper administration route must be decided based on the area of the eye being affected and the specific disease state. Additionally, the administration route should not hinder or affect the normal function of the eye. The three main routes of administration for ocular drug delivery include topical, systemic and injectables.

2.3.1 Topical Administration

Topical formulations include any formulation that is applied directly to the surface of the eye such as solutions, suspensions, gels, emulsions, ointments and ocular inserts. These formulations are typically used to treat inflammation of the eye (i.e. keratitis, uveitis, and conjunctivitis) among other non-chronic illnesses. Drug delivery via topical instillation is the most ideal route of administration for the eye, due to easy administration, noninvasive, high patient compliance and little to no irritation (Gaudana, Ananthula, Parenky, & Mitra, 2010; Patel, Cholkar, Agrahari, & Mitra, 2013). However, it's ease of use comes with a number of disadvantages. First of all, it's only ideal for treatment of the anterior segment as increased tear rate turnover, reflex blinking, nasolacrimal drainage and permeation barriers result in less than 5% delivery to the posterior tissues (Gulsen & Chauhan, 2004). Static barriers include the permeation issues posed by the corneal, retinal pigment epithelium and scleral tissues along with the tear film layers. Permeability through the cornea and sclera is inversely proportional to the size of the molecule (Gaudana et al., 2010). The tear film layers consist of an outermost oil layer, middle aqueous layer and a mucin layer that is nearest to the corneal surface. Therefore, the ability for a topical formulation to penetrate these layers depends on the lipophilicity of the drug and excipient properties. Dynamic

barriers include lymphatic flow in the conjunctival tissue and episclera, along with the blood flow in the choroid and conjunctival tissues (Kim, Lutz, Wang, & Robinson, 2007).

2.3.2 Systemic Delivery

Systemic delivery, either orally or parenterally, is an alternative to topical treatments when patients lack administration compliance. Additionally, systemic delivery to the eye has been suggested for posterior delivery; however, it is limited due to the presence of blood-aqueous and blood-retinal barriers and the miniscule volume of the eye relative to the whole body. The blood-aqueous barrier restricts entrance of solutes into the aqueous humor, while the blood-retinal barrier prevents entrance of therapeutic entities into the vitreous humor (Barar, Javadzadeh, & Omidi, 2008; Pitkanen, Ranta, Moilanen, & Urtti, 2005). Drugs taken orally or parenterally can easily penetrate the choroid due to its enhanced vascularization; however, the blood-retinal barrier prevents further transfer of the drug to the retina. Oral delivery is sometimes used concurrently with topical therapy to enhance the therapeutic effect.

2.3.3 Injectables

Due to the aforementioned disadvantages of topical formulations and low ocular bioavailability of systemic delivery, injections have become a common technique for the treatment of ocular diseases. Furthermore, ocular injections are often implemented when a chronic long-term ocular illness is present. For instance, intracameral injections are used to provide higher levels of drug to the anterior segment. This treatment is attractive when patient compliance for eye drops instillation is low. Additionally, systemic side effects are decreased. Intravitreal injections are targeted to the vitreous humor and are used to treat posterior segment conditions. Even though intravitreal injections provide more localized delivery, they still have disadvantages of cataract formation, hemorrhage, retinal detachment, poor patient compliance, and repeat injection is necessary (Bochot & Fattal, 2012; Geroski & Edelhauser, 2000). Periocular delivery is less

invasive compared to intravitreal injections as the drug can reach the posterior segment via subconjunctival, subtenon and retrobulbar injections (Gaudana et al., 2010). Subconjunctival injectables provides sustained release to both posterior and anterior segments of the eye; however, the circulation in surrounding tissues can decrease the ocular bioavailability to the targeted location. Subtenon injections result in high drug levels in the vitreous but can result in subconjunctival hemorrhaging and chemosis. Retrobulbar administration yields enhanced local doses of anesthetics but can lead to respiratory arrest.

Drug delivery to the eye is a very challenging field as a number of static and dynamic barriers exist. No single drug delivery system is capable of avoiding all of the barriers presented by the eye; however, each system has specific benefits over other systems.

2.4 Ophthalmic Drug Delivery Systems

The types of ophthalmic drug delivery systems range from the traditional topical formulations to controlled release implants. Each type of ocular drug delivery system is sterile and has benefits towards specific types of conditions. Furthermore, each system has individual advantages as well as disadvantages. The remainder of this chapter will discuss the specific benefits and drawbacks of conventional ocular formulations along with the various routes of administration.

2.4.1 Conventional Ophthalmic Delivery Systems

Eye drop formulations include solutions, suspensions, ointments, emulsions, and gels; with eye drops making up 90% of marketed ophthalmic formulations (Le Bourlais et al., 1998). The remaining 10% includes: injectable, ocular inserts and oral products(Lang, 1995). All of the liquid formulations are advantageous due to the ease of administration, rapid absorption, long shelf life, better patient compliance, and lower visual and systemic side effects. However, only ~20% of the formulation is retained in the conjunctival sac after instillation due to increased lacrimation

and reflex blinking(Schoenwald, 1990). This means that the remainder of the drug is spilled from the eye, absorbed through the lymphatic system or drained through the nasolacrimal tract. The rate at which a drug is absorbed or drained from the eye depends on the dosage form.

2.4.1.1 Solutions & Suspensions

Suspensions and solutions are both easy to administer; however, suspensions contain dispersed insoluble drug particles that lead to irritation and increased lacrimation upon instillation. The lacrimation increases tear turnover rate and decreases the amount of time that the drug has to permeate the cornea or sclera. Solutions are the most desirable topical formulation as they don't cause irritation since the drug is completely solubilized. Permeation enhancers can be added to the formulations to improve permeation through the ocular tissues, while viscosity enhancers can be added to improve the retention on the ocular surface (Keister, Cooper, Missel, Lang, & Hager, 1991). Furthermore, cyclodextrins can be implemented to transform a suspension into a solution (Loftssona & Jarvinen, 1999). Overall, solutions and suspensions are the patient-preferred products; however, the disadvantage of decreased residence time and low permeation are still prevalent. Current commercial examples of solutions are Visine® and Xiidra®, while commercial suspension examples include: TobraDex® and Besivance®.

2.4.1.2 Emulsions, Ointments & Gels

Emulsions formulations for ophthalmic delivery offer prolonged drug release, improved solubility and bioavailability (Vandamme, 2002). Oil in water (o/w) emulsions are commonly preferred for ocular purposes due to less irritation and higher ocular tolerance. Restasise™ and AzaSite® are examples of ophthalmic o/w emulsions. Studies have demonstrated that emulsions lead to increased precorneal residence time.

Ointments and gels have an increased residence time in the eye due to the higher viscosity of the vehicle; however, this can lead to blurred vision and matting of the eyelids (Sasaki et al., 1999). Ointments are a mixture of both solid and semisolid paraffin wax, which melts upon instillation in the eye due to the temperature increase. Contrarily, ophthalmic gels are formulated using hydrophilic polymers that can either remain a gel or form stimuli-responsive gels. Stimuli-responsive gels are liquid in a normal environment and transform into a gel upon instillation in the eye, this is termed *in-situ* gelation (Makwana, Patel, & Parmar, 2016). Environmental stimuli can be physical (light and temperature), chemical (pH, redox potential, electrolyte) or biological (enzymes). The gels remain in the conjunctival sac allowing for slow release of the drug to the ocular surface. *In-situ* gels are beneficial because it combines the benefits of both solutions and ointments: easy administration at room temperature and longer residence time once instilled in the eye (Al-Kinani et al., 2017).

2.4.1.3 Ocular Inserts

Ocular inserts are sterile products that allow for increased residence and sustained release of the drug to the ocular surface, typically used to treat dry eye syndrome and keratitis sicca. There is a plethora of types of ocular inserts and the mechanism of release is dependent upon the solubility of the insert. Ocular inserts provide accurate dosing, reduction of systematic absorption and increased patient compliance. However, ocular inserts have the following disadvantages: foreign object sensation felt by patients, movement in the eye, vision interference and the insert can be lost unintentionally (Kumari, Sharma, Garg, & Garg, 2010). Ophthalmic inserts can be categorized into three main groups: insoluble, bioerodible and soluble. Insoluble inserts are further divided into three subcategories: osmotic, diffusion and contact lenses. Diffusion inserts are composed of a drug reservoir and a semi-permeable membrane. Lachrymal fluid penetrates the membrane leading to diffusion of the drug through the membrane. Osmotic inserts can contain a single drug

reservoir with (or without) an osmotic solute dispersed in a polymer matrix. Conversely, the insert can contain two separate compartments: one containing the drug and the second containing the osmotic solute. Contact lenses are made of either a hydrophobic or hydrophilic polymeric matrix capable of retaining aqueous or solid drug components (Gulsen & Chauhan, 2004). After instillation the drug release is rapid, followed by a slow decline in release rate (Lee & Robinson, 1986). Soluble inserts are made from either natural, synthetic or semi-synthetic polymers; therefore, they dissolve upon interaction with the tear fluid and do not need to be removed. Bioerodible ocular inserts consist of hydrophobic bioerodible polymers, that slowly erodes upon mixing with the tear fluid to slowly release drug. Examples of commercial ocular inserts are Ocusert®, Ocufit® SR, and Minidisc® (Yasukawa, Ogura, Kimura, Sakurai, & Tabata, 2006).

2.5 Conclusions

The eye is a very complex organ that can become stricken by a number of illnesses. In order to successfully deliver drugs and treat conditions, the proper dosage form and route of administration must be determined. Each conventional dosage form has specific advantages; however, a number of static and dynamic barriers still exist. Therefore, it is imperative to explore different routes of administration and alternative ways to enhance ophthalmic formulations. This dissertation will focus on the improvement of ophthalmic drug delivery using cyclodextrins and polymers. Chapters 3-6 will cover the formulation of novel ophthalmic drug delivery systems. Chapter 3 discusses the solubility improvement of a common ocular NSAID, nepafenac by complexing with HPBCD. This complexation was then formulated into an in-situ gel system for the improved residence time of nepafenac on the ocular surface, the preparation of this formulation is discussed in Chapter 4. Chapter 5 focuses on the complexation of HPBCD with the corticosteroid, difluprednate. Chapter 6 describes the use of PLGA biodegradable microneedles to delivery difluprednate to the posterior segment of the eye.

2.6 References

Al-Kinani, A. A., Zidan, G., Elsaid, N., Seyfoddin, A., Alani, A. W. G., & Alany, R. G. (2017). Ophthalmic gels: Past, present and future. *Adv Drug Deliv Rev*. doi:10.1016/j.addr.2017.12.017

Barar, J., Javadzadeh, A. R., & Omidi, Y. (2008). Ocular novel drug delivery: impacts of membranes and barriers. *Expert Opinion on Drug Delivery, 5*(5), 567-581. doi:10.1517/17425240802095061

Bochot, A., & Fattal, E. (2012). Liposomes for intravitreal drug delivery: a state of the art. *J Control Release, 161*(2), 628-634. doi:10.1016/j.jconrel.2012.01.019

College, W. C. M. (2018). Corneal and Anterior Segment Diseases. Retrieved from http://weillcornelleye.org/services/corneal_diseases.html

Gaudana, R., Ananthula, H. K., Parenky, A., & Mitra, A. K. (2010). Ocular drug delivery. *AAPS J, 12*(3), 348-360. doi:10.1208/s12248-010-9183-3

Geroski, D. H., & Edelhauser, H. F. (2000). Drug delivery for posterior segment eye disease. *Invest Ophthalmol Vis Sci, 41*(5), 961-964.

Gulsen, D., & Chauhan, A. (2004). Ophthalmic drug delivery through contact lenses. *Investigative Ophthalmology & Visual Science, 45*(7), 2342-2347. doi:10.1167/iovs.03-0959

Keister, J. C., Cooper, E. R., Missel, P. J., Lang, J. C., & Hager, D. F. (1991). Limits on Optimizing Ocular Drug Delivery. *Journal of Pharmaceutical Sciences, 80*(1), 50-53. doi:DOI 10.1002/jps.2600800113

Kim, S. H., Lutz, R. J., Wang, N. S., & Robinson, M. R. (2007). Transport barriers in transscleral drug delivery for retinal diseases. *Ophthalmic Res, 39*(5), 244-254. doi:10.1159/000108117

Kumari, A., Sharma, P. K., Garg, V. K., & Garg, G. (2010). Ocular inserts - Advancement in therapy of eye diseases. *J Adv Pharm Technol Res, 1*(3), 291-296. doi:10.4103/0110-5558.72419

Lang, J. C. (1995). Ocular Drug-Delivery Conventional Ocular Formulations. *Advanced Drug Delivery Reviews, 16*(1), 39-43. doi:Doi 10.1016/0169-409x(95)00012-V

Le Bourlais, C., Acar, L., Zia, H., Sado, P. A., Needham, T., & Leverge, R. (1998). Ophthalmic drug delivery systems - Recent advances. *Progress in Retinal and Eye Research, 17*(1), 33-58. doi:Doi 10.1016/S1350-9462(97)00002-5

Lee, V. H., & Robinson, J. R. (1986). Topical ocular drug delivery: recent developments and future challenges. *J Ocul Pharmacol, 2*(1), 67-108.

Loftssona, T., & Jarvinen, T. (1999). Cyclodextrins in ophthalmic drug delivery. *Advanced Drug Delivery Reviews, 36*(1), 59-79. doi:Doi 10.1016/S0169-409x(98)00055-6

Makwana, S. B., Patel, V. A., & Parmar, S. J. (2016). Development and characterization of in-situ gel for ophthalmic formulation containing ciprofloxacin hydrochloride. *Results Pharma Sci, 6*, 1-6. doi:10.1016/j.rinphs.2015.06.001

Patel, A., Cholkar, K., Agrahari, V., & Mitra, A. K. (2013). Ocular drug delivery systems: An overview. *World J Pharmacol, 2*(2), 47-64. doi:10.5497/wjp.v2.i2.47

Pitkanen, L., Ranta, V. P., Moilanen, H., & Urtti, A. (2005). Permeability of retinal pigment epithelium: Effects of permeant molecular weight and lipophilicity. *Investigative Ophthalmology & Visual Science, 46*(2), 641-646. doi:10.1167/iovs.04-1051

Sasaki, H., Yamamura, K., Mukai, T., Nishida, K., Nakamura, J., Nakashima, M., & Ichikawa, M. (1999). Enhancement of ocular drug penetration. *Critical Reviews in Therapeutic Drug Carrier Systems, 16*(1), 85-146.

Schoenwald, R. D. (1990). Ocular drug delivery. Pharmacokinetic considerations. *Clin Pharmacokinet, 18*(4), 255-269.

Vandamme, T. F. (2002). Microemulsions as ocular drug delivery systems: recent developments and future challenges. *Progress in Retinal and Eye Research, 21*(1), 15-34. doi:Pii S1350-9462(01)00017-9

Doi 10.1016/S1350-9462(01)00017-9

Yasukawa, T., Ogura, Y., Kimura, H., Sakurai, E., & Tabata, Y. (2006). Drug delivery from ocular implants. *Expert Opin Drug Deliv, 3*(2), 261-273. doi:10.1517/17425247.3.2.261

Zinn, K. M., & Mockel-Pohl, S. (1973). Fine structure and function of ocular tissues. The cornea and sclera. *Int Ophthalmol Clin, 13*(3), 93-107.

Chapter 3. Improved Ocular Delivery of Nepafenac by Cyclodextrin Complexation

In part: Shelley, H., Grant, M., Smith, F.T. et al. AAPS PharmSciTech (2018). https://doi.org/10.1208/s12249-018-1094-0

3.1 Abstract

Nepafenac is a nonsteroidal anti-inflammatory drug (NSAID), currently only available as 0.1% ophthalmic suspension (Nevanac®). This study utilized hydroxypropyl-β-cyclodextrin (HPBCD) to increase the water solubility and transcorneal permeation of nepafenac. The nepafenac-HPBCD complexation in the liquid and solid states were confirmed by phase solubility, differential scanning calorimetry (DSC), X-ray diffraction (XRD), Fourier transform infrared spectroscopy (FTIR) and nuclear magnetic resonance spectroscopy (NMR) analyses. Nepafenac 0.1% ophthalmic solution was formulated using HPBCD (same pH and osmolality as that of Nevanac®) and pig eye trans-corneal permeation was studied versus Nevanac®. Furthermore, nepafenac content in cornea, sclera, iris, lens, aqueous humor, choroid, ciliary body, retina, and aqueous humor was studied in a continuous isolated pig eye perfusion model in comparison to suspension and Nevanac®. Permeation studies using porcine corneas revealed that the solution formulation had a permeation rate 18 times higher than Nevanac®. Furthermore, the solution had 11 times higher corneal retention than Nevanac®. Drug distribution studies using porcine eyes revealed that the solution formulation enables detectable levels in various ocular tissues while the drug was undetectable by Nevanac®. The ocular solution formulation has a significantly higher drug concentration in the cornea compared to the suspension or Nevanac®.

3.2 Introduction

Nepafenac is a COX-1 and COX-2 inhibiting non-steroidal anti-inflammatory drug (NSAID). It is commonly used to treat post-operative pain and inflammation in the cornea, following ocular procedures such as Lasik and cataracts surgery (Ahuja, Dhake, Sharma, & Majumdar, 2008; Gaynes & Onyekwuluje, 2008; Jones & Neville, 2013). It is a prodrug and it is rapidly metabolized to amfenac by intraocular hydrolases after its corneal permeation. Compared to other ocular NSAIDs, such as bromfenac and ketorolac, nepafenac has a higher permeation rate and faster onset of action (Walters, Raizman, Ernest, Gayton, & Lehmann, 2007).

Currently, the only commercial available dosage form of nepafenac is a suspension, Nevanac 0.1% ®. This is due to the low water solubility of the nepafenac, 0.0197 mg/mL. Suspension formulation has the disadvantage that it causes blurred vision, foreign particle sensation and may cause irritation of the eye; ointments and gels may cause similar problems (Patel, Cholkar, Agrahari, & Mitra, 2013). The irritation may leads to increased lacrimation causing the drug to be removed from the eye. This rapid removal of the formulation limits the residence time of the drug, thereby decreasing the ability of the drug to penetrate the cornea. Additionally, the tear fluid volume only holds 7-10µL, while a formulation droplet contains 50-100µL (Saettone, 2002). The formulation that exceeds the tear volume is removed by either spillage, lacrimation, or adsorption into the conjunctiva (which then enters the systemic circulation) (Pharmacy). Therefore, a huge problem is that less than 10% of the drug is absorbed into the eye; this is wasteful of the drug and not cost effective. The amount of drug capable of permeating the cornea is proportional to the soluble fraction of drug. Therefore, in the case of suspensions, the permeation could be lower when compared to solutions due to the low fraction of soluble drug; even though suspensions have proven to be superior in precorneal residence time compared to solutions (Sieg & Robinson, 1975). Additionally, solution formulations are widely accepted by patients due to ease of

application and low irritation effects; thus, creating a nepafenac solution may be beneficial in terms of enhanced permeation and patient acceptance (Duong, Westfield, & Chalkley, 2007).

Cyclodextrins are cone-shaped, cyclic oligosaccharides with a hydrophobic core and a hydrophilic shell; therefore, these molecules are ideal for encapsulating and increasing the water solubility, stability, dissolution rate, and bioavailability for a variety of guest molecules (Bekers, Uijtendaal, Beijnen, Bult, & Underberg, 1991). When cyclodextrins are combined with a lipophilic drug in an aqueous environment several water molecules are released from the hydrophobic cyclodextrin core, this is said to be the driving force of the complexation (Liu & Guo, 2002). Next, the water-fearing drug seeks refuge from the aqueous environment by entering the hydrophobic core of the cyclodextrin (Del Valle, 2004). This complexation gives the drug a hydrophilic shell, without altering the molecular structure or drug properties (Sahoo, Diinawaz, & Krishnakumar, 2008). For successful delivery to the corneal surface the drug must possess both hydrophilic and lipophilic properties, so that it can pass through the tear film, which consists of both lipid and aqueous layers. By complexing the drug with cyclodextrin, the drug has both hydrophobic (core drug) and hydrophilic (outer CD shell) properties (Loftsson & Stefansson, 1997). Cyclodextrins have been shown to enhance permeation of lipophilic drugs for improved delivery through the tear film, which can lead to higher bioavailability at the ocular epithelium (Loftsson & Stefansson, 2007; Tiwari, Tiwari, & Rai, 2010; Uekama, 2004). Furthermore, cyclodextrins alter the biological membrane by interacting with the membrane, unlike traditional penetration enhancers which disrupt the ocular barrier (Challa, Ahuja, Ali, & Khar, 2005; Tiwari et al., 2010). Hydroxypropyl-β-cyclodextrin (HPBCD) is a more water-soluble derivative of the parent molecule, β-cyclodextrin (18mg/mL), with a water solubility of more than 500 mg/mL. It has been suggested that when applied to the eye, HPBCD does not pass through the corneal epithelium because the ocular membrane has low affinity for the hydrophilic cyclodextrin; therefore, the cyclodextrin remains in the tear film while the drug partitions into the eye (Loftsson & Stefansson, 1997). After the formulation is

administered to the eye, the cyclodextrin inevitably ends up in the gastrointestinal tract via the nasolacrimal duct. However, no gastrointestinal damage is experienced as the normal usage of HPBCD is less than 1/10th of the toxic level (1.7mg/kg/day) (Loftssona & Jarvinen, 1999). Additionally, studies conducted on rabbits showed that HPBCD was well tolerated and nontoxic up to a concentration of 45% (Jansen T, 1990; Jonathan C. Javitt, 1994). Nepafenac can be encapsulated within the hydrophobic HPBCD core, thereby increasing the water solubility of the drug leading to a solution formulation. The complex allows the cyclodextrin to carry the drug across through the lipid, aqueous and mucin layers of the tear fluid to the lipophilic corneal epithelium. The objective of this work is to improve the water solubility and subsequent ocular bioavailability of nepafenac by complexation with HPBCD to produce a solution formulation. The solutions are widely accepted for ocular use based on their clarity and lack of particulate irritation of a suspension. By formulating nepafenac into a solution, we can overcome the disadvantages of currently marketed suspension formulation, Nevanac®. In addition, we performed ocular perfusion studies in porcine eyes to determine the drug distribution in various ocular tissues, in comparison to suspension and Nevanac® formulations. Due to the difficulty of obtaining human corneas, porcine corneas have been used in lieu of human corneas. Porcine eyes are comparable to the tensile strength and stress-strain curve of human eyes; therefore, are considered a suitable alternative (Zeng, Yang, Huang, Lee, & Lee, 2001).

3.3 Experimental Methods

3.3.1 Materials

Nepafenac raw material was purchased from Hangzhou Yuhao Chemical Technology Co., Ltd. Trappsol hydroxypropyl-β-cyclodextrin was obtained from CTD Holdings, Inc. Sodium Chloride and Ethyl Alcohol (100%) was purchased from Letco Medical. Methocel E15 Premium LV Hydroxypropyl methylcellulose (HPMC) was obtained from Dow Chemical Company.

Benzalkonium Chloride (BKC) was purchased from Spectrum Chemical Mfg. Corp. The D_2O used was 99.9% NMR grade, purchased from Merck, Switzerland. All solvents used for high performance liquid chromatography (HPLC) were of analytical or HPLC grade.

3.3.2 Preparation of the Nepafenac/ HPBCD Mixtures

3.3.2.1 Dry Mixture (DM)

The dry mixture (DM) of nepafenac and HPBCD was prepared by gently mixing equimolar (0.2 mM) amounts of drug and HPBCD with a mortar and pestle until a homogenous mixture was produced. The mixture was then stored in a glass vial on the benchtop until needed for analysis.

3.3.2.2 Kneaded Mixture (KM)

The kneaded mixture (KM) of nepafenac and HPBCD was prepared by adding 50:50 methanol:H_2O dropwise to an equimolar mixture of drug and HPBCD until a homogenous paste is formed. The mixture is then left in a desiccator overnight until a dry mixture is obtained; the subsequent mixture was stored in a glass vial on the benchtop until needed for analysis.

3.3.2.3 Freeze Dried Mixture (FD)

Nepafenac was dissolved in acetonitrile and added to an aqueous solution of HPBCD at a molar ratio of 1:1. The solution was kept in a freezer for two days at -80°C. Once the solution was frozen it was subjected to freeze-drying in a Labconco Freezone 4.5 with a Welch 8917 vacuum pump, until a dry fluffy mixture was obtained (approximately 24 hours). The freeze-dried mixture (FD) was then stored in a glass vial on the benchtop until needed for analysis.

3.3.2.4 Rotary Evaporation Mixture (RM)

HPBCD was added to a solution of Nepafenac in methanol at a molar ratio of 1:1. The solution was then placed on Buchi Rotovapor R-210 for 30 minutes at 40°C in complete vacuum. Once

the methanol had evaporated completely, the mixture was placed in the desiccator for 24 hours until a dry flaky mixture was obtained.

3.3.3 Phase Solubility Studies

Phase solubility studies on nepafenac with HPBCD were performed according to Higutchi and Connors (Higuchi, 1965). Increasing molar concentrations (10, 20, 50, 100, 150, 200, 250 mM) of HPBCD were dissolved in 1mL of water using 5mL polypropylene tubes. Excess amounts of nepafenac (above the solubility limit) were added to the HPBCD solutions and then sonicated for 30 minutes. The mixtures were then placed on a magnetic stirrer and stirred for 24 hours. The mixtures were then left on the benchtop for 24 hours for equilibration. Following equilibration, the mixtures were filtered using 0.45 micron nylon membrane filter, diluted appropriately and analyzed for nepafenac concentration by HPLC.

The complexation efficiency (CE), which reveals the ratio of HPBCD to nepafenac, can be calculated by the following equation (Eleamen et al., 2017):

$$CE = \frac{slope}{1-slope} \qquad \text{Eq.1}$$

Using Eq. 1, the affinity constant (K) between HPBCD and nepafenac was calculated based on the data provided by the phase solubility results:

$$K = \frac{CE}{S_o} \qquad \text{Eq. 2}$$

where S_o is the solubility of free nepafenac in water, without the addition of HPBCD. Furthermore, the change in Gibbs free energy was calculated:

$$\Delta G = -RTlnK \qquad \text{Eq. 3}$$

where R is the ideal gas constant (8.314 J/molK) and T is the temperature (295 K).

3.3.4 High Performance Liquid Chromatography (HPLC) Analysis

An Alliance Waters e2695 Separations Module and a Waters 2998 Photodiode Array Detector was used for the nepafenac analysis. A Kinetix C18 5µm, 150mm x 4.60mm reversed-phase HPLC column was employed for nepafenac analysis. The mobile phase consisted of 40:60 acetonitrile: water. Samples were eluted at a flow rate of 1mL/min at ambient temperature. The absorbance wavelength set at 254nm, with an injection volume of 10 µL.

3.3.5 Characterization of Nepafenac/HPBCD Complex

3.3.5.1 Differential Scanning Calorimetry (DSC)

DSC analysis of nepafenac, HPBCD and various mixtures (DM, KM, FD and RM) were performed using 2910 differential scanning calorimeter (TA Instruments). Samples were weighed (~10 mg) and placed in a non-hermetic aluminum pans and sealed with an encapsulating press. The samples were heated under an inert atmosphere of nitrogen with a temperature range of 30-220°C with a scanning rate of 10°C/min. Empty aluminum pans were used as a reference.

3.3.5.2 X-Ray Diffraction (XRD)

X-Ray Diffraction of nepafenac, HPBCD and various mixtures (DM, KM, FD, RM) were performed using a Bruker D-8 x-ray diffractometer. The samples were exposed to copper Kα radiation honed through a 1.0mm slit, voltage: 40kV, current: 40Ma, 2θ range: 0-60.

3.3.5.3 Molecular Docking

The Surflex Dock program, along with the Sybyl-X 1.3 package was used to estimate the molecular interactions between HPBCD and nepafenac prior to NMR studies. Nepafenac and HPBCD were prepared using the sketch function in Sybyl and both molecules were minimized using the Tripos force field. HPBCD was solvated using the solvate function in Sybyl and water

molecules within the HPBCD cavity were eliminated to allow nepafenac to bind. The solvated structure was then used to create the protomol with the threshold set to 0.42 and the bloat equal to one.

3.3.5.4 ^{1}H-NMR Spectroscopy

^{1}H-NMR spectra for nepafenac, HPBCD, and RM were recorded using a Varian 400 MHz Premium Shielded NMR. Nepafenac was heated to 40°C in D_2O, while the HPBCD and RM complex was analyzed unheated in D_2O.

3.3.5.5 Fourier Transform Infrared Spectroscopy (FT-IR)

FT-IR spectra for nepafenac, HPBCD, and various mixtures (DM, KM, FD, and RM) were recorded using a Perkin Elmer Spectrum 400 FT-IR/FT-NIR Spectrophotometer with a resolution of 4cm^{-1} and the detector scanned a range from 4000 cm^{-1}-650 cm^{-1}.

2.3.6 Ex-vivo Corneal Permeation Experiments

3.3.6.1 Corneal Excision

Porcine eyes were obtained from Auburn University Lambert-Powell Meats Laboratory (Auburn University, Auburn AL) and stored in 4°C until needed for the experiment. The animals were sacrificed according to the Institutional Animal Care and Use Committee (IACUC) approved protocol (SOP 2015-2727). The excess tissue was first cut from the globe and the corneas were excised from the globe using a 3.0mm slit eagle blade to create an insertion point between the iris and the cornea. Corneal scissors were used to excise the cornea and the corneas were rinsed with tap water and then placed in phosphate buffered saline (PBS) at pH=7.4 until used in the permeation studies. The permeation studies began within 2 hours of excision.

3.3.6.2 Corneal Permeation Study

Franz Diffusion Cell apparatus was assembled to hold the cornea in position during the permeation experiments. The following formulations were tested: nepafenac solution, nepafenac suspension, and Nevanac®. Nepafenac solution was prepared to contain 0.1% nepafenac, 6.05% HPBCD, 0.5% hydroxypropyl methylcellulose E15, 0.76% sodium chloride, 1.4% ethanol, 0.005% of a 0.25% benzalkonium chloride solution and water. The nepafenac suspension was prepared to contain 0.1% nepafenac, 0.5% hydroxypropyl methylcellulose E15, 0.76% sodium chloride, 1.4% ethanol, 0.005% of a 0.25% benzalkonium chloride solution and water. Osmolality of both the solution and suspension formulations was adjusted similar to lachrymal secretions. Each formulation was tested in 4 replicate permeation experiments. The receptor cell was filled with 5 mL PBS buffer (pH 7.4) containing 10% ethanol (to maintain sink conditions). Nepafenac has a solubility of 0.925 µg/mL in PBS (pH=7.4), which was increased by 35 fold due to inclusion of 10% ethanol. Studies have shown that corneal cell viability is not harmed at an ethanol concentration of 10% (Chen, Chang, Lee, Javier, & Azar, 2002). The corneas were placed on the receptor cell with the outer surface of the cornea facing up, the donor cell was placed on top of the cornea and both half cells were clamped together. The donor cell was filled with 0.5mL of the formulation and covered with Parafilm®. The receptor cell was sampled (1 mL) at 1, 2, 4, 6, 8, 12, and 24 h, and replenished with fresh PBS buffer (pH 7.4) containing 10% ethanol. The samples were assayed by HPLC method as described earlier.

3.3.6.3 Extraction of Nepafenac from Corneas

Following the 24-hour permeation study, the formulation was removed from the donor chamber using a dropper pipette, and the cornea was cleaned with PBS buffer (pH 7.4) containing 10% ethanol using cotton swabs. The active diffusion area of the cornea was cut, weighed, minced and placed in individual vials with 2mL of the HPLC mobile phase (acetonitrile: water 60:40). The vials were then sonicated for 30 minutes, and left to sit for 24 hours at 4^{o}C to extract any drug that

is retained in the cornea. The vials were sonicated again for 30 minutes and then the supernatant was filtered through 0.45 µm Nylon membrane filter and assayed by HPLC.

3.3.7 Ocular Distribution of Nepafenac in Isolated Perfused Eyes

Porcine eyes of either sex were freshly obtained from Lambert-Powell Meats Laboratory (Auburn University, Auburn AL) immediately following euthanasia. The animals were sacrificed according to the Institutional Animal Care and Use Committee (IACUC) approved protocol (SOP 2015-2727). All eyes were used within 4 hours of euthanasia to maintain the integrity of the entire globe. The excess adnexal tissue was trimmed from the ocular globe and placed in PBS pH 7.4 until ready for perfusion (Abarca, Salmon, & Gilger, 2013). The eyes were perfused with Dulbecco's Modified Eagle's Medium F12 (DMEM) under constant oxygen O_2 supply. The perfusion was started 30 minutes prior to the drug application and throughout the entirety of the study. A major artery of each eye was identified, split open with a 3.0 mm slit Eagle blade, cannulated and secured in place with Scotch® super glue gel. The eyes were then placed in a stainless-steel strainer on top of a beaker, which allowed for the collection of the DMEM medium from the veins. An Ismatec® peristaltic pump (Cole-Parmer GmbH, Wertheim, Germany) was employed to run the oxygenated DMEM through the cannulated eyes (Figure 3.1). As previously described, perfusion was started at a flow rate 0.25–0.8 mL/min and increased to 1.04 ml /min (Abarca et al., 2013; Mains, Tan, Wilson, & Urquhart, 2012). Adequate arterial perfusion was determined by observing flow of media exiting vortex veins. The following formulations were tested: nepafenac solution, nepafenac suspension, and Nevanac®. 50 µL of the solution, suspension, or commercial product was pipetted onto each of the corneas every 15 minutes for one hour. After one hour, the eyes were frozen instantly using CO_2 and then stored in a freezer at -80°C to prevent transfer of drug between tissues until needed for dissection. For dissection, the frozen eye was placed on a cold ceramic tile and all the ocular tissues were subsequently removed: cornea, aqueous humour,

lens, iris, ciliary body, vitreous humor, sclera, retina and choroid. Each tissue was soaked in 40:60 acetonitrile:water for 24 hours in individual vials, then filtered with 0.45 µm Nylon membrane filters and analyzed via HPLC. The entire ocular distribution experimentation was repeated on all three formulations for a period of 2 hours. At the end of 2 hours, the eyes were frozen instantly as described under 1 hour experiment, ocular tissues were subsequently collected, drug was extracted and assayed as described earlier.

3.3.7 Statistical Analysis

All results are presented as mean ± standard error of mean (SEM). The calibration curve for nepafenac was tested over the following concentration range: 20-400µg/mL (slope: y=29281x; R=0.9998). The cumulative amount of drug permeated through unit area of cornea was plotted as a function of time. The steady state flux ($\mu g/cm^2/h$) was derived by performing linear regression on the cumulative corneal permeation amount ($\mu g/cm^2$) versus time (h). The amount of drug (mg) retained in the cornea was normalized to 1 gram of cornea. Analysis of variance was performed to determine the level of significance between the means. Mean differences with $P < 0.05$ were significant. Statistical analysis was performed using GraphPad Prism for Windows, GraphPad Software, La Jolla California USA.

3.4. Results & Discussion

3.4.1 Phase Solubility Studies

The phase solubility studies indicate a linear (A_L) type phase diagram and 1:1 complex (Figure 3.2), meaning one HPBCD molecule is needed to complex one nepafenac molecule. The stability rate constants 3665 M^{-1} and 4296M^{-1}, respectively, for water and PBS, indicative of strong association between Nepafenac and HPBCD (Bramhane et al., 2016; Liao et al., 2016). The change in Gibbs free energy, ΔG, values were -20.45 kJ/mol and -20.06 kJ/mol, respectively for

water and PBS, the negative value is indicative of a spontaneous complex formation (Tang et al., 2015).

3.4.2 Characterization of Nepafenac/HPBCD Complex in the solid state

The solid state characterization of nepafenac-HPBCD complex would be very helpful to understand the physico-chemical interactions between the drug and CD, and if the drug in the form of an inclusion complex would remain stable in the formulation. The DM, KM would serve as controls for comparing the physical and chemical interactions to the complex formation by the FD and RM (Liu & Guo, 2002).

3.4.2.1 Differential Scanning Calorimetry (DSC)

The sharp endothermic peak at 187°C in nepafenac represents its melting point (Figure 3.3A). On the contrary, HPBCD displays a broad endothermic peak between 40-100°C which is indicative of the loss of water molecules from the cyclodextrin (Oprean et al., 2016; Tang, Tang, et al., 2016). The dry and kneaded mixtures of nepafenac and HPBCD show the two original profiles superimposed upon one another, meaning there was no interaction between HPBCD and nepafenac (Tang, Ma, et al., 2016). This can be explained by the fact that in order for a complexation to occur between nepafenac and HPBCD some water must be included to initiate complexation (Alves-Silva, Sa-Barreto, Lima, & Cunha-Filho, 2014). The nepafenac melting peak has almost completely disappeared in the freeze-dried mixture and is completely absent in the rotovap mixture. The results for both mixtures indicate a new solid state exists due to formation of an inclusion complex. Incomplete complexation in the FD may be due to the affinity of the HPBCD for the higher polarity mixture (acetonitrile/water) over methanol and the low temperature of the freeze-drying process.

3.4.2.2 X-Ray Diffraction (XRD)

The powder XRD data is shown in Figure 3.3B. Nepafenac (1) displays crystalline properties, which is known by the distinctive sharp diffraction peaks (Alonso et al., 2016; Oprean et al., 2016). HPBCD (2) is well known as an amorphous solid hence showed no diffraction peaks. For the freeze-dried and rotovap mixtures (5, 6), the XRD profile shows only amorphous characteristics, meaning the nepafenac is encapsulated within the HPBCD. This is not seen in the dry or kneaded mixtures (3, 4), the two characteristics (crystalline and amorphous) seem to be superimposed upon one another, indicating complexation has not occurred (Braga et al., 2016).

3.4.2.3 Molecular Docking

The molecular docking software predicted that the left terminal side of the nepafenac, including the far-left aromatic phenyl ring and half of the middle aromatic ring, would be encapsulated in the hydrophobic core of the HPBCD (Figure 3.4). This can be explained by the fact that the left side of nepafenac is more nonpolar; therefore, it shields itself from the aqueous environment in the hydrophobic core. The right side consists of more hydrophilic components: amino substituted ring and amide-containing side chain, which is why it is exposed to the aqueous environment. Molecular docking has been applied to other experiments to show the orientation of complexation with HPBCD (Liao et al., 2016; Matencio, Hernandez-Gil, Garcia-Carmona, & Lopez-Nicolas, 2017; Zhang, Liu, Yang, Chen, & Jiao, 2017).

3.4.2.4 ^{1}H-NMR Spectroscopy

Proton NMR revealed that the first aromatic ring of nepafenac is completely encapsulated in the HPBCD core (Figure 3.5). The first aromatic ring is shown by the two peaks (labelled ‘1’, Figure 3.5) where the 5 protons are distributed: with the three ‘a’ protons in the first peak and the two ‘b’ protons in the second peak. In the rotovap mixture, the first peak partially merges into the second peak, but when this peak shifts it leaves a proton behind forming a new peak, so now the first peak at 7.6 has 1 proton and the second peak at 7.45 has 4 protons. These shifts are all due to

change of the environment caused by the interactions with the cyclodextrin, suggesting this entire aromatic ring is caged by HPBCD. Hydrogen ‘e’ shifts from 7.308 to 7.123 indicative of a major change in the environment, while hydrogen ‘f’ shifts less (6.662 to 6.617), indicative of a weaker influence by HPBCD. Additionally, hydrogen g shifts from 7.315 to 7.364, suggesting as weak complexation.

3.4.2.5 Fourier transform infrared spectroscopy (FT-IR)

The infrared spectrum from FT-IR for nepafenac, HPBCD, dry, kneaded, freeze-dried, and rotovap mixtures are shown in Figure 3.6. The O-H stretching vibration of HPBCD is displayed in the peaks 3600-3000 cm^{-1}, while the C-H stretching vibration is shown in the 3021-2783cm^{-1} and the sharp peak at 1021.62cm^{-1} is C-O stretching vibration (Wei et al., 2017). Nepafenac has characteristic N-H peaks at 3437.97 and 3316.45 cm^{-1}, with a carbon peak at 1673.87 cm^{-1}. Additionally, the C-N stretch of the aliphatic amine is at 1236.51, with the N-H bend from the primary amine at 1552 cm^{-1}. For the secondary amine, the C-N stretch of aromatic amine is located at 1282.02 and 1330.05 cm^{-1} ("IR Spectroscopy Tutorials: Amines ")("IR Spectroscopy Tutorials: Amines ")("IR Spectroscopy Tutorials: Amines ")("IR Spectroscopy Tutorials: Amines ")("IR Spectroscopy Tutorials: Amines "). Based on the docking experiment, it is evident that a portion of nepafenac is lodged HPBCD core, meaning the secondary amine is completely complexed, while the primary amine portion is not as complexed. This is evident by the larger decrease in peak size of the secondary amine (1282.02 & 1332.58 cm^{-1}) compared to the primary amine (1552.52 cm^{-1}), since cyclodextrin is strongly complexed with the benzene ring portion it is blocking transmission signals in the mixtures.

3.4.3 Corneal Permeation

Studies have shown that the epithelial barrier of the cornea maintains integrity up to 6 hours; however, we conducted the study for 24 hours to see if there was a presence of a linearity in the

permeation rate (Abarca, Cuming, Duran, & Ramapuram, 2015). The permeation profiles of nepafenac solution and the two suspension formulations across isolated porcine corneas are presented in Figure 3.7. The solution has achieved enhanced permeation as compared to suspension and commercial product. The HPBCD: nepafenac complexation increased the water solubility of the drug, leading to increased permeability through ocular tissues. The flux across the cornea for the solution was 5 and 18 times higher than the suspension (without HPBCD) and Nevanac®, respectively ($p<0.001$). Additionally, the amount of nepafenac retained in the cornea (µg /g) was 4 and 11 times higher than the suspension and Nevanac® formulations, respectively.

3.4.4 Distribution of Nepafenac in Isolated Perfused Eyes

Isolated perfused eye studies mimic in vivo conditions such as tissue viability, temperature and circulation in the eye, which enable us to determine drug distribution in the ocular tissues following topical application (Abarca et al., 2013). Nepafenac is commonly used to treat pain and inflammation in the anterior segment of the eye such as the cornea, sclera, iris, and ciliary body (Walters et al., 2007). The ocular distribution studies were performed for one and two hours, where 50µL of the formulation was applied every 15 minutes throughout the duration of the study. Following each study, the individual tissues were dissected and the drug levels in each tissue were determined via HPLC. As shown in Figure 3.8A, after 1 hour, only the solution formulation provided detectable amounts of nepafenac in a majority of the ocular tissues. The suspension and Nevanac formulations showed detectable levels only in the cornea, sclera, and aqueous humour, and the drug was not detectable in the remaining ocular tissues. The solution formulation produced much higher drug levels than suspension or Nevanac in cornea, sclera and aqueous humor ($P<0.05$). However, there was a larger amount of nepafenac deposited to the cornea which is considered the target site of action for nepafenac (Gaynes & Onyekwuluje, 2008). This suggests that the cyclodextrin, in addition to serving as a drug solubilizer, may have acted as a

permeation enhancer allowing nepafenac to diffuse through individual tissues faster than the suspended drug (Masson, Loftsson, Masson, & Stefansson, 1999). No significant difference was observed between the suspension and Nevanac®. The accumulated drug concentration in the tissues was too low to be significantly different for the one-hour samples, however the two hour data set provided more comparable information. The solution successfully delivered drug to all ocular tissues in detectable quantities except the vitreous humour (Figure 3.8B). Even after 2 hours, only the solution formulation provided nepafenac in the detectable levels in most ocular tissues. The suspension and Nevanac formulations showed detectable levels only in cornea, sclera, iris, and aqueous humour, and the drug was not detectable in other ocular tissues such as retina, lens and vitreous humour. It is difficult for topical formulations to deliver drugs to the posterior segment of the eye due to the tear film layers and anterior epithelium layers (Tahara, Karasawa, Onodera, & Takeuchi, 2017). The mucin layer of the tear film provides a lipophilic protective layering over the glycocalyx of the ocular surface (Gaudana, Ananthula, Parenky, & Mitra, 2010). Furthermore, the cornea and sclera prevent entry of foreign molecules to the posterior tissues of the eye. The cornea contains tight junctions that prevent the penetration of drugs, while drug permeation through the sclera is dependent on the size and charge of the drug molecule (Prausnitz & Noonan, 1998). “A study in humans found the Cmax of nepafenac in the aqueous humor to be 205.3 ng/mL at a tmax of 30min (Walters et al., 2007). After two hours of perfusion we had an average concentration 79 of μg/mL in the aqueous humor. The stark difference is due to the fact that the perfusion model does not have a culdesac/eyelid to hold the initial formulation, meaning some of the formulation falls off of the eye and the only drug that is absorbed is that which sticks to the eye. Additionally, the circulation is not perfectly mimicked, this can lead to decrease in the amount of drug distributed to the desired tissues. The solution formulation produced much higher drug levels in cornea, iris and aqueous humor when compared to the suspension or Nevanac ($P<0.05$).

The solution provided a significantly higher amount of drug in the cornea compared to Nevanac®, following the two hours of perfusion ($p<0.001$). This is due to the enhanced solubility resulting from the HPBCD complexation (Tiwari et al., 2010). In agreement with the one-hour results, there was no significant difference in drug accumulation between the suspension formulation and Nevanac®. Thus, the solution formulation displayed properties that led to a higher permeation rate and enhanced drug delivery compared to the suspension and Nevanac®. Previous work, which studied the impact of ocular perfusion after intravitreal and suprachoroidal administration, used the same model in isolated perfused pig eyes as in the current work. The main conclusion of that paper showed no significant differences in tissue dye concentrations in nonperfused eyes compared to perfused eyes following hydrophilic drug delivered intravitreally or with a lipophilic drug injected either intravitreally or into the suprachoroidal space (Abarca et al., 2013). Therefore, the dynamics of the perfusion fluid have no significant effect on drug permeation.

3.5 Conclusions

Nepafenac: HP-β-CD complexation in liquid and solid states were demonstrated. The stability rate constants of 3665 M-1 and 4296 M-1, in water and phosphate buffered saline (PBS), respectively; suggest strong association of nepafenac with HPBCD. This allowed the formulation of a 0.1% solution, for comparison with the 0.1% Nevanac® suspension. Permeation studies using porcine corneas revealed that the solution had a permeation rate 18 times higher than Nevanac®. Furthermore, the solution had 11 times higher corneal retention than Nevanac®. Drug distribution studies using porcine eyes revealed that the solution formulation enables detectable levels in various ocular tissues while the drug was undetectable in most tissues when using Nevanac®. Furthermore, the ocular solution provided a significantly higher drug concentration in the cornea compared to the suspension or Nevanac®. Thus, a solution with enhanced trans-corneal permeation of nepafenac was achieved.

3.6 Acknowledgements

Authors acknowledge Dow Chemical Company and Auburn University Lambert-Powell Meats Laboratory for their generosity.

3.7 References

Abarca, E. M., Cuming, R., Duran, S., & Ramapuram, J. (2015). Development of an ex-vivo trans-corneal permeation model in horses: Epithelial barrier evaluation. *Investigative Ophthalmology & Visual Science, 56*(7).

Abarca, E. M., Salmon, J. H., & Gilger, B. C. (2013). Effect of Choroidal Perfusion on Ocular Tissue Distribution After Intravitreal or Suprachoroidal Injection in an Arterially Perfused Ex Vivo Pig Eye Model. *Journal of Ocular Pharmacology and Therapeutics, 29*(8), 715-722. doi:10.1089/jop.2013.0063

Ahuja, M., Dhake, A. S., Sharma, S. K., & Majumdar, D. K. (2008). Topical ocular delivery of NSAIDs. *AAPS J, 10*(2), 229-241. doi:10.1208/s12248-008-9024-9

Alonso, E. C., Riccomini, K., Silva, L. A., Galter, D., Lima, E. M., Durig, T., . . . Marreto, R. N. (2016). Development of carvedilol-cyclodextrin inclusion complexes using fluid-bed granulation: a novel solid-state complexation alternative with technological advantages. *J Pharm Pharmacol, 68*(10), 1299-1309. doi:10.1111/jphp.12601

Alves-Silva, I., Sa-Barreto, L. C. L., Lima, E. M., & Cunha-Filho, M. S. S. (2014). Preformulation studies of itraconazole associated with benznidazole and pharmaceutical excipients. *Thermochimica Acta, 575*, 29-33. doi:10.1016/j.tca.2013.10.007

Bekers, O., Uijtendaal, E. V., Beijnen, J. H., Bult, A., & Underberg, W. J. M. (1991). Cyclodextrins in the Pharmaceutical Field. *Drug Development and Industrial Pharmacy, 17*(11), 1503-1549. doi:Doi 10.3109/03639049109026630

Braga, M. A., Martini, M. F., Pickholz, M., Yokaichiya, F., Franco, M. K., Cabeca, L. F., . . . de Paula, E. (2016). Clonidine complexation with hydroxypropyl-beta-cyclodextrin: From physico-chemical characterization to in vivo adjuvant effect in local anesthesia. *J Pharm Biomed Anal, 119*, 27-36. doi:10.1016/j.jpba.2015.11.015

Bramhane, D. M., Kulkarni, P. A., Martis, E. A., Pissurlenkar, R. R., Coutinho, E. C., & Nagarsenker, M. S. (2016). Characterization of pioglitazone cyclodextrin complexes: Molecular modeling to in vivo evaluation. *J Pharm Bioallied Sci, 8*(2), 161-169. doi:10.4103/0975-7406.171680

Challa, R., Ahuja, A., Ali, J., & Khar, R. K. (2005). Cyclodextrins in drug delivery: an updated review. *AAPS PharmSciTech, 6*(2), E329-357. doi:10.1208/pt060243

Chen, C. C., Chang, J. H., Lee, J. B., Javier, J., & Azar, D. T. (2002). Human corneal epithelial cell viability and morphology after dilute alcohol exposure. *Invest Ophthalmol Vis Sci, 43*(8), 2593-2602.

Del Valle, E. M. M. (2004). Cyclodextrins and their uses: a review. *Process Biochemistry, 39*(9), 1033-1046. doi:10.1016/S0032-9592(03)00258-9

Duong, H. V. Q., Westfield, K. C., & Chalkley, T. H. F. (2007). Ketorolac tromethamine LS 0.4% versus nepafenac 0.1% in patients having cataract surgery - Prospective randomized double-masked clinical trial. *Journal of Cataract and Refractive Surgery, 33*(11), 1925-1929. doi:10.1016/j.jcrs.2007.07.017

Eleamen, G. R. A., da Costa, S. C., Lima-Neto, R. G., Neves, R. P., Rolim, L. A., Rolim-Neto, P. J., . . . Oliveira, E. E. (2017). Improvement of Solubility and Antifungal Activity of a New Aminothiophene Derivative by Complexation with 2-Hydroxypropyl-beta-cyclodextrin. *Journal of the Brazilian Chemical Society, 28*(1), 116-125. doi:10.5935/0103-5053.20160153

Gaudana, R., Ananthula, H. K., Parenky, A., & Mitra, A. K. (2010). Ocular Drug Delivery. *Aaps Journal, 12*(3), 348-360. doi:10.1208/s12248-010-9183-3

Gaynes, B. I., & Onyekwuluje, A. (2008). Topical ophthalmic NSAIDs: a discussion with focus on nepafenac ophthalmic suspension. *Clin Ophthalmol, 2*(2), 355-368.

Higuchi, T., & Connors, K. A. . (1965). Phase Solubility Techniques. *Advances in Analytical Chemistry and Instrumentation, 4*, 117-212.

IR Spectroscopy Tutorials: Amines *IR Spectroscopy Tutorials.* Retrieved from www.orgchemboulder.com/spectroscopy/irtutor/aminesir.shtml

Jansen T, X. B., Mesens J, Borgers M. (1990). Beta-cyclodextrins as vehicles in eye-drop formulations: an evaluation of their effecst on rabbit corneal epithelium. *Lens Eye Toxic Res., 7*(3-4), 459-468.

Jonathan C. Javitt, N. B. J., Peter Mcdonnell. (1994).

Jones, B. M., & Neville, M. W. (2013). Nepafenac: An Ophthalmic Nonsteroidal Antiinflammatory Drug for Pain After Cataract Surgery. *Annals of Pharmacotherapy, 47*(6), 892-896. doi:10.1345/aph.1R757

Liao, Y., Zhang, X., Li, C., Huang, Y., Lei, M., Yan, M., . . . Zhao, C. (2016). Inclusion complexes of HP-beta-cyclodextrin with agomelatine: Preparation, characterization, mechanism study and in vivo evaluation. *Carbohydr Polym, 147*, 415-425. doi:10.1016/j.carbpol.2016.04.022

Liu, L., & Guo, Q. X. (2002). The driving forces in the inclusion complexation of cyclodextrins. *Journal of Inclusion Phenomena and Macrocyclic Chemistry, 42*(1-2), 1-14. doi:Doi 10.1023/A:1014520830813

Loftsson, T., & Stefansson, E. (1997). Effect of cyclodextrins on topical drug delivery to the eye. *Drug Development and Industrial Pharmacy, 23*(5), 473-481. doi:Doi 10.3109/03639049709148496

Loftsson, T., & Stefansson, E. (2007). Cyclodextrins in ocular drug delivery: theoretical basis with dexamethasone as a sample drug. *Journal of Drug Delivery Science and Technology, 17*(1), 3-9.

Loftssona, T., & Jarvinen, T. (1999). Cyclodextrins in ophthalmic drug delivery. *Adv Drug Deliv Rev, 36*(1), 59-79.

Mains, J., Tan, L. E., Wilson, C., & Urquhart, A. (2012). A pharmacokinetic study of a combination of beta adrenoreceptor antagonists - In the isolated perfused ovine eye. *European Journal of Pharmaceutics and Biopharmaceutics, 80*(2), 393-401. doi:10.1016/j.ejpb.2011.11.006

Masson, M., Loftsson, T., Masson, G., & Stefansson, E. (1999). Cyclodextrins as permeation enhancers: some theoretical evaluations and in vitro testing. *Journal of Controlled Release, 59*(1), 107-118. doi:Doi 10.1016/S0168-3659(98)00182-5

Matencio, A., Hernandez-Gil, C. J., Garcia-Carmona, F., & Lopez-Nicolas, J. M. (2017). Physicochemical, thermal and computational study of the encapsulation of rumenic acid by natural and modified cyclodextrins. *Food Chemistry, 216*, 289-295. doi:10.1016/j.foodchem.2016.08.023

Oprean, C., Mioc, M., Csanyi, E., Ambrus, R., Bojin, F., Tatu, C., . . . Soica, C. (2016). Improvement of ursolic and oleanolic acids' antitumor activity by complexation with hydrophilic cyclodextrins. *Biomed Pharmacother, 83*, 1095-1104. doi:10.1016/j.biopha.2016.08.030

Patel, A., Cholkar, K., Agrahari, V., & Mitra, A. K. (2013). Ocular drug delivery systems: An overview. *World J Pharmacol, 2*(2), 47-64. doi:10.5497/wjp.v2.i2.47

Pharmacy, U. o. N. C. E. S. o. Sterile Compounding: Ophthalmics.

Prausnitz, M. R., & Noonan, J. S. (1998). Permeability of cornea, sclera, and conjunctiva: A literature analysis for drug delivery to the eye. *Journal of Pharmaceutical Sciences, 87*(12), 1479-1488. doi:DOI 10.1021/js9802594

Saettone, M. F. (2002). *Progress and Problems in Ophthalmic Drug Delivery*. Retrieved from

Sahoo, S. K., Diinawaz, F., & Krishnakumar, S. (2008). Nanotechnology in ocular drug delivery. *Drug Discovery Today, 13*(3-4), 144-151. doi:10.1016/j.drudis.2007.10.021

Sieg, J. W., & Robinson, J. R. (1975). Vehicle effects on ocular drug bioavailability i: evaluation of fluorometholone. *J Pharm Sci, 64*(6), 931-936.

Tahara, K., Karasawa, K., Onodera, R., & Takeuchi, H. (2017). Feasibility of drug delivery to the eye's posterior segment by topical instillation of PLGA nanoparticles. *Asian Journal of Pharmaceutical Sciences, 12*(4), 394-399. doi:10.1016/j.ajps.2017.03.002

Tang, P., Li, S., Wang, L., Yang, H., Yan, J., & Li, H. (2015). Inclusion complexes of chlorzoxazone with beta- and hydroxypropyl-beta-cyclodextrin: Characterization, dissolution, and cytotoxicity. *Carbohydr Polym, 131*, 297-305. doi:10.1016/j.carbpol.2015.05.055

Tang, P., Ma, X., Wu, D., Li, S., Xu, K., Tang, B., & Li, H. (2016). Posaconazole/hydroxypropyl-beta-cyclodextrin host-guest system: Improving dissolution while maintaining antifungal activity. *Carbohydr Polym, 142*, 16-23. doi:10.1016/j.carbpol.2016.01.042

Tang, P., Tang, B., Wang, Q., Xu, K., Xiong, X., & Li, H. (2016). Effect of hydroxypropyl-beta-cyclodextrin on the bounding of salazosulfapyridine to human serum albumin. *Int J Biol Macromol, 92*, 105-115. doi:10.1016/j.ijbiomac.2016.07.033

Tiwari, G., Tiwari, R., & Rai, A. K. (2010). Cyclodextrins in delivery systems: Applications. *J Pharm Bioallied Sci, 2*(2), 72-79. doi:10.4103/0975-7406.67003

Uekama, K. (2004). Design and evaluation of cyclodextrin-based drug formulation. *Chem Pharm Bull (Tokyo), 52*(8), 900-915.

Walters, T., Raizman, M., Ernest, P., Gayton, J., & Lehmann, R. (2007). In vivo pharmacokinetics and in vitro pharmacodynamics of nepafenac, amfenac, ketorolac, and bromfenac. *J Cataract Refract Surg, 33*(9), 1539-1545. doi:10.1016/j.jcrs.2007.05.015

Wei, Y. Q., Zhang, J., Zhou, Y., Bei, W. Y., Li, Y., Yuan, Q. P., & Liang, H. (2017). Characterization of glabridin/hydroxypropyl-beta-cyclodextrin inclusion complex with robust solubility and enhanced bioactivity. *Carbohydrate Polymers, 159*, 152-160. doi:10.1016/j.carbpol.2016.11.093

Zeng, Y. J., Yang, J., Huang, K., Lee, Z. H., & Lee, X. Y. (2001). A comparison of biomechanical properties between human and porcine cornea. *Journal of Biomechanics, 34*(4), 533-537. doi:Doi 10.1016/S0021-9290(00)00219-0

Zhang, C. L., Liu, J. C., Yang, W. B., Chen, D. L., & Jiao, Z. G. (2017). Experimental and molecular docking investigations on the inclusion mechanism of the complex of phloridzin and hydroxypropyl-beta-cyclodextrin. *Food Chemistry, 215*, 124-128. doi:10.1016/j.foodchem.2016.07.155

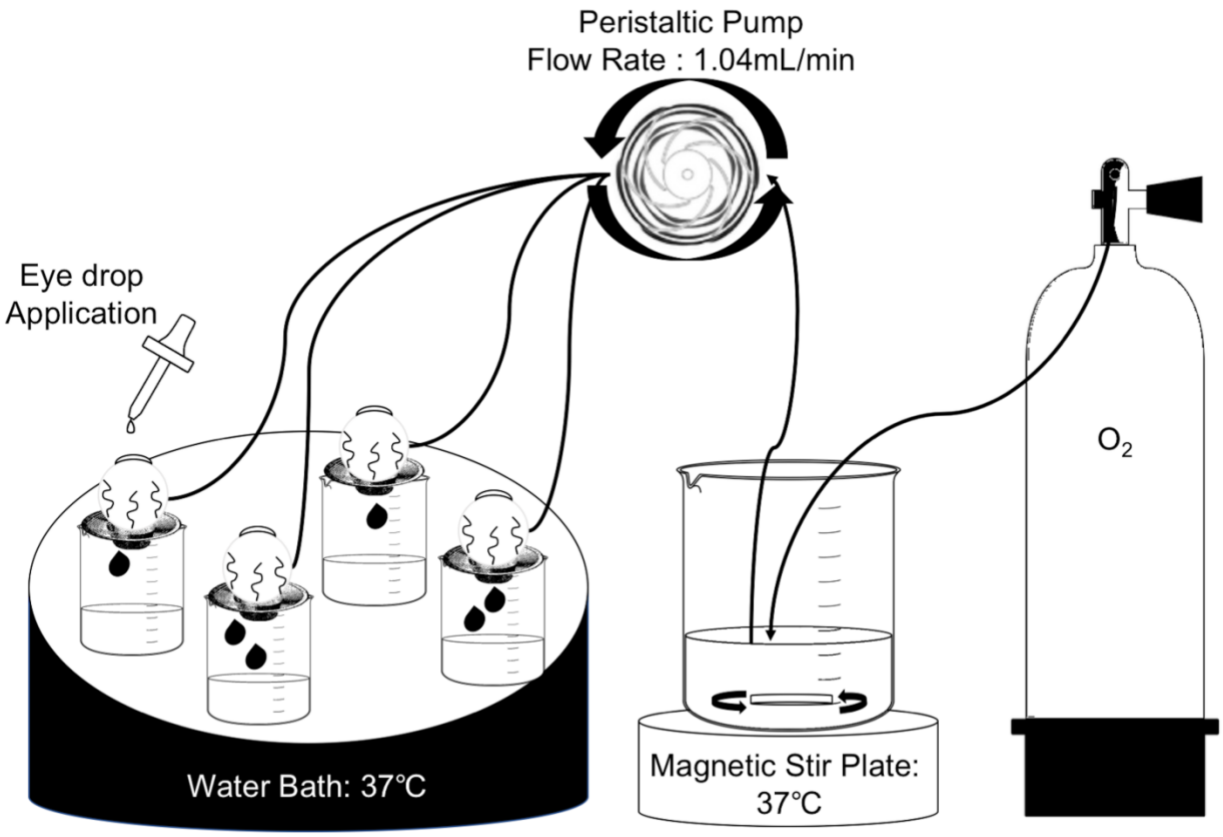

Figure 3.1: Arterial perfusion of the porcine eye for drug distribution in the ocular tissues.

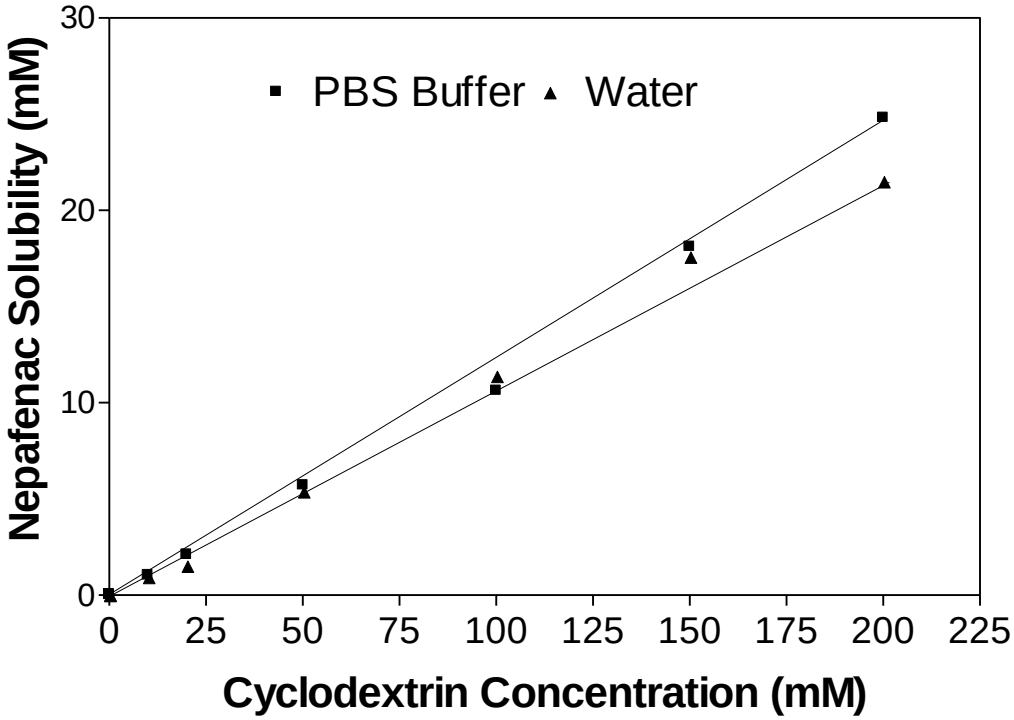

Figure 3.2: Phase solubility studies for nepafenac and HPBCD in PBS and water.

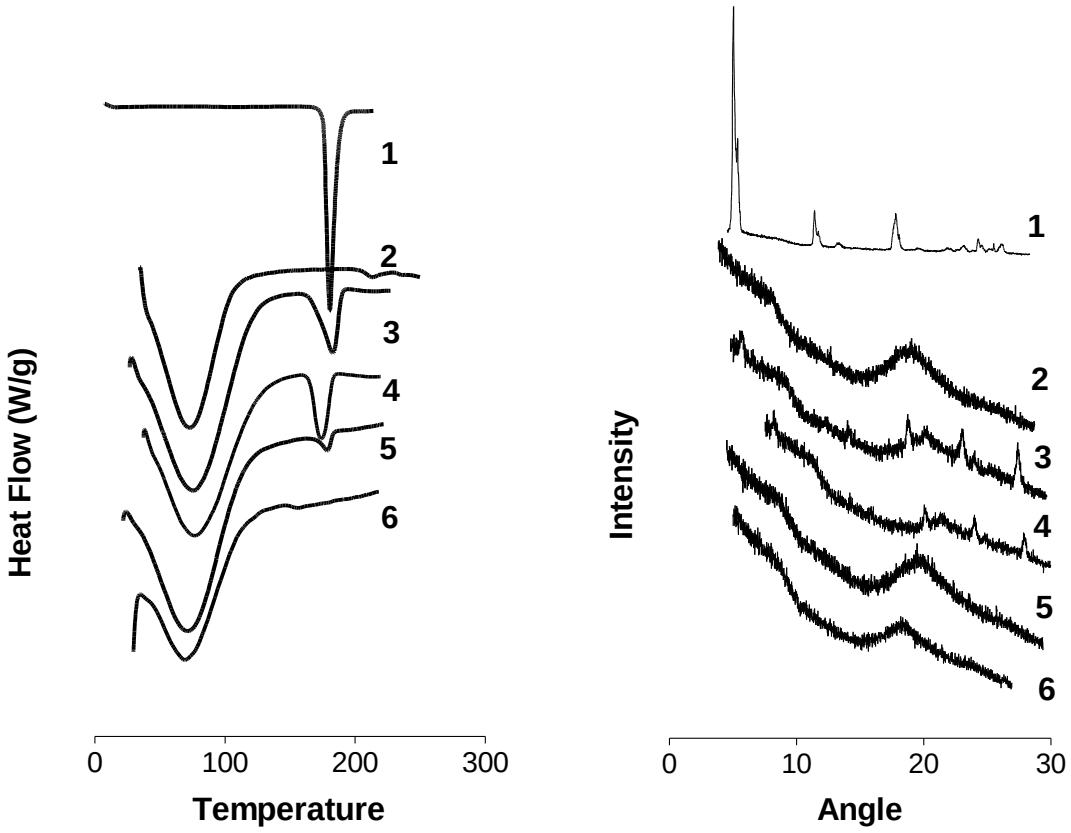

Figure 3.3: Differential scanning calorimetry (a) and x-ray diffractometry data (b) confirm complexation in the solid state (1, nepafenac; 2, hpbcd; 3, dry mix; 4, kneaded mix; 5, freeze-dried mix; 6, rotovap mix).

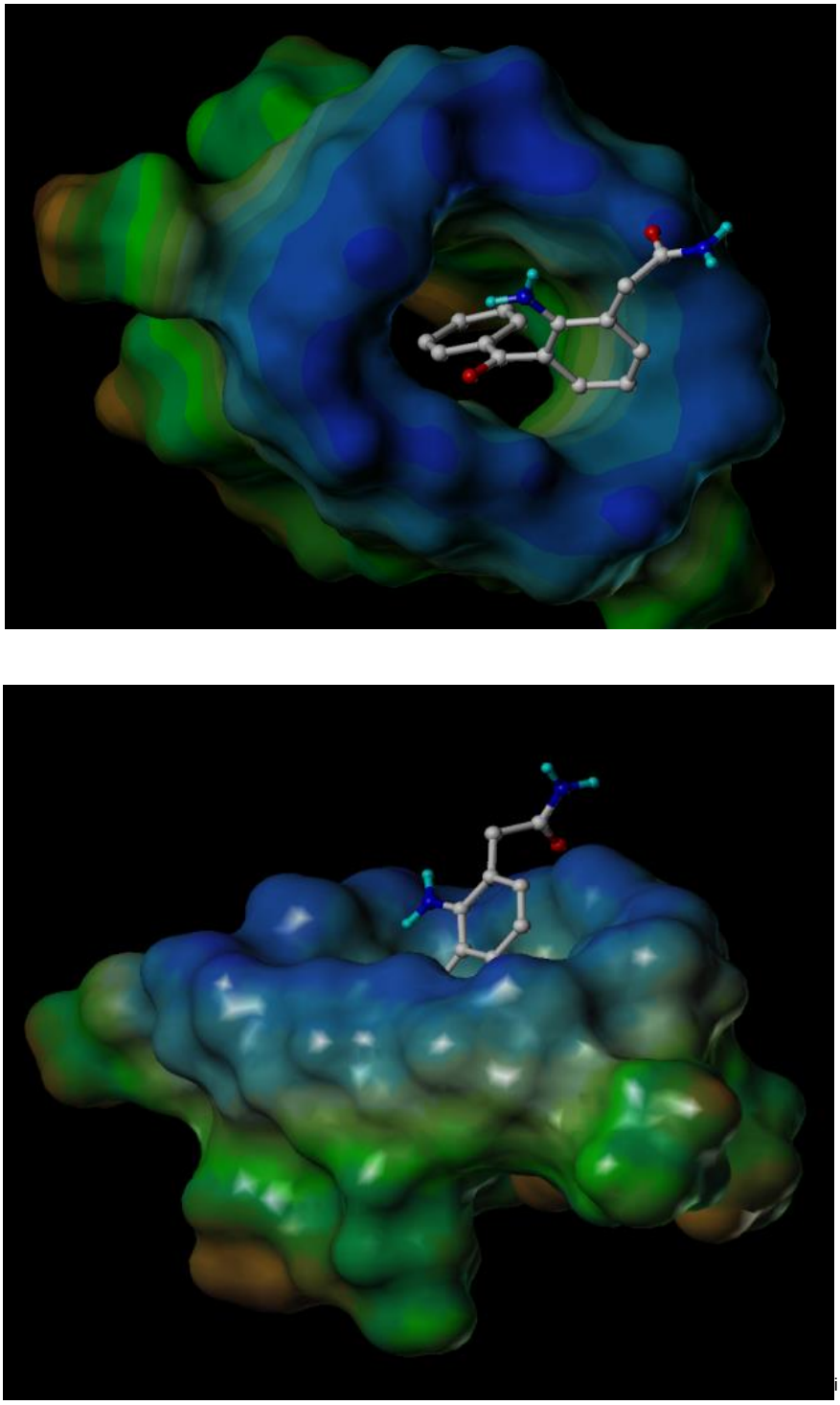

Figure 3.4: Molecular docking simulated the interaction between nepafenac and HPBCD. Lipophilic areas are indicated by lighter gray, whereas hydrophilic areas are shown by darker gray.

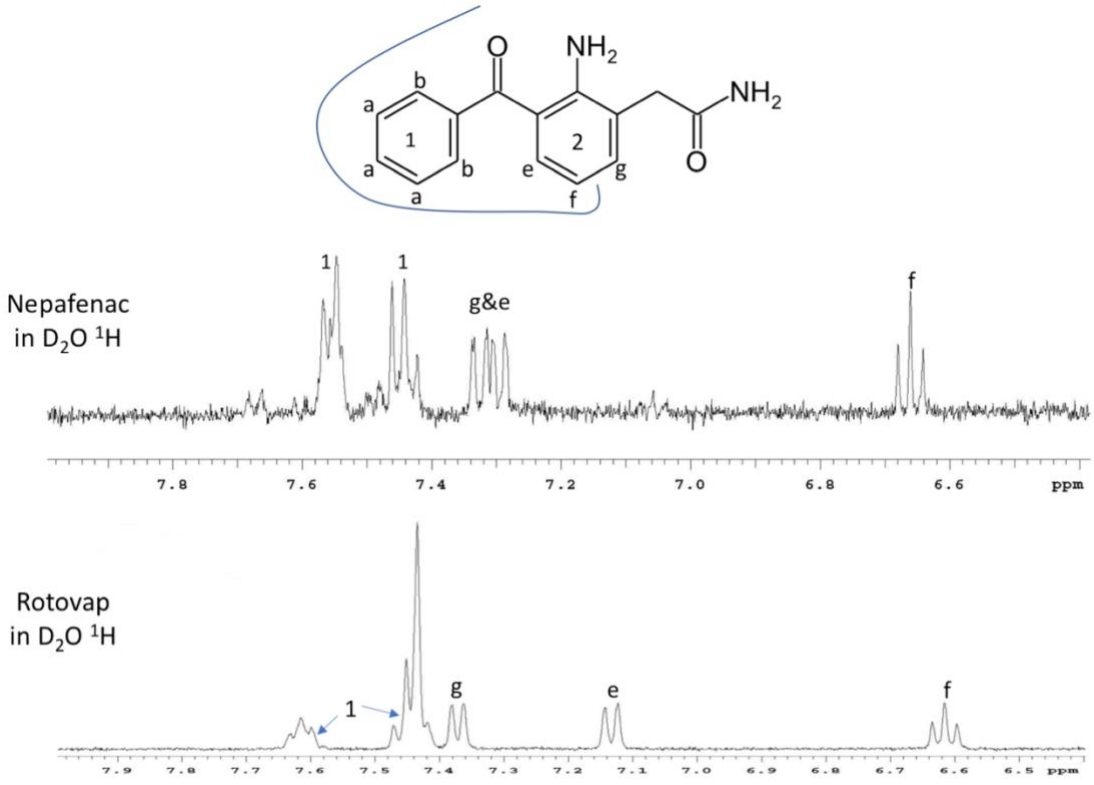

Figure 3.5**:** Proton NMR of nepafenac (top) and the inclusion complex prepared by rotovap (bottom).

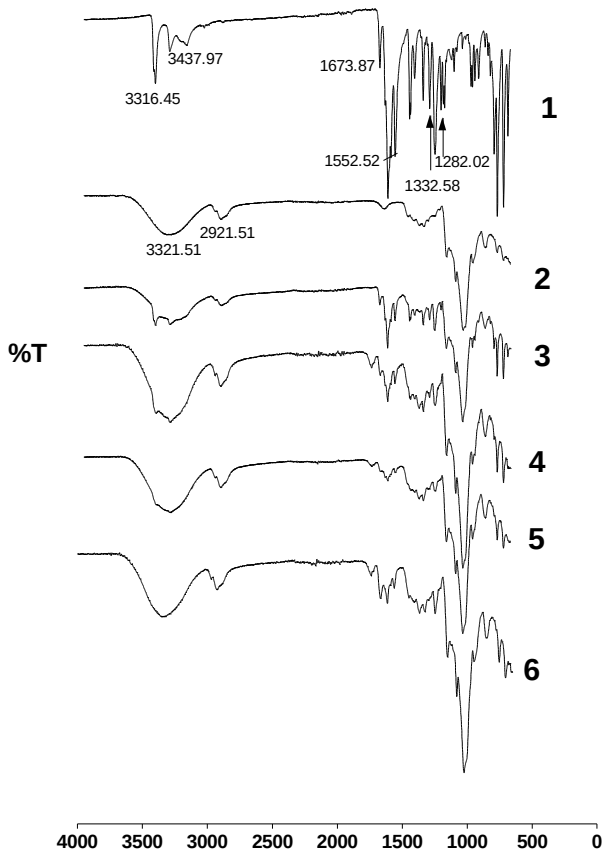

Figure 3.6: FT-IR data of various nepafenac-HPβCD mixtures to confirm the inclusion complex formation in the solid state. (1, nepafenac; 2, hpbcd; 3, dry mix; 4, kneaded mix; 5, freeze-dried mix; 6, rotovap mix).

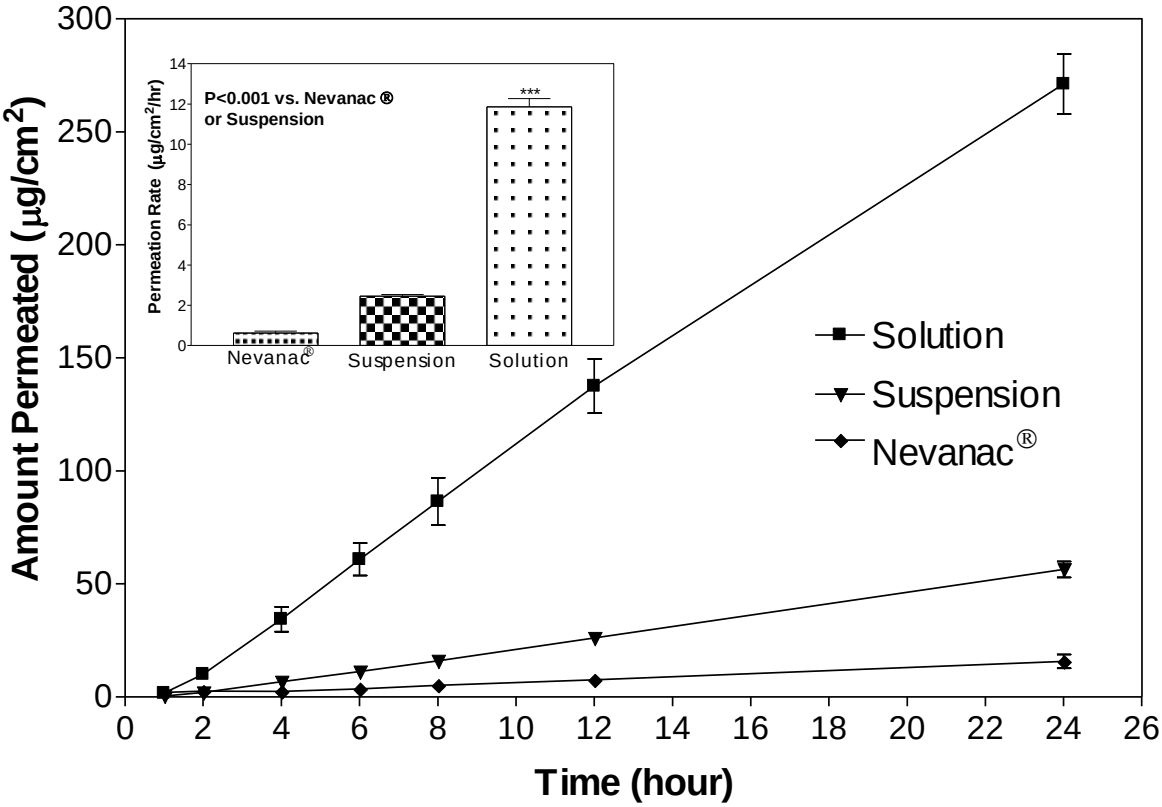

Figure 3.7: Permeation of nepafenac across porcine cornea; inset: permeation rate (steady state flux).

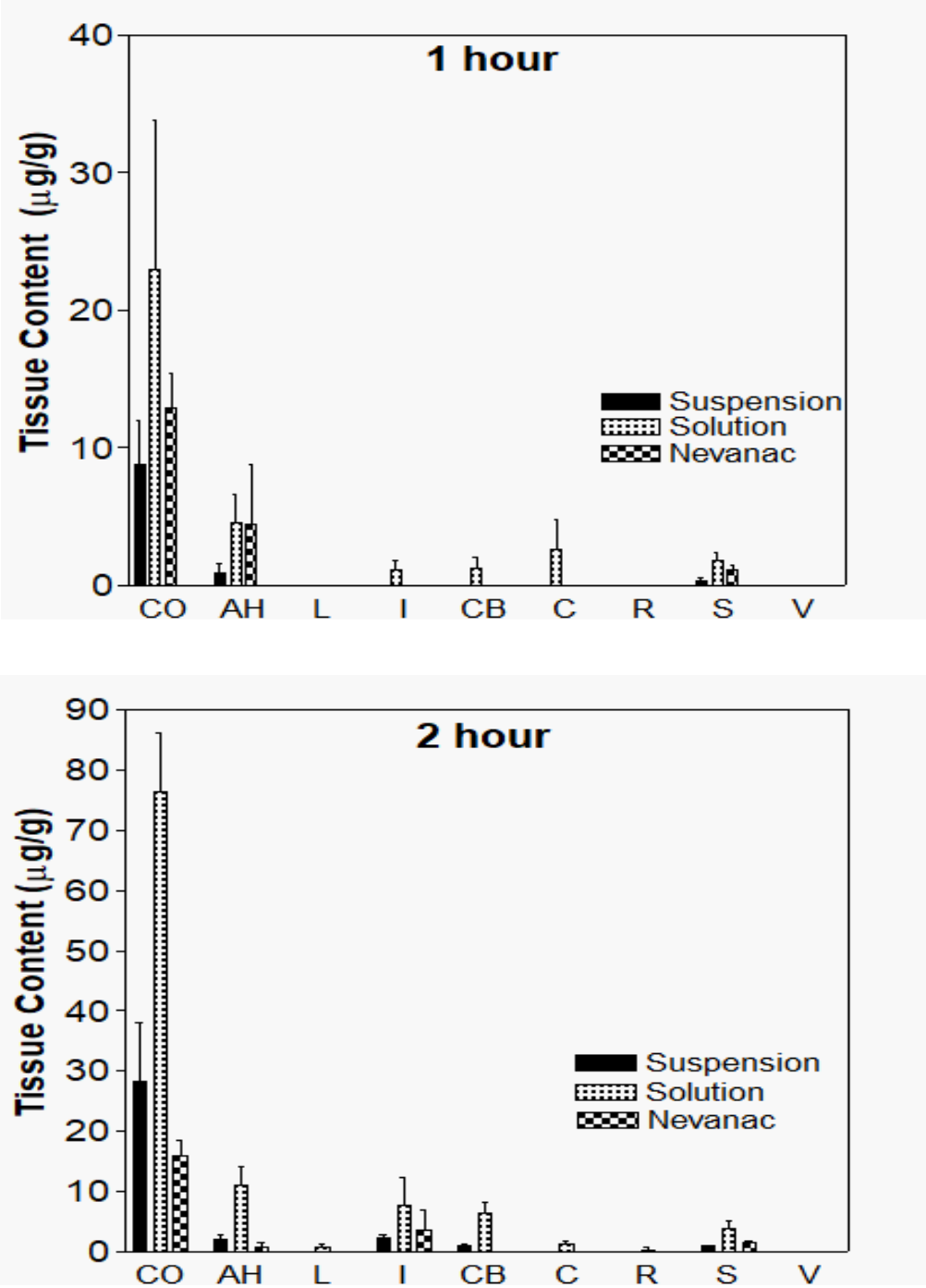

Figure 3.8: Ocular distribution of Nepafenac in isolated porcine eyes in a continuous perfusion model. The experiments were terminated at 1 and 2 hour time points and various ocular tissues were collected, and nepafenac in the tissues was quantified. [CO, Cornea; AH, Aqueous Humour; L, Lens; I, Iris; CB, Ciliary Body; C, Choroid; R, Retina; S, Sclera; V, Vitreous Humour. Error bars represent standard error mean (SEM).

Chapter 4. *In-Situ* Gel of Nepafenac/Hydroxypropyl-B-Cyclodextrin Complex for Sustained Drug Release to the Cornea

4.1 Abstract

Nepafenac is a water insoluble nonsteroidal anti-inflammatory drug, which is available as an ophthalmic suspension (Nevanac®). Suspensions are undesirable for two reasons: they tend to cause foreign body sensation and lacrimation, which could limit residence time and drug bioavailability. This decreases the amount of time the drug has to reach the site of action, the cornea. Previously, we improved the solubility and ocular permeability of nepafenac by complexing the drug with hydroxypropyl-β-cyclodextrin. In this study, we utilized the complex to formulate an ion-activated in-situ gel system using sodium alginate, Protanal PH 1033, to increase the residence time and to reduce repeat eye drop instillation. Rheological properties of the formulations revealed that the viscosity of the optimized formulation was increased 30-fold when exposed to the STF (35°C). Permeation studies showed that the drug concentration of the in-situ formulations were approximately 10 times higher than the commercial product, Nevanac® ($P<0.001$). Additionally, the in-situ gel formulations had 5-fold higher concentrations of nepafenac retained in the cornea when compared to Nevanac® ($P < 0.001$). Finally, ex-vivo drug distribution studies in the porcine eye perfusion model revealed a higher drug retention in various ocular tissues such as cornea, sclera, retina, as compared to Nevanac®.

4.2 Introduction

Nepafenac is a non-steroidal anti-inflammatory drug used to treat post-operative pain and inflammation in the cornea following ocular surgeries, such as cataracts and Lasik corrective surgery. Due to the extreme water insoluble nature of the drug, nepafenac is only currently commercially available as an ophthalmic suspension, Nevanac®. Suspensions could cause blurred vision, foreign particle sensation and/or irritation in the eye, leading to increased lacrimation, causing the drug to be removed from the eye by either drainage or spillage (Patel, Cholkar, Agrahari, & Mitra, 2013; Sawarkar, Ravikumar, & Pashte, 2016). This rapid removal of the formulation limits the residence time of the drug, meaning a very low fraction of the administered dose of the drug is absorbed to the site of action, such as the cornea or sclera, while the remaining drug is absorbed systemically (Mohanambal, Arun, & Sathali, 2011). This could lead to significant drug wastage and possible adverse effects (Almeida, Amaral, Lobao, & Lobo, 2014). Typically, a formulation is drained from the eye within 5 minutes of instillation (Cohen, Lobel, Trevgoda, & Peled, 1997). Furthermore, patient compliance is reduced when a formulation is uncomfortable (S.B. Makwana, V.A. Patel, & Parmar, 2015). In general, it is possible to achieve higher drug absorption, better ocular bioavailability and longer residence time by improving the water solubility of an insoluble drug and by increasing the retention time by formulating a solution with in situ gelling characteristics. Previously, we have shown that hydroxypropyl-β-cyclodextrin (HPBCD) can increase both the water solubility and bioavailability of nepafenac(Haley Shelley, 2018). By formulating an *in situ* gel with Protanal PH 1033 sodium alginate, we could increase residence time of the drug in the cul-de-sac of the eye for prolonged contact and better absorption.

Alginates are a group of naturally occurring non-toxic mucoadhesive gelling agents derived from a variety of brown seaweeds known as phylum phaeophyceae (Anderson, Brydon, Eastwood, & Sedgwick, 1991). Gelation occurs when the alginates interact with divalent cations and the cations

bind to the guluronate blocks of the sodium alginate. Cross-linking of the cation-guluronate blocks then yields a gel-like structure. Sodium alginate has been utilized as a viscosity enhancer, for ophthalmic formulations (Szekalska, Pucilowska, Szymanska, Ciosek, & Winnicka, 2016). Additionally, the gel formation is beneficial because the gel matrix allows for a slow steady release of drug at the application site. More specifically, sodium alginate can provide sustained drug release for ocular delivery due to the mucoadhesive properties and enhanced viscosity (Almeida et al., 2014; Gupta et al., 2015; Pawar, Kashyap, Malhotra, & Sindhu, 2013). The two most important factors in producing an effective *in-situ* gelling system are the gelling capacity and viscosity (Srividya, Cardoza, & Amin, 2001). The formulation should have a low viscosity at room temperature for easy instillation, but upon administration the formulation interacts with the calcium ions in the tear fluid to form a gel matrix, providing controlled drug release (Z. D. Liu et al., 2006). Draize ocular irritation studies on rabbits for sodium alginates were found to be non-irritating to the eye (Z. D. Liu et al., 2006; Mandal, Thimmasetty, Prabhushankar, & Geetha, 2012). The aim of this work is to formulate an *in-situ* gel for improved residence time and sustained release of nepafenac to the ocular surface. Protanal PH 1033 was selected as the gelling agent, because low amounts of the polymer form a strong gel due to the high guluronic acid content (Cohen et al., 1997). The ability of the *in-situ* gel to increase retention on the eye was compared to Nevanac® in ex-vivo porcine perfusion eye model.

4.3 Experimental Methods

4.3.1 Materials

Nepafenac was obtained from Hangzhou Yuhao Chemical Technology Co. Ltd. (Hangzhou, China). Hydroxypropyl-β-cyclodextrin was purchased from CTD Holdings, Inc.(Alachua, FL). Protanal (sodium alginate) was kindly provided by FMC BioPolymer (Philadelphia, PA). All

chemicals and solvents used were of either USP grade or High Performance Liquid Chromatography (HPLC) grade and purchased from VWR Scientific (Suwanee, GA).

4.3.2 High Performance Liquid Chromatography (HPLC) Analysis

An Alliance Waters e2695 Separations Module and a Waters 2998 Photodiode Array Detector was used for quantifying nepafenac in the formulation, release, permeation and tissue retention studies. A Kinetix C18 reversed-phase HPLC column (5µm particles, 150mm x 4.6mm) was employed for nepafenac analysis. The mobile phase consisted of 40:60 acetonitrile: water set at a flow rate of 1mL/min. The absorbance wavelength was set at 254nm, with an injection volume of 10 µL.

4.3.3 Gelation Capacity & Clarity Tests

Protanal PH 1033 and HPMC E15, E50, or K4M were mixed together in varying concentrations to determine the gelation capacity of each formulation. Gelation capacity tests were performed by placing one drop (20-50 µL) of each mixture into 2mL of simulated tear fluid (STF) using a dropper. STF had the following composition: 670mg sodium chloride, 200mg sodium bicarbonate, 8mg calcium chloride dihydrate, volume filled to 100mL with milli Q water (Edman, 1993). The appearance of each gel was visually evaluated as described by Asasutjarit et al (Asasutjarit, Thanasanchokpibull, Fuongfuchat, & Veeranondha, 2011). The mixtures which displayed the best gelation capacity were used for further formulation development.

4.3.4 Rheology Studies

The rheology properties of each *in-situ* gel system was tested before and after the addition of STF using Bohlin CVO plate and cone rheometer (Worcestershire, UK). The viscosity of each formulation was measured at both 25°C and 35°C (surface temperature of the eye)(Efron, Young, & Brennan, 1989) with increasing shear rate from 0 to 100s^{-1} (Liu et al., 2010). The rheology tests

were conducted in triplicates for statistical analysis. The mixtures that displayed the lowest initial viscosity with the largest increase in viscosity, following the addition of STF, were used for preparing the *in-situ* gel systems.

4.3.5 Formulation Development

The nepafenac in-situ gel was prepared by weighing the drug (0.1%) in a 20mL glass vial, the drug was then wetted with (1.4%) ethanol (190-proof). HPβCD (6.0%) was subsequently added and half of the volume was made up with isotonic 1.9% boric acid buffer solution (pH=6.00). The mixture was sonicated until the drug was completely dissolved. Following dissolution, the desired concentration of gel former (sodium alginate/HPMC) was added followed by 0.005% benzylkonium chloride solution. The volume was brought to 100% using the isotonic 1.9% boric acid buffer. The formulation was kept under constant stirring using a magnetic stir bar until a clear solution was achieved. The nepafenac content of the formulation was assayed by HPLC.

4.3.6 Particle Size

The particle size of the *in-situ* gel formulation and Nevanac®was measured using a PSS Nicomp 380 ZLS Particle Sizing System, Port Richey, FL. 5uL of each formulation was diluted in 1mL of milli-Q water prior to analysis. Particle size distribution of the formulations was carried out by dynamic light scattering method using Nicomp 380 ZLS particle size analyzer (Particle Sizing Systems, Santa Barbara, CA). 5μL of each formulation was diluted in 1mL of milli-Q water prior to analysis. The particle size distribution plots were obtained in the intensity-weighed mode for each formulation. Mean particle size and polydispersity index of the formulations after appropriate dilutions were calculated.

3.3.7 pH & Osmolality Measurement

The pH of each formulation was measured using an Accumet XL 150 pH meter (Fisher Scientific, Suwannee, GA). The osmolality of each formulation was determined using a Wescor Vapro 5600 osmometer (Logan, UT) according to the standard procedure provided by the equipment manufacturer.

4.3.8 Ex-vivo Dialysis Membrane Release Experiments

Franz Diffusion Cell apparatus was assembled to hold the dialysis membrane securely in position during the release experiments. The dialysis membranes (Regenerated cellulose, molecular weight cut off 14,000 Da, Fisher Scientific Suwanne, GA) were soaked in water for 30 minutes prior to the experiments. The *in-situ* gel systems were tested and compared to Nevanac®. The receptor cell was filled with 5 mL PBS buffer (pH 7.4) containing 10% ethanol, and the dialysis membrane was placed on the receptor cell and the donor cell was placed on top and the two halves were clamped together. The donor cell was filled with 0.5mL of the *in-situ* gel system and 0.14mL of STF was pipetted on top of the gel; the cell was then covered with Parafilm®. The receptor cell was sampled (1 mL) at 1, 2, 4, 6, 8, 12 and 24 h, replenished with fresh PBS buffer (pH 7.4) containing 10% ethanol to maintain sink conditions. The samples were assayed by HPLC as described earlier. Each formulation was tested in 4 replicates. The release kinetics were modelled using GraphPad Prism (GraphPad Software, La Jolla, CA).

The Korsmeyer-Peppas model was used to describe the drug release from all formulations:

$$\frac{M_t}{M} = K_d t^n \qquad \text{Eq. 1}$$

In this expression, K_m (hr^{-m}) is the kinetic constant and n is the diffusion or release exponent. The constants and exponent are the unknowns and can be determined by fitting the experimental data to the aforementioned equation. Other models were tested as well to determine the best fitting model: Higuchi equation (Higuchi, 1961), Peppas-Stahlin model (Peppas & Sahlin, 1989): zero

and first order release (Wagner, 1969). The model that resulted in the smallest standard error for the individual parameters and highest R^2 value was determined to be the best fitting model.

4.3.9 Ex-vivo Corneal Permeation Experiments

4.3.9.1 Corneal Excision

Porcine eyes were obtained from Auburn University Lambert-Powell Meats Laboratory (Auburn University, Auburn AL) and used freshly on the day of the experiment. The animals were sacrificed according to the Institutional Animal Care and Use Committee (IACUC) approved protocol (SOP 2015-2727). The excess tissue was first cut from the globe and the corneas were excised from the globe using a 3.0mm slit eagle blade to create an insertion point between the iris and the cornea. Corneal scissors were used to excise the cornea and the corneas were rinsed with tap water to remove aqueous humor and then placed in pH 7.4 phosphate buffered saline (PBS) until used in the permeation studies, within 2 hours.

4.3.9.2 Corneal Permeation Study

Franz Diffusion Cell apparatus was assembled to hold the cornea in position during the permeation experiments. Nevanac® and nepafenac in-situ gel systems with varying concentrations of sodium alginate (0.1%, 0.3%, 0.5%) were tested in 4 replicate permeation experiments. The receptor cell was filled with 5 mL PBS buffer (pH 7.4) containing 10% ethanol, to maintain sink conditions. The corneas were placed on the receptor cell with the outer surface of the cornea facing up (convex side); the donor cell was placed on top of the cornea and both half-cells were clamped together The donor cell was filled with 0.5mL of the formulation and 0.14mL of STF was pipetted on top of the in-situ gel; the cell was then covered with Parafilm®. The receptor cell was sampled (1 mL) at 1, 2, 4, 6, 8, 12, and 24 h, replenished with fresh PBS

buffer (pH 7.4) containing 10% ethanol. The samples were assayed by HPLC method as described earlier.

4.3.9.3 Extraction of Nepafenac from Corneas

Following the 24-hour permeation study, the formulation was removed from the donor chamber using a dropper pipette, and the cornea was cleaned with PBS buffer (pH 7.4) containing 10% ethanol using cotton swabs. The active diffusion area of the cornea was cut, weighed, minced and placed in individual vials with 2mL of the HPLC mobile phase (acetonitrile: water 60:40). The vials were then sonicated for 30 minutes and left on the bench for 24 hours at room temperature to extract any drug retained in the cornea. The vials were sonicated again for 30 minutes and the supernatant was filtered through 0.45 µm nylon membrane filter and assayed by HPLC. The extraction method was validated by spiking the corneas with a known amount of Nepafenac and the recovery of the drug from the corneas was determined.

4.3.10 Ocular Distribution of Nepafenac in Isolated Perfused Eyes

Porcine eyes of either sex were freshly obtained from Lambert-Powell Meats Laboratory (Auburn University, Auburn AL) immediately following euthanasia. The animals were sacrificed according to the Institutional Animal Care and Use Committee (IACUC) approved protocol (SOP 2015-2727) for collecting meat. All eyes were used within 4 hours of euthanasia to maintain the integrity of the entire globe. The excess adnexal tissue was trimmed the ocular globe was placed in PBS pH 7.4 until ready for perfusion (Abarca, Salmon, & Gilger, 2013; Mains, Tan, Wilson, & Urquhart, 2012). The eyes were perfused with Dulbecco's Modified Eagle's Medium F12 (DMEM) under constant oxygen supply. The perfusion was started 30 minutes prior to drug application and maintained throughout the entirety of the study. The long posterior ciliary artery of each eye was identified, split open with a 3.0 mm slit Eagle blade, cannulated and secured in place with Scotch® super glue gel. Each eye was then placed in a stainless-steel strainer on top of a 100mL beaker,

which allowed for the collection of the DMEM medium from the veins. An Ismatec® peristaltic pump (Cole-Parmer GmbH, Wertheim, Germany) was employed to perfuse the oxygenated DMEM through the cannulated eyes (Figure 1). As previously described, perfusion was started at a flow rate 0.25–0.8 mL/min and increased to 1 mL/min (Abarca et al., 2013). Adequate arterial perfusion was determined by observing flow of media exiting vortex veins. Ocular distribution of nepafenac from Nevanac® and the F16 *in-situ* gel system was determined. 50 µL of the formulation was pipetted onto each of the corneal surface every 15 minutes for two hours. In the case of the *in-situ* gel system, 14 µL of STF was pipetted on top of the formulation after application to the eye, in order to activate gelation. After two hours, the eyes were frozen instantly using dry ice and stored in a freezer at -80°C to prevent transfer of drug between tissues. For dissection, the frozen eye was placed on a cold ceramic tile and all the ocular tissues were removed: cornea, aqueous humour, iris, ciliary body, sclera, retina, lens, vitreous humour and choroid. The tissue were minced to ensure adequate penetration of the extraction medium. Each tissue was soaked in 2 ml of 40:60 acetonitrile: water for 24 hours in individual vials, then filtered with 0.45 µm Nylon membrane filters and analyzed via HPLC.

The extraction method was validated by spiking a known concentration of nepafenac (10µg/Ml) in each ocular tissue and determining the recovery of drug the tissue. For these experiments, the tissues that were not in contact with nepafenac were used. The recovery of nepafenac from the tissues was determined in 4 replicates from the following tissue: cornea, sclera, aqueous humor, iris, ciliary body, choroid and retina.

The tissue samples were collected in frozen condition, and minced within a 5 mL polypropylene tube. The tissues were added with 2 mL of nepafenac solution (10 µg/mL) in the acetonitrile: water (4:6) mixture and sonicated for 30 min and stored overnight. The following day, the samples were filtered using 0.45 micron Nylon membrane filters and and assayed by HPLC. The nepafenac

recovery (%) from the tissues was calculated as the ratio of the amount of nepafenac extracted from the spiked tissue to the amount of nepafenac extracted from the solution in the absence of the tissues but processed by the same procedure.

4.3.11 Statistical Analysis

All results are presented as mean ± standard error of mean (SEM). The cumulative amount of nepafenac permeated through unit area of cornea was plotted as a function of time. In vitro steady-state flux was calculated from the slope of the linear portion of the plot. The amount of drug (μg) retained in the cornea was normalized to 1 gram of cornea. Analysis of variance was performed to determine the level of significance between the means. Mean differences with $P < 0.05$ were considered significant (GraphPad Prism, La Jolla, CA).

4.4 Results & Discussion

4.4.1 Gelation Capacity & Clarity Tests

Aqueous solutions of varying concentrations of HPMC and alginates were formulated to determine the gelation capacity of each mixture (Table 4.1). All formulations were transparent in appearance. The gelation capacity was evaluated based on the rate of gelation and length of time until the gel completely dissolved, after interaction with STF. The following key was used to evaluate the gelation capacity of each formulation: -, no gelation occurred; +, gels rapidly/dissolves after minutes; ++, gels instantly/remains a gel for hours; +++: gels instantly/remains a gel for longer than 8 hours (Z. Liu et al., 2006). Formulation A3 did not form a gel upon instillation into STF. A1, A2, A8, A15 & A16 formed gels rapidly and dissolved minutes later. A4-A7 rapidly formed a gel and dissolved within 2 hours. A9-A14 & A17 formed gels immediately and remained gels for more than 8 hours. However, formulations A11 & A14 formed a gel without the addition of STF; therefore, this formulation could not be used for *in-situ* gel drug

delivery. A12, A13, A15-A17 formulations were used to produce placebo *in-situ* gel systems for rheology studies corresponding to the following placebo names P12, P13, P15, P16 and P17.

4.4.2 Rheology Studies

Rheology studies were first performed on placebo formulations: P12, P13 and P15-P17. The viscosity of each formulation was determined before and after the addition of STF at 25°C and 35°C (Figure 4.1A & 4.1B). All placebo formulations exhibited psuedoplastic flow: the viscosity was high during interblinking, and is low during blinking. This is desirable for ophthalmic formulations, since the shear rate during blinking is 4250-28,500 s^{-1} and 0.03s^{-1} during interblinking (Almeida et al., 2014). Mixing HPMC with sodium alginate improves the rheological properties (Z. D. Liu et al., 2006; Makwana, Patel, & Parmar, 2016; Mandal et al., 2012), as evident by visually inspecting the formulations. The initial viscosity of all HPMC/sodium alginate mixtures had a significantly higher viscosity ($P<0.05$) compared to sodium alginate alone at a given concentration. The HPMC/sodium alginate mixtures had initial viscosities ranging from 2-3 Pas, which is consistent with the final viscosity of previously reported *in-situ* ophthalmic gels; therefore, these viscosities would be too high to be easily administered at room temperature (Al-Kassas & El-Khatib, 2009; Gupta et al., 2007; Liu et al., 2010; Srividya et al., 2001). Of all the mixtures, P16 had the lowest viscosity before the addition of STF and the largest gelation capacity, yielding a 9.2 fold increase at 35°C and a 9.4 fold increase at 25°C. The second highest gelation increase was produced by P13, resulting in a 5.6 (35°C) and 3.6 fold (25°C) increase in viscosity. P17 increased by of 4.7 (35°C) and 2 (25°C) fold, respectively. Similarly, P12 increased by 2.6 (35°C) and 2 (25°C) fold, while P15 did not display an increase at either temperature, since it contained an inadequate amount of sodium alginate. All of the placebo formulations displayed a slightly lower initial viscosity at 35°C due to the fact that alginate viscosity decreases as

temperature increases (Alginate Industry Co., 2018). The aforementioned placebo formulations were tested in triplicates and the average of the measurements was recorded as the viscosity.

Based on these results, rheology studies were conducted on nepafenac *in-situ* gel systems F15, F16, & F17 corresponding to the original formulations A15-A17 (Figure 4.2). HPMC was excluded from the formulations, as the placebo studies revealed that the addition of HPMC did not strengthen the gelation capacity of sodium alginate. All formulations had an increase in initial viscosity at both temperatures, due to the addition of drug; however, the gelation capacity of each formulation was not affected. As with the placebos, all formulations had a decrease in initial viscosity after heating to 35°C. Again, F15 did not display any gelation due to the low content of sodium alginate in the formulation. F16 and F17 both displayed good gelation capacity, meaning the formulation had a lower initial viscosity and once mixed with the STF the viscosity increased significantly. F16 maintained the highest increase viscosity after the addition of STF with a 31.9 times increase at 35°C and 10.5 times increase at 25°C. F17 had the second highest viscosity change, 3.8 time increase at 35°C and 2.4 times increase at 25°C. Even though F17 displayed the most viscous formulation following the addition of STF, the initial viscosity of F17 at administration room temperature was very viscous (~4Pas); therefore, it would not be easily administered. Finally, all *in-situ* gel systems had pseudoplastic flow, which is desirable for ophthalmic formulations. The nepafenac *in-situ* gel system rheology tests were conducted in triplicates for statistical analysis.

4.4.3 Particle Size

The particles sizes and polydispersity index (PDI) for all the *in-situ* gel systems and the commercial formulation, Nevanac®, are displayed in Table 4.2.

4.4.4 pH & Osmolality Measurement

The pH and osmolality of formulations F15-F17 were all within the normal tolerable range for ophthalmic formulations (Table 4.2) (Baranowski, Karolewicz, Gajda, & Pluta, 2014; McElhiney & American Pharmacists Association., 2013).

4.4.5 Ex-vivo Dialysis Membrane Release Experiments

The slope of the linear portion of the plot, from 0 to 8 hours, was used to calculate the release rate. All *in-situ* gel systems displayed a significantly higher diffusion rate compared to Nevanac® ($P<0.05$) (Figure 4.3), resulting in a 75%, 56%, and 62% drug release for F15, F16, and F17; respectively, while the commercial product only released 39%. The increased release rate is due to a higher solubilized fraction of nepafenac, thereby improving dissolution. All formulations displayed sustained release over the 24-hour period, without the occurrence of a burst effect. The Korsmeyer-Peppas (Peppas, 1985), Higuchi equation (Higuchi, 1961), Peppas-Stahlin (Peppas & Sahlin, 1989), and first order release (Wagner, 1969) equations were all applied to the release data for all *in-situ* gels and Nevanac®. The Korsmeyer-Peppas equation determines the mechanism of release from a hydrophilic matrix by solving for the value for *n;* where $n=0.5$ corresponds to Fickian diffusion, $n=1$ refers to zero order kinetics and $0.5<n<1$ describes non-Fickian diffusion. The Higuchi equation describes Fickian diffusion while the Peppas-Sahlin equation is a modified version of the Korsmeyer-Peppas model which describes a release mechanism that is dependent on both diffusion and relaxation of the polymer. The Peppas-Sahlin equation was initially determined to be the best-fit model for the *in-situ* gel systems based on the low standard error values of individual parameters and high R^2 values. Negative values were obtained for the relaxational constant, meaning that the diffusion mechanism dominated the release compared to the relaxational contribution of the polymer (Babu, 2016; Bacaita, Ciobanu, Popa, Agop, & Desbrieres, 2014). The values for the relaxational constant were considered negligible compared to the diffusion constant; therefore, the data could be fitted to the original

Korsmeyer-Peppas model to determine the type of diffusion involved in the release (Eq. 2). All *in-situ* gel systems displayed anomalous or non-Fickian diffusion since the calculated *n* values were greater than 0.5. This is due to the swelling of the sodium alginate following by the diffusion of drug from the alginate matrix (Mohanan & Vishalakshi, 2009). The commercial product, Nevanac®, contains Carbomer 974P which is a highly cross-linked bioadhesive polymer that enables near zero or anomalous release rate, this was confirmed by the *m* value given by the Korsmeyer-Peppas model (Nahid Sharmin, 2010). The values K_d, *n* and R^2 *for each formulation* are provided in Table 4.3.

4.4.6 Ex-Vivo Corneal Permeation Studies

All of the *in-situ* gel systems had a significantly higher permeation rate through the cornea compared to Nevanac® ($p<0.001$) (Figure 4.4). Again, all formulations displayed a slow steady permeation profile over the 24-hour period, without a burst effect. This observation is due to the slow release of drug through the *in-situ* gel matrix. The highest permeation was found using the F15 formulation due to the low viscosity both before and after the addition of STF ($P<0.05$). No significant difference was observed between the permeation rates of F16 and F17. Therefore, F16 will be used for perfusion studies as it contains the minimum amount of sodium alginate needed to produce a successful *in-situ* gel system for the sustained delivery of nepafenac. *In-situ* gel systems showed approximately 6 to 8 fold higher retention in the corneas as compared to Nevanac® ($P<0.001$) (Figure 4.5). This observation is a result of the increased solubility of the nepafenac due to complexation with HPβCD, permeation enhancement effect, which yielded increased corneal permeation of the drug.

4.4.7 Ex-Vivo Corneal Perfusion Studies

Ocular drug distribution studies were performed using the F16 formulation; as it displayed the lowest initial viscosity and largest increase in viscosity after mixing with STF and contained the

minimum amount of sodium alginate needed to form an ocular *in-situ* gel. F15 did not increase in viscosity after the addition of STF; due to the small amount of sodium alginate. Contrarily, F17 had a too viscous initial viscosity which would not be easily administered at room temperature. Perfusion studies revealed that an increase in the retention of the drug on the sclera ($P<0.001$) was achieved using F16, allowing for improved residence time of the formulation on the ocular surface. Additionally, the amount of nepafenac retained in the cornea was significantly higher for F16 compared to Nevanac® ($P<0.001$). This is because after the STF interacts with the *in-situ* gel system, it rapidly forms a gel allowing for longer retention on the scleral surface. An increased accumulation of nepafenac in the posterior segment of the eye (ciliary body, sclera, choroid, and retina) was achieved by the in-situ gel system compared to Nevanac® (Figure 4.6). Nepafenac was not detected in the vitreous humor or lens. This increase in posterior drug concentration is due to the permeation enhancing effects of the HPβCD complexation allowing nepafenac to permeating deeper into the posterior tissues.

Previous work, which studied the impact of ocular perfusion after intravitreal and suprachoroidal administration, used the same model in isolated perfused pig eyes as in the current work. The main conclusion of this paper showed no significant differences in tissue dye concentrations in nonperfused eyes compared to perfused eyes following hydrophilic drug delivered intravitreally or with a lipophilic drug, injected either intravitreally or into the suprachoroidal space (Abarca et al., 2013). Therefore, there the dynamics of the perfusion fluid have no significant effect on drug permeation, other than keeping the ocular globe viable during the study period. The extraction efficiency for all tissues was over 80% with the exception of the lens (58.89 ± 4.49), sclera (40.08 ± 5.67) and vitreous humour (33.02 ± 7.02). The lens and vitreous humor disintegrated and formed a gelatinous substance upon mixing with the mobile phase; therefore, a low extraction efficiency resulted. Furthermore, the sclera was the largest quantity of tissue and is extremely

hydrophobic, leading to a low extraction efficiency as the drug is retained in the hydrophobic tissue.

4.5 Conclusions

Ion-activated *in-situ* gel systems for the enhanced retention of nepafenac on the corneal surface were formulated. Mixtures containing HPMC produced high viscosity formulations that could not be easily administered at room temperature; therefore, *in-situ* gel systems were formulated with sodium alginate only for the remainder of the studies. The addition of the nepafenac yielded an increased initial viscosity in all of the *in-situ* gel systems. All formulations displayed release kinetics followed by analogous diffusion as described by the Korsmeyer-Peppas equation. Permeation studies using porcine corneas revealed that all *in-situ* gel systems had significantly higher permeation and retention in the cornea compared to Nevanac®. Ocular drug distribution studies, using the *in-situ* gel system in whole porcine eye perfusion showed a significantly higher amount of drug retained by many of the ocular tissue as compared to Nevanac®. Therefore, an increased accumulation of drug in the posterior segment was achieved using the *in-situ* gel system compared to Nevanac®. Also, an ion-activated *in-situ* gel system, using Protanal PH 1033, yielded the sustained release of nepafenac to the cornea.

4.6 Acknowledgements

Authors acknowledge FMC Biopolymer and Auburn University Lambert-Powell Meats Laboratory for their generosity. Authors also acknowledge the financial support provided by the intramural grant program of the Auburn University.

4.7 References

Abarca, E. M., Salmon, J. H., & Gilger, B. C. (2013). Effect of Choroidal Perfusion on Ocular Tissue Distribution After Intravitreal or Suprachoroidal Injection in an Arterially Perfused Ex Vivo Pig Eye Model. *Journal of Ocular Pharmacology and Therapeutics, 29*(8), 715-722. doi:10.1089/jop.2013.0063

Al-Kassas, R. S., & El-Khatib, M. M. (2009). Ophthalmic controlled release in situ gelling systems for ciprofloxacin based on polymeric carriers. *Drug Delivery, 16*(3), 145-152. doi:10.1080/10717540802689008

Alginate Industry Co., L. (2018). Property of Alginate. Retrieved from http://www.iroalginate.com/property.htm

Almeida, H., Amaral, M. H., Lobao, P., & Lobo, J. M. S. (2014). In situ gelling systems: a strategy to improve the bioavailability of ophthalmic pharmaceutical formulations. *Drug Discovery Today, 19*(4), 400-412. doi:10.1016/j.drudis.2013.10.001

Anderson, D. M., Brydon, W. G., Eastwood, M. A., & Sedgwick, D. M. (1991). Dietary effects of sodium alginate in humans. *Food Addit Contam, 8*(3), 237-248. doi:10.1080/02652039109373974

Asasutjarit, R., Thanasanchokpibull, S., Fuongfuchat, A., & Veeranondha, S. (2011). Optimization and evaluation of thermoresponsive diclofenac sodium ophthalmic in situ gels. *Int J Pharm, 411*(1-2), 128-135. doi:10.1016/j.ijpharm.2011.03.054

Babu, B. R. B. a. K. N. (2016). Calculation of predominant drug release mechanism using Peppas-Sahlin

model (substitution method): A linear regression approach. *International Journal of Pharmacy, 6*(4), 128-137.

Bacaita, E. S., Ciobanu, B. C., Popa, M., Agop, M., & Desbrieres, J. (2014). Phases in the temporal multiscale evolution of the drug release mechanism in IPN-type chitosan based hydrogels. *Physical Chemistry Chemical Physics, 16*(47), 25896-25905. doi:10.1039/c4cp03389b

Baranowski, P., Karolewicz, B., Gajda, M., & Pluta, J. (2014). Ophthalmic Drug Dosage Forms: Characterisation and Research Methods. *Scientific World Journal*. doi:Artn 861904

10.1155/2014/861904

Cohen, S., Lobel, E., Trevgoda, A., & Peled, Y. (1997). A novel in situ-forming ophthalmic drug delivery system from alginates undergoing gelation in the eye. *Journal of Controlled Release, 44*(2-3), 201-208. doi:Doi 10.1016/S0168-3659(96)01523-4

Edman, P. (1993). *Biopharmaceutics of ocular drug delivery*. Boca Raton, Fla.: CRC Press.

Efron, N., Young, G., & Brennan, N. A. (1989). Ocular Surface-Temperature. *Current Eye Research, 8*(9), 901-906.

Gupta, H., Aqil, M., Khar, R. K., Ali, A., Bhatnagar, A., & Mittal, G. (2015). An alternative in situ gel-formulation of levofloxacin eye drops for prolong ocular retention. *Journal of Pharmacy and BioAllied Sciences, 7*(1), 9-14. doi:10.4103/0975-7406.149810

Gupta, H., Jain, S., Mathur, R., Mishra, P., Mishra, A. K., & Velpandian, T. (2007). Sustained ocular drug delivery from a temperature and pH triggered novel in situ gel system. *Drug Delivery, 14*(8), 507-515. doi:10.1080/10717540701606426

Haley Shelley, M. G., Forrest T. Smith, Eva M. Abarca, R. Jayachandra Babu. (2018). Improved Ocular Delivery of Nepafenac by Cyclodextrin Complexation. *AAPS PharmSciTech*. doi:10.1208/s12249-018-1094-0

Higuchi, T. (1961). Rate of Release of Medicaments from Ointment Bases Containing Drugs in Suspension. *Journal of Pharmaceutical Sciences, 50*(10), 874-&. doi:DOI 10.1002/jps.2600501018

Liu, Y. J., Liu, J. P., Zhang, X. L., Zhang, R. D., Huang, Y. L., & Wu, C. J. (2010). In Situ Gelling Gelrite/Alginate Formulations as Vehicles for Ophthalmic Drug Delivery. *AAPS PharmSciTech, 11*(2), 610-620. doi:10.1208/s12249-010-9413-0

Liu, Z., Li, J., Nie, S., Liu, H., Ding, P., & Pan, W. (2006). Study of an alginate/HPMC-based in situ gelling ophthalmic delivery system for gatifloxacin. *Int J Pharm, 315*(1-2), 12-17. doi:10.1016/j.ijpharm.2006.01.029

Liu, Z. D., Li, J. W., Nie, S. F., Liu, H., Ding, P. T., & Pan, W. S. (2006). Study of an alginate/HPMC-based in situ gelling ophthalmic delivery system for gatifloxacin. *International Journal of Pharmaceutics, 315*(1-2), 12-17. doi:10.1016/j.ijpharm.2006.01.029

Mains, J., Tan, L. E., Wilson, C., & Urquhart, A. (2012). A pharmacokinetic study of a combination of beta adrenoreceptor antagonists - In the isolated perfused ovine eye. *European Journal of Pharmaceutics and Biopharmaceutics, 80*(2), 393-401. doi:10.1016/j.ejpb.2011.11.006

Makwana, S. B., Patel, V. A., & Parmar, S. J. (2016). Development and characterization of in-situ gel for ophthalmic formulation containing ciprofloxacin hydrochloride. *Results Pharma Sci, 6*, 1-6. doi:10.1016/j.rinphs.2015.06.001

Mandal, S., Thimmasetty, M. K., Prabhushankar, G., & Geetha, M. (2012). Formulation and evaluation of an in situ gel-forming ophthalmic formulation of moxifloxacin hydrochloride. *Int J Pharm Investig, 2*(2), 78-82. doi:10.4103/2230-973X.100042

McElhiney, L. F., & American Pharmacists Association. (2013). *Compounding guide for ophthalmic preparations*. Washington, D.C.: American Pharmacists Association.

Mohanambal, E., Arun, K., & Sathali, A. A. H. (2011). Formulation and Evaluation of pH-triggered in situ Gelling System of Levofloxacin. *Indian Journal of Pharmaceutical Education and Research, 45*(1), 58-64.

Mohanan, A., & Vishalakshi, B. (2009). Swelling and Diffusion Characteristics of Interpenetrating Network Films Composed of Sodium Alginate and Gelatin: Transport of Azure B.

International Journal of Polymeric Materials, 58(11), 561-580. doi:10.1080/00914030903035469

Nahid Sharmin, M. E. A. M., Reza-Ul Jalil. (2010). A Novel Method to Study the Effect of pH and Excipients on Water

Uptake and Swelling Behaviour of Carbopol Polymers *Bangladesh Pharmaceutical Journal, 13*(2), 1-7.

Patel, A., Cholkar, K., Agrahari, V., & Mitra, A. K. (2013). Ocular drug delivery systems: An overview. *World J Pharmacol, 2*(2), 47-64. doi:10.5497/wjp.v2.i2.47

Pawar, P., Kashyap, H., Malhotra, S., & Sindhu, R. (2013). Hp-beta-CD-Voriconazole In Situ Gelling System for Ocular Drug Delivery: In Vitro, Stability, and Antifungal Activities Assessment. *BioMed Research International*. doi:Artn 341218

10.1155/2013/341218

Peppas, N. A. (1985). Analysis of Fickian and Non-Fickian Drug Release from Polymers. *Pharmaceutica Acta Helvetiae, 60*(4), 110-111.

Peppas, N. A., & Sahlin, J. J. (1989). A Simple Equation for the Description of Solute Release .3. Coupling of Diffusion and Relaxation. *International Journal of Pharmaceutics, 57*(2), 169-172. doi:Doi 10.1016/0378-5173(89)90306-2

S.B. Makwana, V.A. Patel, & Parmar, S. J. (2015). Development and Characterization of in-situ gel for ophthalmic formulation containing ciproflaxin hydrochloride. *Results in Pharma Sciences*. doi:10.1016/j.rinphs.2015.06.001

Sawarkar, S., Ravikumar, P., & Pashte, S. (2016). In-Situ Ophthalmic Gel Forming Solution of Moxifloxacin Hydrochloride for Sustained Ocular Delivery. *International Journal of Pharmaceutical Sciences and Research, 7*(3), 1192-1205. doi:10.13040/Ijpsr.0975-8232.7(3).1192-05

Srividya, B., Cardoza, R. M., & Amin, P. D. (2001). Sustained ophthalmic delivery of ofloxacin from a pH triggered in situ gelling system. *Journal of Controlled Release, 73*(2-3), 205-211.

Szekalska, M., Pucilowska, A., Szymanska, E., Ciosek, P., & Winnicka, K. (2016). Alginate: Current Use and Future Perspectives in Pharmaceutical and Biomedical Applications. *International Journal of Polymer Science*. doi:Artn 7697031

10.1155/2016/7697031

Wagner, J. G. (1969). Interpretation of percent dissolved-time plots derived from in vitro testing of conventional tablets and capsules. *J Pharm Sci, 58*(10), 1253-1257.

Table 4.1 Combinations of HPMC & alginates formulations for gelation capacity

Formulation	HPMC Grade	HPMC (w/v%)	Alginate (w/v%)	Gelling Capacity
A1	**--**	**--**	**0.2**	**+**
A2	**--**	**--**	**0.35**	**+**
A3	**E15**	**4**	**0.2**	**-**
A4	**E15**	**6**	**0.2**	**++**
A5	**E50**	**1**	**0.2**	**++**
A6	**E50**	**2**	**0.2**	**++**
A7	**E50**	**3**	**0.2**	**++**
A8	**--**	**--**	**0.4**	**+**
A9	**E15**	**1**	**0.5**	**+++**
A10	**E50**	**1**	**0.5**	**+++**
A11	**K4M**	**1**	**0.5**	**+++**
A12	**E15**	**0.5**	**0.5**	**+++**
A13	**E50**	**0.5**	**0.5**	**+++**
A14	**K4M**	**0.5**	**0.5**	**+++**
A15	**--**	**--**	**0.1**	**+**
A16	**--**	**--**	**0.3**	**+**
A17	**--**	**--**	**0.5**	**+++**

Note: +: gels rapidly, dissolves after minutes; ++: gels instantly, remains a gel for hours; +++: gels instantly, remains a gel for more than 8 hr; -: no gelation occurred

Table 4.2: Characteristics and properties of each nepafenac formulation

Formulation	% Protanal PH 1033	mOsm/kg	pH	Particle Size(μm)	PDI %
Nevanac	**-**	**305**	**7.4**	**2.0**	**1.525**
F15	**0.1**	**319**	**5.63**	**4.7**	**1.094**
F16	**0.3**	**363**	**5.62**	**2.0**	**1.158**
F17	**0.5**	**342**	**5.73**	**0.7**	**0.736**

Table 4.3: Parameters derived from Korsmeyer-Peppas equation for each nepafenac formulation

Formulation	K_d	n	R^2
F15	**4.349E-02**	**0.7505**	**0.9745**
F16	**4.714E-02**	**0.6565**	**0.9963**
F17	**4.584E-02**	**0.6790**	**0.9966**
Nevanac 0.1% ®	**3.267E-02**	**0.6559**	**0.9262**

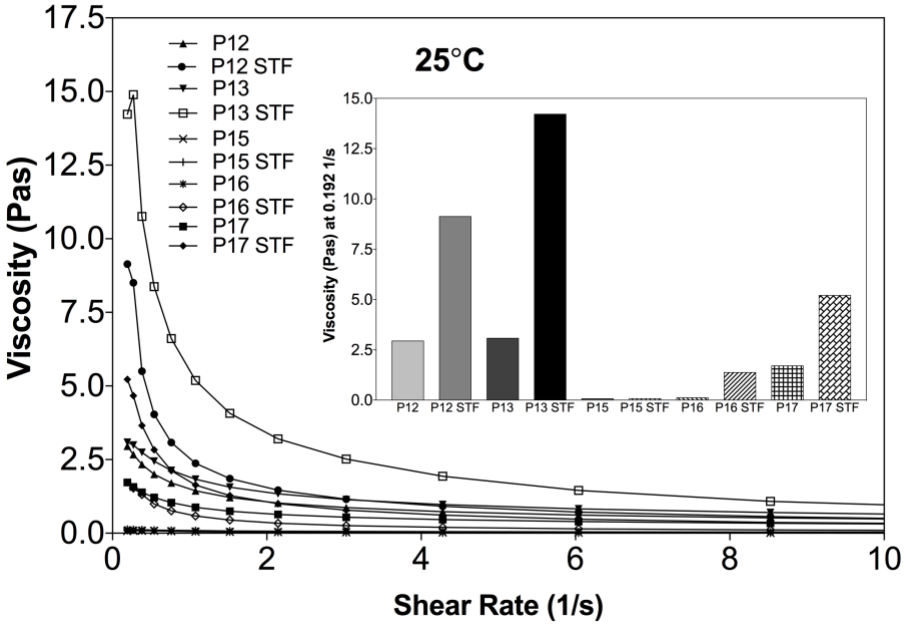

ii

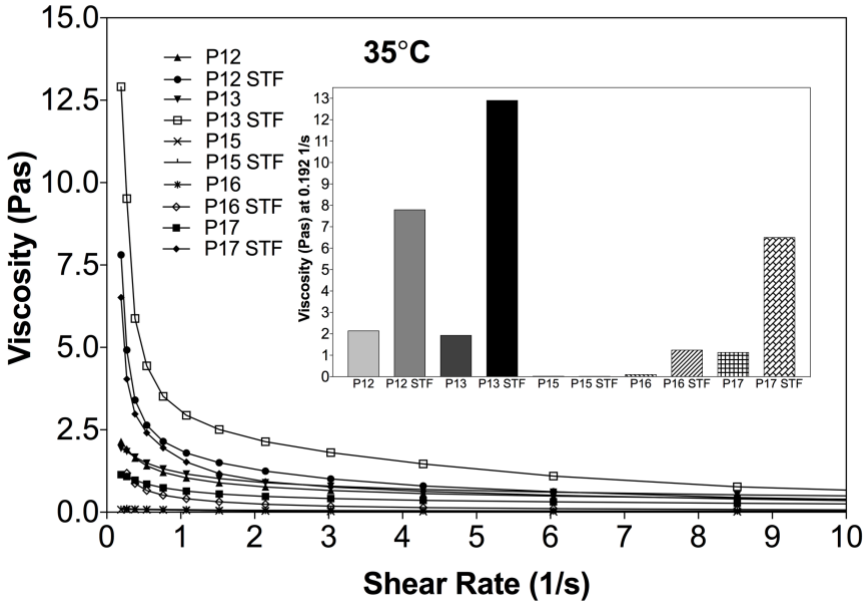

Figure 4.1: Rheology studies conducted on placebo formulations before and after the addition of STF at 25°C (left) and 35°C (right). Inset of viscosity at specific shear rate ($0.192s^{-1}$).

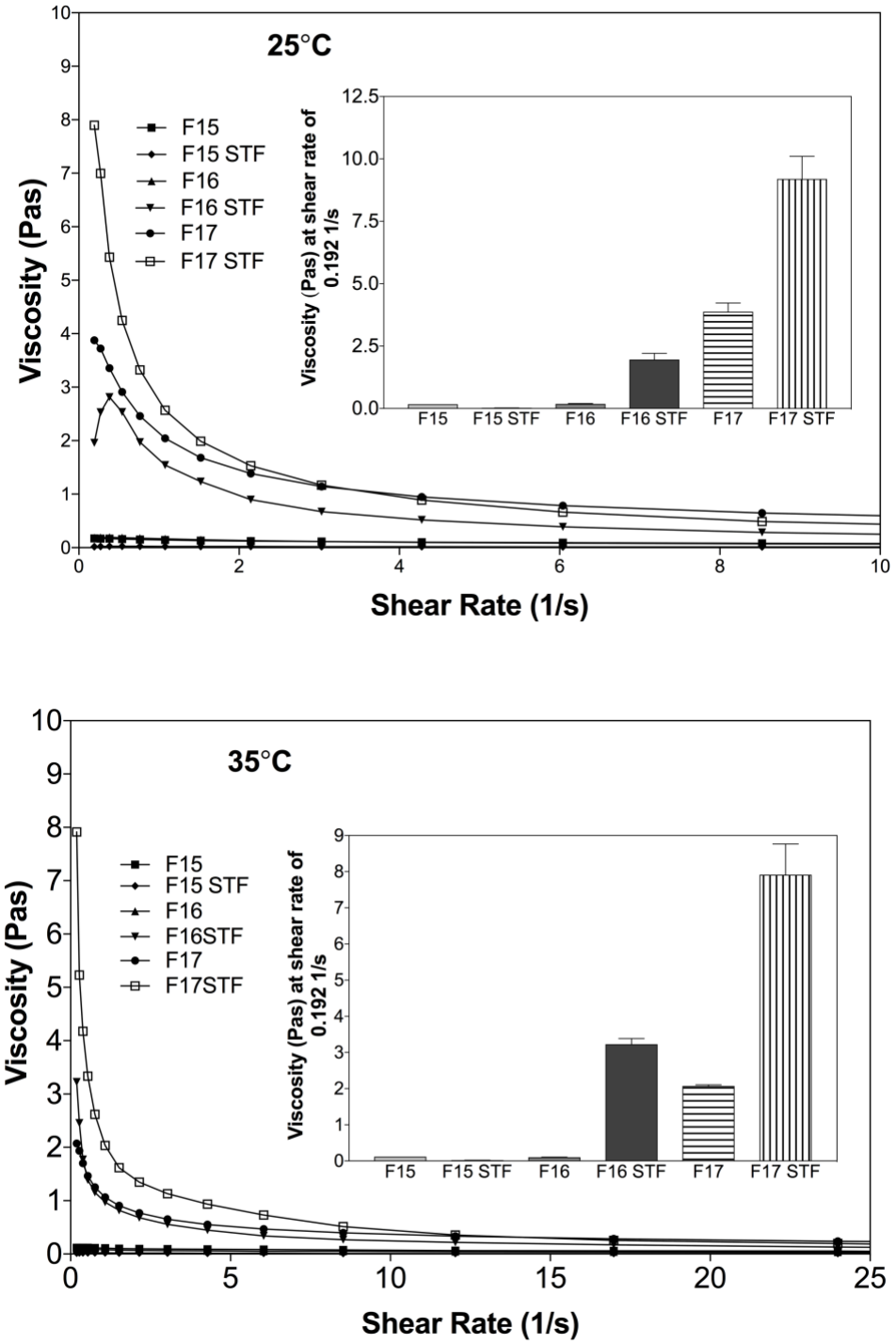

Figure 4.2: Rheology studies conducted on nepafenac in-situ gel systems before and after the addition of STF at 25°C (left) and 35°C (right). Inset of viscosity at specific shear rate ($0.192s^{-1}$).

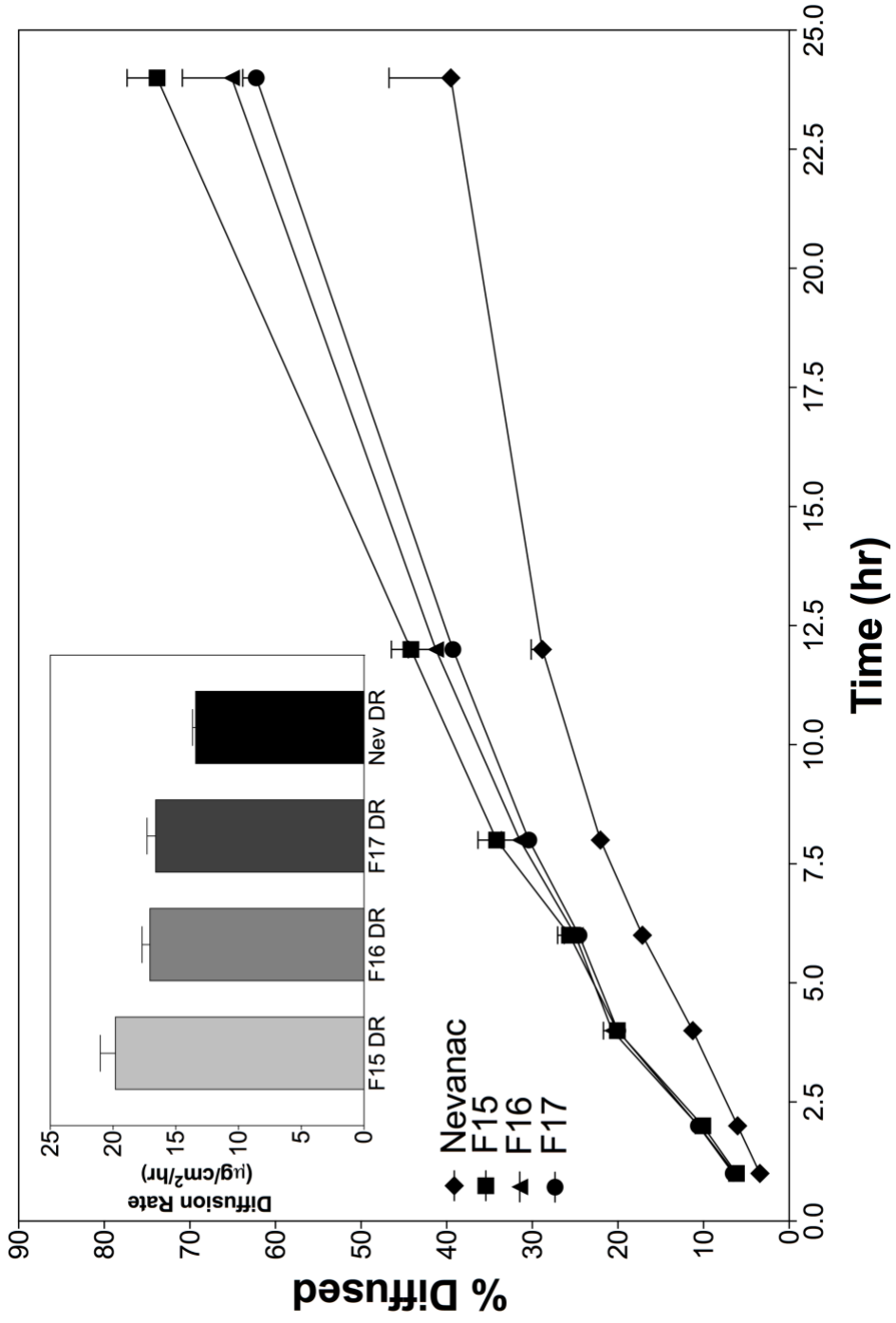

Figure 4.3: Nepafenac In-situ gel system release studies across dialysis membranes; Inset: diffusion rate.

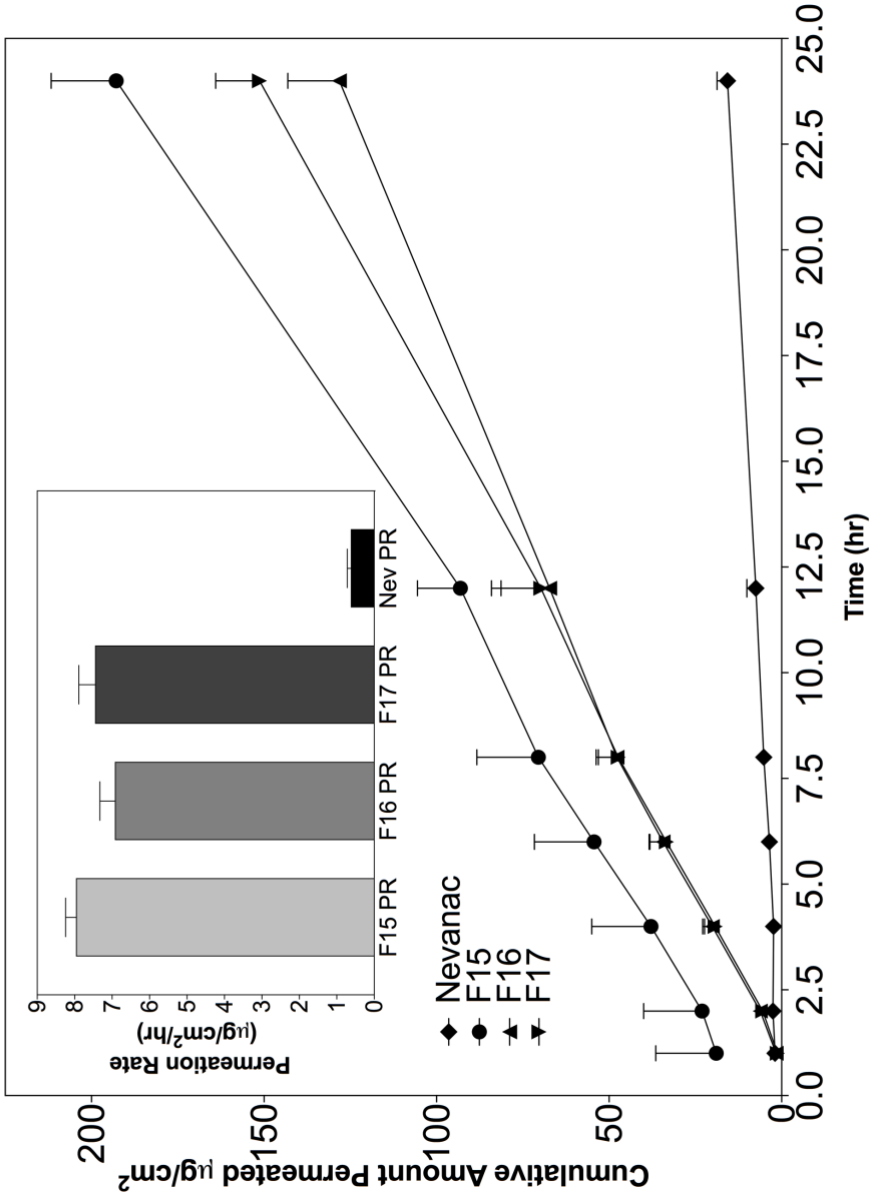

Figure 4.4: Permeation of Nepafenac in-situ gel system across porcine cornea; Inset: Permeation rate (steady state flux).

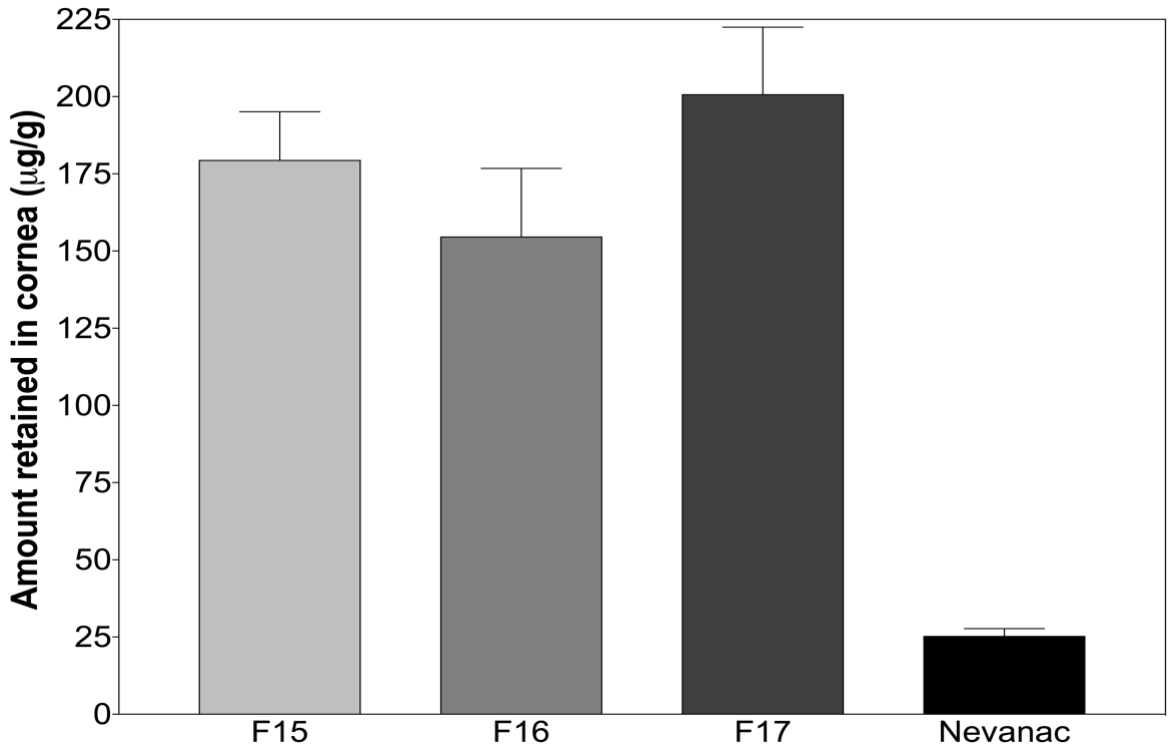

Figure 4.5: Corneal retention of nepafenac from applied in-situ gel systems and the commercial product.

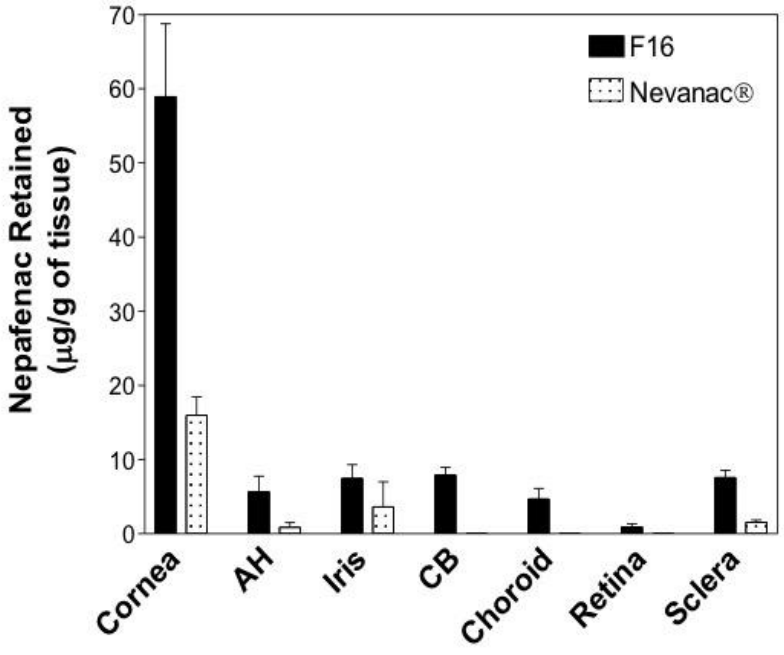

Figure 4.6: Ocular distribution of Nepafenac in isolated porcine eyes in a continuous perfusion model. The experiments were terminated after 2 hours. Nepafenac in various ocular tissues was quantified. [CO, Cornea; AH, Aqueous Humour; L, Lens; I, Iris; CB, Ciliary Body; C, Choroid; R, Retina; S, Sclera].

Chapter 5. Characterization of Difluprednate-Hydroxypropyl-β-Cyclodextrin Inclusion Complex for Ocular Delivery

5.1 Abstract

Difluprednate (DFP) is a recently approved corticosteroid used to treat pain and inflammation of the eye following ocular surgeries. This study characterizes hydroxypropyl-β-cyclodextrin (HPBCD)-DFP inclusion complex in the liquid and solid states for improved ocular delivery of DFP. The phase solubility profile of HPBCD and DFP provided an Ap-type relationship. Molecular docking studies, differential scanning calorimetry (DSC), and Fourier transform infrared spectroscopy (FT-IR), all suggested the solid state complexation of DFP with HPBCD. Difluprednate 0.05% ophthalmic solution was formulated using HPBCD, which provided 16 and 26 times higher trans-corneal permeation when compared to the suspension (no HPBCD) and Durezol®, respectively ($P<0.001$). Additionally, ocular drug distribution studies conducted in continuously perfused whole porcine eyes showed DFP permeated into all of the ocular tissues in much higher amounts than Durezol®. The ophthalmic solution based on HPBCD in this study is iso-osmotic, safe and very effective as compared to Durezol®.

5.2 Introduction

Difluoroprednisolone butyrate acetate, or difluprednate (DFP), is a corticosteroid prodrug that is rapidly metabolized to difluoroprednisolone butyrate by deacetylation after penetration into the eye and was approved for treatment of anterior uveitis in 2008 (Tajika, Isowaki, & Sakaki, 2011). Anterior uveitis is the inflammation of the middle layer of the eye: iris and ciliary body (Figure 5.1). Difluprednate is the first strong ophthalmic steroid to be developed in the past four decades and the first to be approved for both postoperative pain and inflammation (Jamal & Callanan, 2009; Korenfeld et al., 2009; Mulki & Foster, 2011). Prednisolone acetate (Pred Forte 1%™) remains the gold standard for topical anti-inflammatory treatment for uveitis; however, it has not been shown to effectively reduce pain. When compared to prednisolone, DFP is noninferior when dosed half as often (4 vs. 8 times a day) and has a comparable safety profile (Foster et al., 2010). Additionally, DFP has a 56 times stronger glucocorticoid binding affinity than prednisolone, which yields higher specificity, better tissue penetration and greater potency (Donnenfeld, 2011; Tajika, Waki, Tsuzuki, Kida, & Sakaki, 2011). Also, it was shown that DFP was faster at reducing all patients' symptoms such as: lacrimation, ocular pain, photophobia, and blurry vision (Foster et al., 2010) and visual rehabilitation, when compared to prednisolone (Mulki & Foster, 2011).

Due to the extreme low water solubility of DFP (0.0097mg/mL), the only commercial formulation is a 0.05% oil-in-water ophthalmic emulsion, Durezol®. Emulsions are a superior delivery system to suspensions; however, they still have the disadvantage of instability due to creaming, coalescence, and flocculation which can lead to dosing errors (Jamal & Callanan, 2009). Furthermore, all liquid ophthalmic preparations lack long residence time, meaning they need to be administered by the patient multiple times a day (Sultana, Jain, Aqil, & Ali, 2006). However, it is better for the drug to be in solution when administered to the eye, as it helps bypass the multiple layers of the tear film and tissues, successfully reaching the anterior uvea. Since DFP is an

extremely lipophilic compound, it would be beneficial if this drug is presented to eye as a hydrophilic caged compound using cyclodextrins, yielding better solubility and ocular absorption. To date, only emulsion formulation has been attempted for DFP and this was prior to drug approval in 2008, thus the alternative formulation possibilities using DFP are relatively unexplored (Yamaguchi et al., 2005).

Cyclodextrins are cyclic oligosaccharides with a truncated cone structure, having a hydrophobic inner surface and a hydrophilic outer shell. These unique structural features enable trapping hydrophobic drug molecules of appropriate dimensions in their hydrophobic domains (Hayiyana et al., 2016; Vieira et al., 2015). The physical entrapment (inclusion complexation) increases water solubility, dissolution, rate, stability, and bioavailability of drug molecules (Del Valle, 2004; Liu & Guo, 2002; Malaquias et al., 2018). In the case of ocular drug delivery, a drug must possess both lipophilic and hydrophilic properties in order to successfully penetrate through the tear film layers, which are comprised of both lipid and aqueous layers. Cyclodextrins have been proven to provide enhanced permeation of complexed drug molecules, giving way for improved delivery through the tear film, yielding higher bioavailability at the corneal epithelium (Loftsson & Stefansson, 2007; Tiwari, Tiwari, & Rai, 2010; Uekama, 2004). Additionally, cyclodextrins avoid disruption of the ocular barrier like traditional permeation enhances. Instead, cyclodextrins alter the biological membrane by interacting with the membrane (Challa, Ahuja, Ali, & Khar, 2005; Tiwari et al., 2010).

Hydroxypropyl-β-cyclodextrin (HPBCD) is a highly-water soluble derivative of the parent molecule, β-cyclodextrin. Research suggests that when an ophthalmic formulation containing HPBCD is applied to the eye, the HPBCD does not pass through the corneal epithelium due to the low affinity between the hydrophobic ocular membrane and hydrophilic cyclodextrin (Loftsson & Stefansson, 1997). Therefore, the cyclodextrin is drained via the nasolacrimal duct to the gastrointestinal tract. Additionally, no damage occurs in the gastrointestinal tract, as normal usage

of HPBCD is less than 1/10th of the toxic level (1.7mg/kg/day) (Loftsson & Jarvinen, 1999). Studies conducted on rabbits revealed that HPBCD was nontoxic and well tolerated up to a concentration of 45% (Jansen, Xhonneux, Mesens, & Borgers, 1990; Javitt, Javitt, & Mcdonnell, 1994). Thus, we hypothesize DFP can be encapsulated within the hydrophobic HPBCD core, yielding an increase in drug water solubility, allowing for the preparation of an ophthalmic solution formulation. The complex allows the drug to be transported via HPCBD across through the lipid, aqueous and mucin layers of the tear fluid to the lipophilic corneal epithelium. This leads to an increase in the amount of drug absorbed to the cornea, without causing irritation or blurred vision, producing a more desirable formulation for patients. Therefore, in this study, DFP-HPBCD complexation was characterized for improved water solubility and subsequent ocular bioavailability. The DFP properties were advantageously modified to achieve better permeation across ocular tissue to enable a non-inferior ophthalmic solution formulation at a lower dose.

5.3 Experimental Methods

5.3.1 Materials

Difluprednate was purchased from Chemieliva Pharmaceutical CO., LTD., Chongqing China. Trappsol hydroxypropyl-β-cyclodextrin was obtained from CTD Inc. (Alachua, FL). Sodium Chloride USP and Ethyl Alcohol (200 proof) USP were purchased from Letco Medical. Benzalkonium Chloride (BKC) NF was purchased from Spectrum Chemical Mfg. Corp (Gardena, CA). All solvents used for high performance liquid chromatography (HPLC) were of analytical or HPLC grade, were purchased from VWR Scientific (Atlanta GA).

5.3.2 Preparation of the Difluprednate/ HPBCD Mixtures

5.3.2.1 Dry Mixture (DM)

The dry mixture (DM) of DFP and HPBCD was prepared by gently mixing 1:2 molar amounts of drug and HPBCD with a mortar and pestle until a homogenous mixture was produced. The mixture was then stored in a glass vial at ambient temperature until needed for analysis.

5.3.2.2 Kneaded Mixture (KM)

The kneaded mixture (KM) of DFP and HPBCD was prepared by adding 50:50 methanol:H_2O dropwise to an 1:2 molar mixture of drug and HPBCD until a homogenous paste is formed. The mixture was then left in a desiccator overnight until a dry mixture is obtained; the subsequent mixture was stored in a glass vial at ambient temperature until needed for analysis.

5.3.2.3 Rotary Evaporation Mixture (RM)

HPBCD was added to a solution of DFP in 50:50 methanol:acetonitrile at 1:2 molar ratio (DFP to HPBCD). The solution was then placed in a Buchi Rotovapor R-210 for 30 minutes at 40°C in vacuum. Once the solvent had evaporated completely, the flask was placed in the desiccator for 24 hours until a dry flaky mixture was obtained. The mixture was collected, gently powdered and stored in a glass vial at ambient temperature until needed for analysis.

5.3.3 Phase Solubility Studies

Phase solubility studies on DFP with HPBCD were performed according to Higuchi and Connors (Higuchi & Connors, 1965). Increasing molar concentrations (25, 50, 100, 150, 200, 250 mM) of HPBCD were dissolved in 1mL of water in 5mL polypropylene tubes. Excess amounts of DFP (above the solubility limit) were added to the HPBCD solutions and then sonicated for 30 minutes. The mixtures were then placed on a magnetic stirrer for 24 hours. The mixtures were then left on the benchtop for 24 hours for equilibration. Following equilibration, the mixtures were filtered using 0.45 micron nylon membrane filters, diluted appropriately and analyzed for DFP concentration by HPLC.

According to Higuchi and Connors, the rate constants of positive-type relationship can be determined if it is assumed that there are two types of complexations taking place (Higuchi & Connors, 1965). The following second order polynomial equation can be applied to positive-type phase solubility data to obtain the unknown parameters:

$$S_t = S_0 + K_{1:1}S_0(L) + K_{1:1}K_{1:2}S_0(L)^2 \qquad \text{Eq. 1}$$

In this expression S_t is the total solubilized concentration of DFP, L is the HPBCD concentration, S_0 is the solubility of free DFP in the absence of HPBCD, $K_{1:1}$ and $K_{1:2}$ *refers* to the stability constant of 1:1 and 1:2 complexes, respectively. Using Eq. 1, the complexation efficiency (*CE*) for each complex between HPBCD and DFP:

$$CE = \frac{K}{S_o} \qquad \text{Eq. 2}$$

Furthermore, the change in Gibbs free energy was calculated:

$$\Delta G = -RTlnK \qquad \text{Eq. 3}$$

Where, R is the ideal gas constant (8.314 J/molK) and T is the temperature (295 K).

5.3.4 High Performance Liquid Chromatography (HPLC) Analysis

An Alliance Waters e2695 Separations Module and a Waters 2998 Photodiode Array Detector was used for quantifying DFP in various formulations and their release and permeation experiments. The HPLC system was interfaced with a workstation installed with Empower 3 software. A Luna C18 (2) 5µm, 150mm x 4.60mm reverse-phase HPLC column was used. The mobile phase consisted of 60:40 acetonitrile: phosphate buffer (10mM, pH=6). Samples were eluted at a flow rate of 1mL/min at ambient temperature. The absorbance wavelength was set at 254nm, with an injection volume of 10 µl.

5.3.5 Characterization of Difluprednate/HPBCD Complex in the solid state

5.3.5.1 Differential Scanning Calorimetry (DSC)

DSC analysis of DFP, HPBCD and various mixtures (DM, KM, RM) were performed using a 2910 differential scanning calorimeter (TA Instruments). Samples were weighed (~10 mg) and placed in a non-hermetic aluminum pans and sealed with an encapsulating press. The samples were heated under an inert atmosphere of nitrogen with a temperature range of 30-220°C with a scanning rate of 10°C/min. Empty aluminum pans were used as a reference.

5.3.5.2 Molecular Docking

HPBCD and DFP were prepared using the 2D sketcher on Maestro, these were subsequently minimized utilizing the OPLS3 force field. The HPBCD was submitted to the protein preparation wizard and the output was used to create the grid file for docking by Glide. The DFP was submitted to Ligprep and the resulting output file was implemented as the ligand for glide docking. The ligand and receptor were subsequently docked. An additional HPBCD molecule was added to the docked structure and the three structures were then solvated with water and submitted to a 100ns dynamics run using the program Desmond. All of the simulations were on Small-Molecule Drug Discovery Suit 2017-4, Schrödinger, LLC, New York, NY, 2018.

5.3.5.3 Fourier Transform Infrared Spectroscopy (FT-IR)

FT-IR spectra for DFP, HPBCD, and various mixtures (DM, KM, FD) were recorded using a Perkin Elmer Spectrum 400 FT-IR/FT-NIR Spectrophotometer with a resolution of 4cm^{-1} and the detector scanned from 4000 cm^{-1}-650 cm^{-1}.

5.3.6 Ex-vivo Dialysis Membrane Release Experiments

Franz diffusion cell apparatus was assembled to hold the dialysis membrane securely in position during the release experiments. The dialysis membranes (Regenerated cellulose, molecular weight cut off 14,000 Da, Fisher Scientific, Suwannee, GA) were soaked in water for 30 minutes prior to starting the experiments. The drug release from solution, suspension and Durezol® formulations were tested. Difluprednate solution was prepared by dissolving 0.05% DFP, 33.4% HPBCD, 0.27% ethanol, 0.01% benzalkonium chloride in water. The DFP suspension was prepared by dispersing 0.05% DFP in an aqueous solution containing 0.27% ethanol, 0.005% benzalkonium chloride. Osmolality of both the solution and suspension formulations was adjusted with sodium chloride to tolerate within the ophthalmic range (McElhiney & American Pharmacists Association., 2013). The receptor cell was filled with 5 mL PBS buffer (pH 7.4) containing 20% ethanol, the donor cell was filled with 0.5mL of the formulation; the cell was then covered with Parafilm®. The receptor cell was sampled (1 mL) at 1, 2, 4, 6, 8, 12, and 24 h replenished with fresh PBS buffer (pH 7.4) containing 20% ethanol. The samples were assayed by HPLC method as described earlier. Each formulation was tested in 4 replicates. The Korsmeyer-Peppas model was used to describe the drug release kinetics of various formulations (Peppas, 1985):

$$\frac{M_t}{M} = K_m t^n$$

In this expression, *Mt* is the cumulative drug released at a specific time, *M* is the total drug in the formulation, K_m is the kinetic constant, *n* is the release exponent; whereas a value of 0.5 for *n* indicated Fickian diffusion, 0.5<n<1 is non-Fickian diffusion and *n*=1 refers to zero order. The constant and exponent are the unknowns and can be calculated by fitting the experimental data to the aforementioned equation. Other models were tested as well to determine the best fitting model: Higuchi equation (Higuchi, 1961), Peppas-Sahlin (Peppas & Sahlin, 1989), zero and first order release (Wagner, 1969). The model that resulted in the smallest standard error for the individual parameters and highest R^2 value was determined to be the best fitting model.

5.3.7 Ex-vivo Corneal Permeation Experiments

5.3.7.1 Corneal Excision

Porcine eyes of either sex were obtained from Auburn University Lambert-Powell Meats Laboratory (Auburn University, Auburn AL) and stored at 4°C until needed. The animals were sacrificed according to the Institutional Animal Care and Use Committee (IACUC) approved protocol (SOP 2015-2727). The excess tissue was first cut from the globe and the corneas were excised from the globe using a 3.0 mm slit eagle blade to create an insertion point between the iris and the cornea. Corneal scissors were used to excise the cornea and the corneas were rinsed with tap water and then placed in phosphate buffered saline (PBS) at pH=7.4 until used in the permeation studies. The permeation studies began within 2 hours of excision.

5.3.7.2 Corneal Permeation Study

Franz Diffusion Cell apparatus was assembled to hold the cornea in position during the permeation experiments. The following formulations were tested: DFP solution, DFP suspension, and Durezol®. Each formulation was tested in 4 replicate permeation experiments. The receptor cell was filled with 5 mL PBS buffer (pH 7.4) containing 20% ethanol to maintain sink conditions (Chen, Chang, Lee, Javier, & Azar, 2002). The corneas were placed on the receptor cell with the outer surface of the cornea facing up, the donor cell was placed on top of the cornea and both half cells were clamped together. The donor cell was filled with 0.5mL of the formulation and covered with Parafilm®. The receptor cell was sampled (1 mL) at 1, 2, 4, 6, 8, 12, and 24 h, and replenished with fresh PBS buffer (pH 7.4) containing 20% ethanol. The samples were assayed by HPLC method as described earlier.

5.3.7.3 Extraction of Difluprednate from Corneas

Following the 24-hour permeation study, the formulation was removed from the donor chamber using a dropper pipette, and the cornea was cleaned with PBS buffer (pH 7.4) containing 20% ethanol, using cotton swabs. The active diffusion area of the cornea was cut, weighed, minced and placed in individual vials with 2mL of the HPLC mobile phase. The vials were then sonicated for 30 minutes and left to sit for 24 hours at 4^{o}C to extract any drug that is retained in the cornea. The vials were sonicated again for 30 minutes and then the supernatant was filtered through 0.45 µm Nylon membrane filter and assayed by HPLC.

5.3.8 Ocular Distribution of Difluprednate in Isolated Perfused Eyes

Porcine eyes of either sex were freshly obtained from Lambert-Powell Meats Laboratory (Auburn University, Auburn AL) immediately following euthanasia. The animals were sacrificed according to the Institutional Animal Care and Use Committee (IACUC) approved protocol (SOP 2015-2727). All eyes were used within 4 hours of euthanasia to maintain the integrity of the entire globe. The excess adnexal tissue was trimmed from the ocular globe and placed in PBS pH 7.4 until ready for perfusion (Abarca, Salmon, & Gilger, 2013). The eyes were perfused with Dulbecco's Modified Eagle's Medium F12 (DMEM) under constant O_2 supply. The perfusion began 30 minutes prior to the drug application and maintained throughout the entirety of the study. A major artery of each eye was identified, split open with a 3.0 mm slit Eagle blade, cannulated and secured in place with Scotch® super glue gel. The eyes were then placed in a stainless-steel strainer on top of a beaker, which allowed for the collection of the DMEM medium from the veins. An Ismatec® peristaltic pump (Cole-Parmer GmbH, Wertheim, Germany) was employed to perfuse the oxygenated DMEM through the cannulated eyes. As previously described, perfusion was started at a flow rate 0.25–0.8 mL/min and increased to 1 ml /min (Abarca et al., 2013; Mains, Tan, Wilson, & Urquhart, 2012). Adequate arterial perfusion was determined by observing flow of media exiting the vortex veins. The following formulations were tested: DFP solution, DFP

suspension, and Durezol®. 50 µL of the formulation was pipetted onto each of the corneas every 15 minutes for one hour. After two hours, the eyes were frozen instantly using CO_2 and then stored in a freezer at -80°C to prevent transfer of drug between tissues until needed for dissection. For dissection, the frozen eye was placed on a cold ceramic tile and all the ocular tissues were subsequently removed: cornea, aqueous humour, lens, iris, ciliary body, vitreous humour, sclera, retina and choroid. Each tissue was soaked in the HPLC mobile phase for 24 hours in individual vials, then filtered with 0.45 µm Nylon membrane filters and analyzed via HPLC.

5.3.8.1 Extraction Efficiency

The DFP extraction efficiency was determined for the aforementioned experimental method of DFP distribution in various ocular tissues. For these experiments, the tissues that were not in contact with DFP were exposed to 2 ml solution of DFP (10 µg/ml) in 60:40 acetonitrile: phosphate buffer. The recovery of DFP from the tissues was determined in 4 replicates for various tissues such as cornea, sclera, ciliary body, choroid, retina, iris, aqueous humour and vitreous humour. The frozen tissue samples were minced in 5 mL polypropylene tubes and added with 2 mL of DFP solution and sonicated for 30 min and stored overnight in the refrigerator. The following day, the samples were filtered using 0.45 micron Nylon membrane filters and assayed by HPLC. The DFP recovery (%) from the tissues was calculated as the ratio of the amount of DFP extracted from the spiked tissue to the amount of DFP extracted from the solution in the absence of the tissues but processed by the same procedure.

5.3.9 Statistical Analysis

All results are presented as mean ± standard error of mean (SEM). The calibration curve for difluprednate was tested over the following concentration range: 20-400µg/mL (slope: y=18005x; R=0.9998). The cumulative amount of drug permeated through unit area of cornea was plotted

as a function of time. *In vitro* steady-state flux was calculated from the slope of the linear portion of the plot. The amount of drug (mg) retained in the cornea was normalized to 1 gram of cornea. Analysis of variance was performed to determine the level of significance between the means. Mean differences with $P < 0.05$ were significant. Statistical analysis was performed using GraphPad Prism for Windows, GraphPad Software, La Jolla California USA.

5.4 Results & Discussion

5.4.1 Phase Solubility Studies

Phase solubility studies allow us to understand the complexation relationship between the drug and the cyclodextrin molecules. The results indicate a second order polynomial (A_P) type phase diagram, meaning more than one HPBCD molecule is needed to solubilize one DFP molecule (Higuchi & Connors, 1965). The data was fitted to the Higuchi equation, which describes positive-type relationships (Eq. 1) and is displayed in Figure 5.2. If two separate complexes are assumed, then a stability constant for each individual complex can be calculated. The stability constant for $K_{1:1}$ and $K_{1:2}$ are is $523M^{-1}$ and $54.7M^{-1}$ for PBS, respectively. The value for $K_{1:1}$ is indicative of strong association between DFP and HPBCD than $K_{1:2}$ suggesting the complexation that is responsible for improved dissolution is primarily the complex described by the rate constant, $K_{1:1}$ (Bramhane et al., 2016; Liao et al., 2016). The change in Gibbs free energy, ΔG, values were -15.30 kJ/mol and -9.78 kJ/mol, respectively for the 1:1 and 1:2 complex. The negative value is indicative of a spontaneous complex formation (Tang et al., 2015).

5.4.2 Characterization of Difluprednate/HPBCD Complex in the solid state

In order to characterize the solid state of the DFP-HPBCD complex, various solid-phase mixtures were prepared for DSC and FT-IR analysis(de Freitas et al., 2012). The dry mixture was prepared without the addition of aqueous/organic solvents, and the kneaded mix was prepared by adding

water/methanol since water is known to assist in the complexation of cyclodextrin molecules (Liu & Guo, 2002).

5.4.2.1 Differential Scanning Calorimetry (DSC)

The sharp endothermic peak at 191°C for DFP (1) represents the melting point of DFP (Figure 5.3). On the contrary, HPBCD (2) displays a broad endothermic peak between 40-100°C which is indicative of the loss of water molecules from the cyclodextrin cavity, upon the addition of heat (Oprean et al., 2016; Tang, Tang, et al., 2016). The dry (3) and kneaded (4) mixtures of DFP and HPBCD show the two original profiles superimposed upon one another, meaning there was no interaction between HPBCD and DFP (Tang, Ma, et al., 2016). This can be explained by the fact that in order for a complexation to occur between DFP and HPBCD some water must be included to initiate complexation (Alves-Silva, Sa-Barreto, Lima, & Cunha-Filho, 2014). Furthermore, the peak of DFP in the dry and kneaded mix is significantly smaller compared to DFP alone due to the higher concentration of HPBCD to the DFP. The DFP peak has completely disappeared in the rotovap mixture suggesting inclusion complex formation and the existence of a new solid phase.

5.4.2.2 Molecular Docking

The molecular docking simulation predicted that two cyclodextrins encapsulate both ends of the DFP molecular, leaving only the side ester chain exposed (Figure 5.4). The ester chain of the molecule is more nonpolar than the aromatic ring portion of the molecule. This is due to the fact that the more nonpolar side of the molecule will seek refuge in the hydrophobic core of the HPBCD more rapidly than the less polar side. Furthermore, the rate constant for the 1:1 complexation can be applied to the ester portion of the molecule and the 1:2 complexation rate constant can be assigned to the left portion of the molecule, containing the aromatic ring. Molecular docking has been applied to other experiments to show the orientation of complexation with HPBCD (Liao et

al., 2016; Matencio, Hernandez-Gil, Garcia-Carmona, & Lopez-Nicolas, 2017; Zhang, Liu, Yang, Chen, & Jiao, 2017).

5.4.2.3 Fourier transform infrared spectroscopy FT-IR

The infrared spectrum from FT-IR for DFP, HPBCD, dry, kneaded, and rotovap mixtures are shown in Figure 5.5. The HPBCD spectra reveals a broad peak at 3336.70 cm^{-1} representing the stretching vibration of the hydroxyl group. DFP has a characteristic peak at 1663.76 cm^{-1} which is representative of the unsaturated ketone/secondary carbonyl, while 1726.96-1754.77 cm^{-1} are the acyclic ketone and esters. The kneaded and dry mixes both display similar profiles that resemble the peaks seen in DFP alone; therefore, it can be said that these mixtures did not form a complex. For the rotovap mixture, the peak at 1754.77 cm^{-1} merges with peak 1726.96 cm^{-1}, while the remainder of the spectrum remains unchanged. This data suggests that the unsaturated ketone/secondary carbonyl is not complexed, whereas the acyclic ketone and esters section is complexed with the HPBCD. However, the molecular docking studies suggested the HPBCD molecules encapsulate both sides of the DFP molecule. This could be due to the fact that the stronger complex ($K_{1:1}$) is representative of the complexation of the more nonpolar (ester) side, while the weaker less frequent complex ($K_{1:2}$) represents the complexation of the aromatic ring side.

5.4.3 Ex-vivo Dialysis Membrane Release Experiments

The solution displayed a significantly higher release compared to the suspension and Durezol® ($P<0.05$). Specifically, the solution had a release rate 1.7 and 5 times higher than the suspension and Durezol®, respectively, as shown in Figure 5.6. The Korsmeyer-Peppas (Peppas, 1985), Higuchi equation (Higuchi, 1961), Peppas-Stahlin (Peppas & Sahlin, 1989), zero and first order release (Wagner, 1969) equations were all applied to the release data for the DFP formulations. The Korsmeyer-Peppas (Eq. 1) equation was determined to be the best fit model for the release

data from all formulations. The exponent of Eq. 1 describes the drug release mechanism; whereas a *n* value of 0.5 corresponds to Fickian diffusion, $n=1$ refers to zero order kinetics and $0.5<n<1$ described non-Fickian diffusion/anomalous release. Both Durezol® and the suspension had an *n* value of 1, meaning they both exhibit zero-order release. Durezol® is an oil-in-water emulsion; therefore, the zero-order release is observed due to the partitioning of the drug from the oil phase to the water phase to the receptor chamber. Additionally, zero order release is often used to describe suspensions because as the suspended particles dissolve, more drug is released from the suspended particles to maintain a constant diffusion gradient. The oil phase in the emulsion and the suspended particles in the suspension act as drug reservoirs, leading to zero-order release kinetics. The solution had a *n* value of 0.81, meaning the formulation displayed first order release kinetics. This is common for solution formulations as the drug particles initially move from a high concentration (donor chamber) to a low concentration (receptor chamber). The R^2 values for the solution, suspension and commercial product are 0.97, 0.99 and 0.94.

5.4.4 Corneal Permeation

The permeation profiles of DFP solution, suspension, and commercial formulation across isolated porcine corneas are shown in Figure 5.7. The solution accomplished improved corneal permeation compared to Durezol® ($P<0.001$). This observation is due to the fact that the complexation between HPBCD and DFP led to an increase in water solubility, which yielded enhanced permeability through ocular tissues (Abarca, Cuming, Duran, & Ramapuram, 2015; Adelli, Balguri, & Majumdar, 2015). The flux across the corneal tissue was 16 and 26 times higher for the solution, when compared the suspension (without HPBCD) and Durezol® ($P<0.05$). Furthermore, the amount of DFP retained in the cornea (μg/g) by the solution (108.3±26.2) was approximately 2.5 times higher than the suspension (37.0±11.2) and Durezol® (41.1±10.2), respectively (Figure 5.8).

5.4.5 Distribution of Nepafenac in Isolated Perfused Eyes

The Isolated perfused porcine eye model closely mimics in vivo conditions such as ocular temperature, circulation and tissue viability, which enables us to determine the distribution of DFP in the individual ocular tissues (Abarca et al., 2013). The solution and Durezol® formulations were both studied. The DFP suspension was excluded as there was no significant difference for corneal retention of the drug in the aforementioned corneal permeation studies. The extraction efficiency for all tissues was 86 to 98% with the exception of the vitreous humor (45.39%± 9.55%). The vitreous humor disintegrated and formed a gelatinous substance upon mixing with the mobile phase; therefore, a low extraction efficiency resulted. The following extraction levels (%) were observed for various tissues, cornea (95.8±0.79), aqueous humor (96.0±1.87), lens (90.2±2.10), iris (96.4±1.26), ciliary body (93.9±11.22), choroid (97.5±3.61), retina (86.6±3.76), sclera (98.4±1.34). As shown in Figure 5.9, the solution displayed drug detection in all ocular tissues while Durezol® had no detectable drug levels in the lens, iris, ciliary body, retina and choroid. This is due to the fact that topical formulations often display difficulty penetrating to the posterior segment because of the anterior permeation barriers, such as tear film layers, cornea and sclera (Gaudana, Ananthula, Parenky, & Mitra, 2010; Prausnitz & Noonan, 1998; Tahara, Karasawa, Onodera, & Takeuchi, 2017). Furthermore, the solution had a significantly higher corneal permeation compared to the Durezol® formulations ($P>0.001$). This is highly desirable because the cornea is the targeted site of action since DFP is rapidly metabolized to the active drug form in the corneal epithelium (Tajika, Isowaki, et al., 2011). This suggests that HPBCD served as both a drug solubilizer and permeation enhancer allowing the drug to penetrate deeper into tissues, bypassing the difficult ocular permeation barriers.

5.5 Conclusions

Phase solubility studies of the DFP:HPBCD complexation revealed a positive-type (Ap) relationship, solid-state characterization (DSC, FT-IR) confirms the existence of a new solid phase for the inclusion complex. The corneal permeation rate of the solution 16 was and 26 times higher than the suspension and Durezol®, respectively. Additionally, the amount of DFP retained in the cornea for the solution was approximately 2.5 fold higher than the suspension and Durezol ®, respectively. Additionally, ocular drug distribution studies conducted in continuously perfused whole porcine eyes showed DFP permeated in all of the ocular tissues in much higher amounts than Durezol®. The ophthalmic solution based on HPBCD in this study is iso-osmotic, safe and very effective as compared to Durezol®.

5.6 Acknowledgements

Authors acknowledge Dow Chemical Company and Auburn University Lambert-Powell Meats Laboratory for their generosity.

5.7 References

Abarca, E. M., Cuming, R., Duran, S., & Ramapuram, J. (2015). Development of an ex-vivo trans-corneal permeation model in horses: Epithelial barrier evaluation. *Investigative Ophthalmology & Visual Science, 56*(7).

Abarca, E. M., Salmon, J. H., & Gilger, B. C. (2013). Effect of Choroidal Perfusion on Ocular Tissue Distribution After Intravitreal or Suprachoroidal Injection in an Arterially Perfused Ex Vivo Pig Eye Model. *Journal of Ocular Pharmacology and Therapeutics, 29*(8), 715-722. doi:10.1089/jop.2013.0063

Adelli, G. R., Balguri, S. P., & Majumdar, S. (2015). Effect of Cyclodextrins on Morphology and Barrier Characteristics of Isolated Rabbit Corneas. *AAPS PharmSciTech, 16*(5), 1220-1226. doi:10.1208/s12249-015-0315-z

Alves-Silva, I., Sa-Barreto, L. C. L., Lima, E. M., & Cunha-Filho, M. S. S. (2014). Preformulation studies of itraconazole associated with benznidazole and pharmaceutical excipients. *Thermochimica Acta, 575*, 29-33. doi:10.1016/j.tca.2013.10.007

Bramhane, D. M., Kulkarni, P. A., Martis, E. A., Pissurlenkar, R. R., Coutinho, E. C., & Nagarsenker, M. S. (2016). Characterization of pioglitazone cyclodextrin complexes: Molecular modeling to in vivo evaluation. *J Pharm Bioallied Sci, 8*(2), 161-169. doi:10.4103/0975-7406.171680

Challa, R., Ahuja, A., Ali, J., & Khar, R. K. (2005). Cyclodextrins in drug delivery: an updated review. *AAPS PharmSciTech, 6*(2), E329-357. doi:10.1208/pt060243

Chen, C. C., Chang, J. H., Lee, J. B., Javier, J., & Azar, D. T. (2002). Human corneal epithelial cell viability and morphology after dilute alcohol exposure. *Invest Ophthalmol Vis Sci, 43*(8), 2593-2602.

de Freitas, M. R., Rolim, L. A., Soares, M. F. D., Rolim-Neto, P. J., de Albuquerque, M. M., & Soares-Sobrinho, J. L. (2012). Inclusion complex of methyl-beta-cyclodextrin and

olanzapine as potential drug delivery system for schizophrenia. *Carbohydrate Polymers, 89*(4), 1095-1100. doi:10.1016/j.carbpol.2012.03.072

Del Valle, E. M. M. (2004). Cyclodextrins and their uses: a review. *Process Biochemistry, 39*(9), 1033-1046. doi:10.1016/S0032-9592(03)00258-9

Donnenfeld, E. D. (2011). Difluprednate for the prevention of ocular inflammation postsurgery: an update. *Clin Ophthalmol, 5*, 811-816. doi:10.2147/OPTH.S6541

Foster, C. S., Davanzo, R., Flynn, T. E., McLeod, K., Vogel, R., & Crockett, R. S. (2010). Durezol (Difluprednate Ophthalmic Emulsion 0.05%) compared with Pred Forte 1% ophthalmic suspension in the treatment of endogenous anterior uveitis. *J Ocul Pharmacol Ther, 26*(5), 475-483. doi:10.1089/jop.2010.0059

Gaudana, R., Ananthula, H. K., Parenky, A., & Mitra, A. K. (2010). Ocular Drug Delivery. *Aaps Journal, 12*(3), 348-360. doi:10.1208/s12248-010-9183-3

Hayiyana, Z., Choonara, Y. E., Makgotloe, A., du Toit, L. C., Kumar, P., & Pillay, V. (2016). Ester-Based Hydrophilic Cyclodextrin Nanosponges for Topical Ocular Drug Delivery. *Curr Pharm Des, 22*(46), 6988-6997. doi:10.2174/1381612822666161216113207

Higuchi, T. (1961). Rate of Release of Medicaments from Ointment Bases Containing Drugs in Suspension. *Journal of Pharmaceutical Sciences, 50*(10), 874-&. doi:DOI 10.1002/jps.2600501018

Higuchi, T., & Connors, K. A. (1965). Phase Solubility Techniques. *Advances in Analytical Chemistry and Instrumentation, 4*, 117-212.

Jamal, K. N., & Callanan, D. G. (2009). The role of difluprednate ophthalmic emulsion in clinical practice. *Clin Ophthalmol, 3*, 381-390.

Jansen, T., Xhonneux, B., Mesens, J., & Borgers, M. (1990). Beta-cyclodextrins as vehicles in eye-drop formulations: an evaluation of their effecst on rabbit corneal epithelium. *Lens Eye Toxic Res., 7*(3-4), 459-468.

Javitt, J. C., Javitt, N. B., & Mcdonnell, P. (1994).

Korenfeld, M. S., Silverstein, S. M., Cooke, D. L., Vogel, R., Crockett, R. S., & Emulsion, D. O. (2009). Difluprednate ophthalmic emulsion 0.05% for postoperative inflammation and pain. *Journal of Cataract and Refractive Surgery, 35*(1), 26-34. doi:10.1016/j.jcrs.2008.09.024

Liao, Y., Zhang, X., Li, C., Huang, Y., Lei, M., Yan, M., . . . Zhao, C. (2016). Inclusion complexes of HP-beta-cyclodextrin with agomelatine: Preparation, characterization, mechanism study and in vivo evaluation. *Carbohydr Polym, 147*, 415-425. doi:10.1016/j.carbpol.2016.04.022

Liu, L., & Guo, Q. X. (2002). The driving forces in the inclusion complexation of cyclodextrins. *Journal of Inclusion Phenomena and Macrocyclic Chemistry, 42*(1-2), 1-14. doi:Doi 10.1023/A:1014520830813

Loftsson, T., & Jarvinen, T. (1999). Cyclodextrins in ophthalmic drug delivery. *Adv Drug Deliv Rev, 36*(1), 59-79.

Loftsson, T., & Stefansson, E. (1997). Effect of cyclodextrins on topical drug delivery to the eye. *Drug Development and Industrial Pharmacy, 23*(5), 473-481. doi:Doi 10.3109/03639049709148496

Loftsson, T., & Stefansson, E. (2007). Cyclodextrins in ocular drug delivery: theoretical basis with dexamethasone as a sample drug. *Journal of Drug Delivery Science and Technology, 17*(1), 3-9.

Mains, J., Tan, L. E., Wilson, C., & Urquhart, A. (2012). A pharmacokinetic study of a combination of beta adrenoreceptor antagonists - In the isolated perfused ovine eye. *European Journal of Pharmaceutics and Biopharmaceutics, 80*(2), 393-401. doi:10.1016/j.ejpb.2011.11.006

Malaquias, L. F. B., Sa-Barreto, L. C. L., Freire, D. O., Silva, I. C. R., Karan, K., Durig, T., . . . Cunha-Filho, M. (2018). Taste masking and rheology improvement of drug complexed

with beta-cyclodextrin and hydroxypropyl-beta-cyclodextrin by hot-melt extrusion. *Carbohydr Polym, 185*, 19-26. doi:10.1016/j.carbpol.2018.01.011

Matencio, A., Hernandez-Gil, C. J., Garcia-Carmona, F., & Lopez-Nicolas, J. M. (2017). Physicochemical, thermal and computational study of the encapsulation of rumenic acid by natural and modified cyclodextrins. *Food Chemistry, 216*, 289-295. doi:10.1016/j.foodchem.2016.08.023

McElhiney, L. F., & American Pharmacists Association. (2013). *Compounding guide for ophthalmic preparations*. Washington, D.C.: American Pharmacists Association.

Mulki, L., & Foster, C. S. (2011). Difluprednate for inflammatory eye disorders. *Drugs Today (Barc), 47*(5), 327-333. doi:10.1358/dot.2011.47.5.1590791

Oprean, C., Mioc, M., Csanyi, E., Ambrus, R., Bojin, F., Tatu, C., . . . Soica, C. (2016). Improvement of ursolic and oleanolic acids' antitumor activity by complexation with hydrophilic cyclodextrins. *Biomed Pharmacother, 83*, 1095-1104. doi:10.1016/j.biopha.2016.08.030

Peppas, N. A. (1985). Analysis of Fickian and Non-Fickian Drug Release from Polymers. *Pharmaceutica Acta Helvetiae, 60*(4), 110-111.

Peppas, N. A., & Sahlin, J. J. (1989). A Simple Equation for the Description of Solute Release .3. Coupling of Diffusion and Relaxation. *International Journal of Pharmaceutics, 57*(2), 169-172. doi:Doi 10.1016/0378-5173(89)90306-2

Prausnitz, M. R., & Noonan, J. S. (1998). Permeability of cornea, sclera, and conjunctiva: A literature analysis for drug delivery to the eye. *Journal of Pharmaceutical Sciences, 87*(12), 1479-1488. doi:DOI 10.1021/js9802594

Sultana, Y., Jain, R., Aqil, M., & Ali, A. (2006). Review of ocular drug delivery. *Curr Drug Deliv, 3*(2), 207-217.

Tahara, K., Karasawa, K., Onodera, R., & Takeuchi, H. (2017). Feasibility of drug delivery to the eye's posterior segment by topical instillation of PLGA nanoparticles. *Asian Journal of Pharmaceutical Sciences, 12*(4), 394-399. doi:10.1016/j.ajps.2017.03.002

Tajika, T., Isowaki, A., & Sakaki, H. (2011). Ocular distribution of difluprednate ophthalmic emulsion 0.05% in rabbits. *J Ocul Pharmacol Ther, 27*(1), 43-49. doi:10.1089/jop.2010.0093

Tajika, T., Waki, M., Tsuzuki, M., Kida, T., & Sakaki, H. (2011). Pharmacokinetic Features of Difluprednate Ophthalmic Emulsion in Rabbits as Determined by Glucocorticoid Receptor-Binding Bioassay. *Journal of Ocular Pharmacology and Therapeutics, 27*(1), 29-34. doi:10.1089/jop.2010.0106

Tang, P., Li, S., Wang, L., Yang, H., Yan, J., & Li, H. (2015). Inclusion complexes of chlorzoxazone with beta- and hydroxypropyl-beta-cyclodextrin: Characterization, dissolution, and cytotoxicity. *Carbohydr Polym, 131*, 297-305. doi:10.1016/j.carbpol.2015.05.055

Tang, P., Ma, X., Wu, D., Li, S., Xu, K., Tang, B., & Li, H. (2016). Posaconazole/hydroxypropyl-beta-cyclodextrin host-guest system: Improving dissolution while maintaining antifungal activity. *Carbohydr Polym, 142*, 16-23. doi:10.1016/j.carbpol.2016.01.042

Tang, P., Tang, B., Wang, Q., Xu, K., Xiong, X., & Li, H. (2016). Effect of hydroxypropyl-beta-cyclodextrin on the bounding of salazosulfapyridine to human serum albumin. *Int J Biol Macromol, 92*, 105-115. doi:10.1016/j.ijbiomac.2016.07.033

Tiwari, G., Tiwari, R., & Rai, A. K. (2010). Cyclodextrins in delivery systems: Applications. *J Pharm Bioallied Sci, 2*(2), 72-79. doi:10.4103/0975-7406.67003

Uekama, K. (2004). Design and evaluation of cyclodextrin-based drug formulation. *Chem Pharm Bull (Tokyo), 52*(8), 900-915.

Vieira, A. C., Ferreira Fontes, D. A., Chaves, L. L., Alves, L. D., de Freitas Neto, J. L., de La Roca Soares, M. F., . . . Rolim-Neto, P. J. (2015). Multicomponent systems with cyclodextrins

and hydrophilic polymers for the delivery of Efavirenz. *Carbohydr Polym, 130*, 133-140. doi:10.1016/j.carbpol.2015.04.050

Wagner, J. G. (1969). Interpretation of percent dissolved-time plots derived from in vitro testing of conventional tablets and capsules. *J Pharm Sci, 58*(10), 1253-1257.

Yamaguchi, M., Yasueda, S., Isowaki, A., Yamamoto, M., Kimura, M., Inada, K., & Ohtori, A. (2005). Formulation of an ophthalmic lipid emulsion containing an anti-inflammatory steroidal drug, difluprednate. *International Journal of Pharmaceutics, 301*(1-2), 121-128. doi:10.1016/j.ijpharm.2005.05.036

Zhang, C. L., Liu, J. C., Yang, W. B., Chen, D. L., & Jiao, Z. G. (2017). Experimental and molecular docking investigations on the inclusion mechanism of the complex of phloridzin and hydroxypropyl-beta-cyclodextrin. *Food Chemistry, 215*, 124-128. doi:10.1016/j.foodchem.2016.07.155

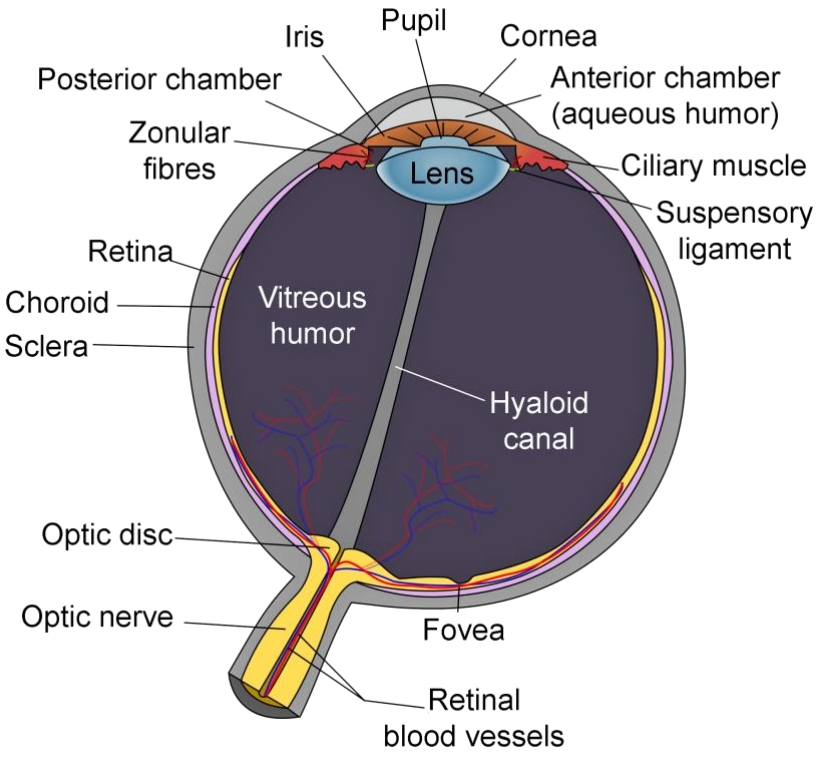

Figure 5.1: Diagram of the eye consisting of the anterior segment (cornea, aqueous humor, lens, iris, and ciliary muscle) and posterior segment (sclera, retina, optic nerve, and choroid).

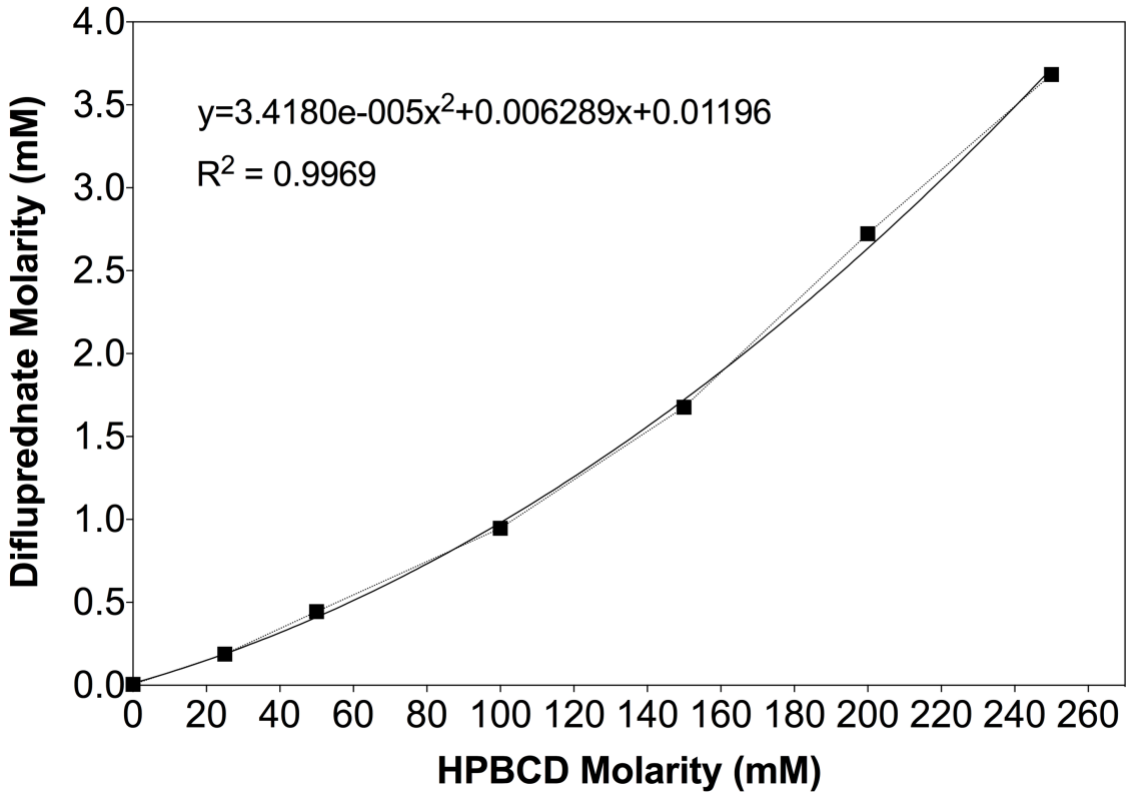

Figure 5.2: Phase solubility studies for difluprednate and HPBCD in PBS.

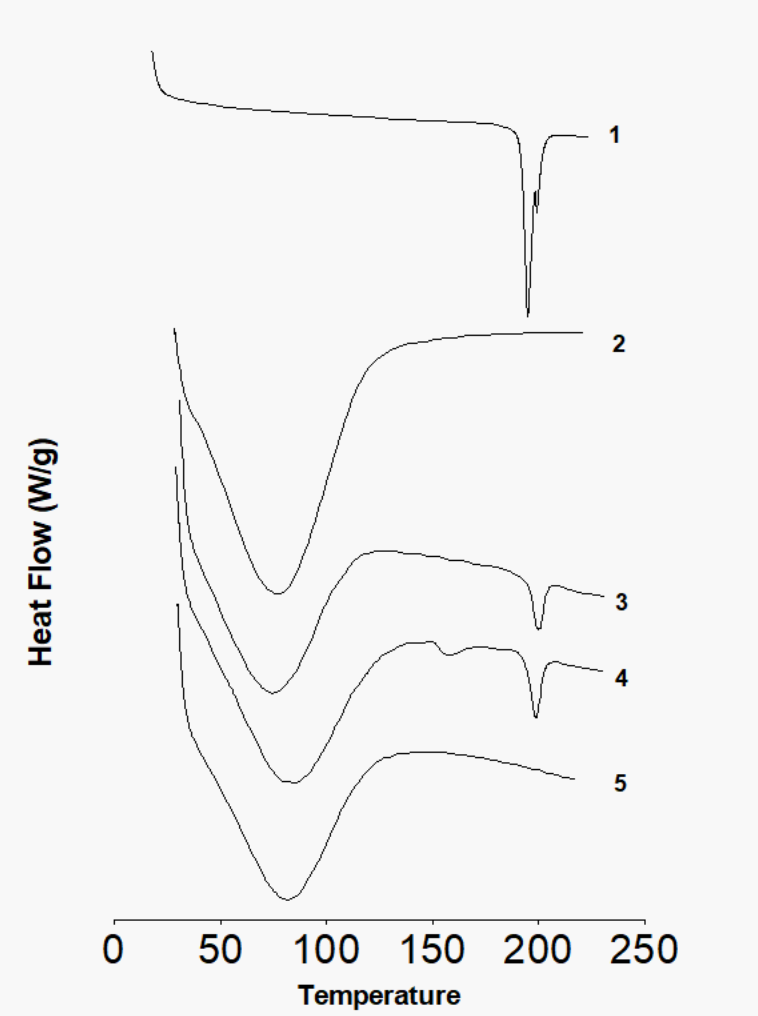

Figure 5.3: Differential Scanning Calorimetry confirmed complexation in the solid state (1, Difluprednate; 2, HPBCD; 3, Dry mix; 4, Kneaded Mix; 5, Rotovap mix)

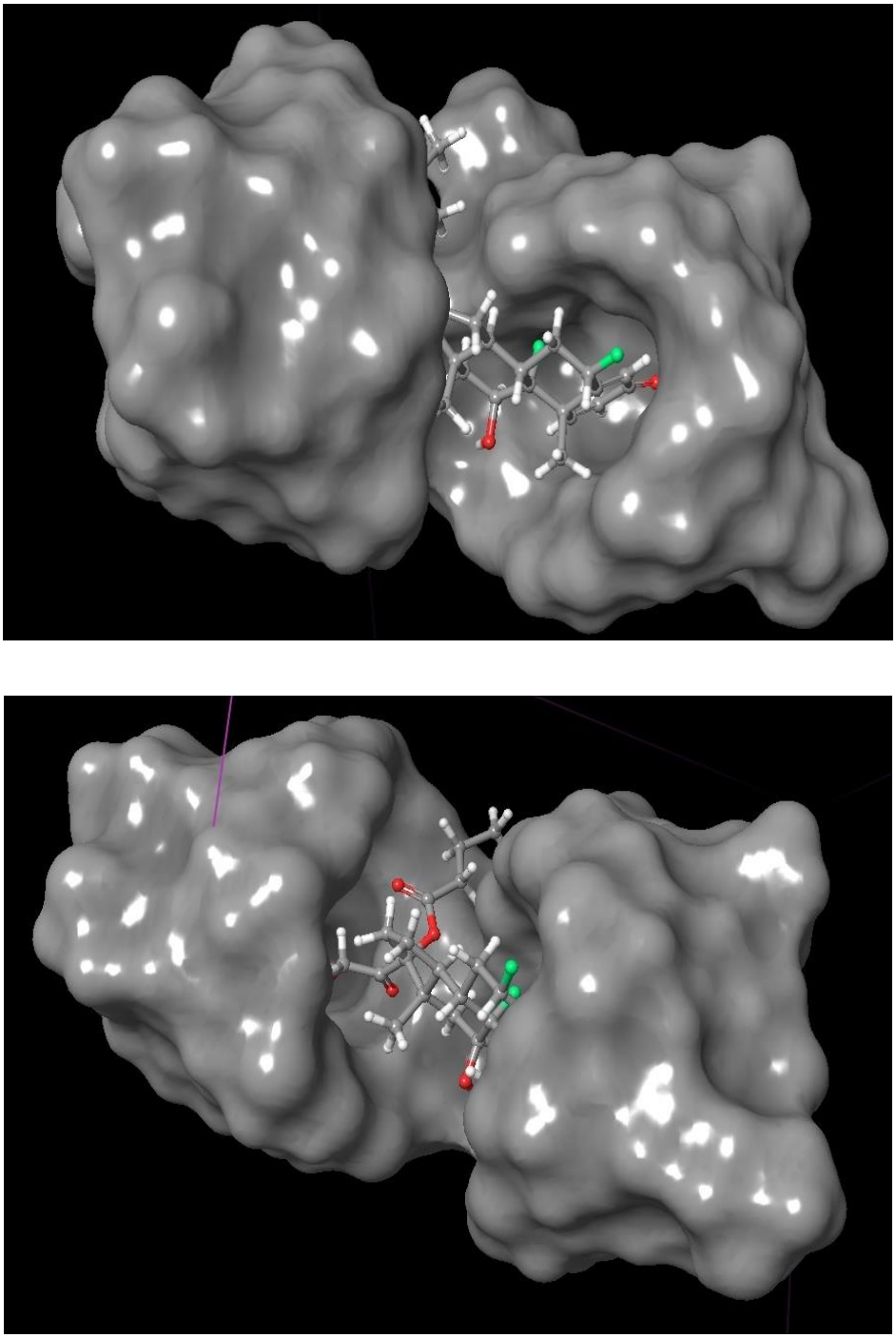

Figure 5.4: Molecular docking simulated the interaction between difluprednate and HPBCD. Green represents Fluorine atoms, white is hydrogen atoms and red is carbon atoms.

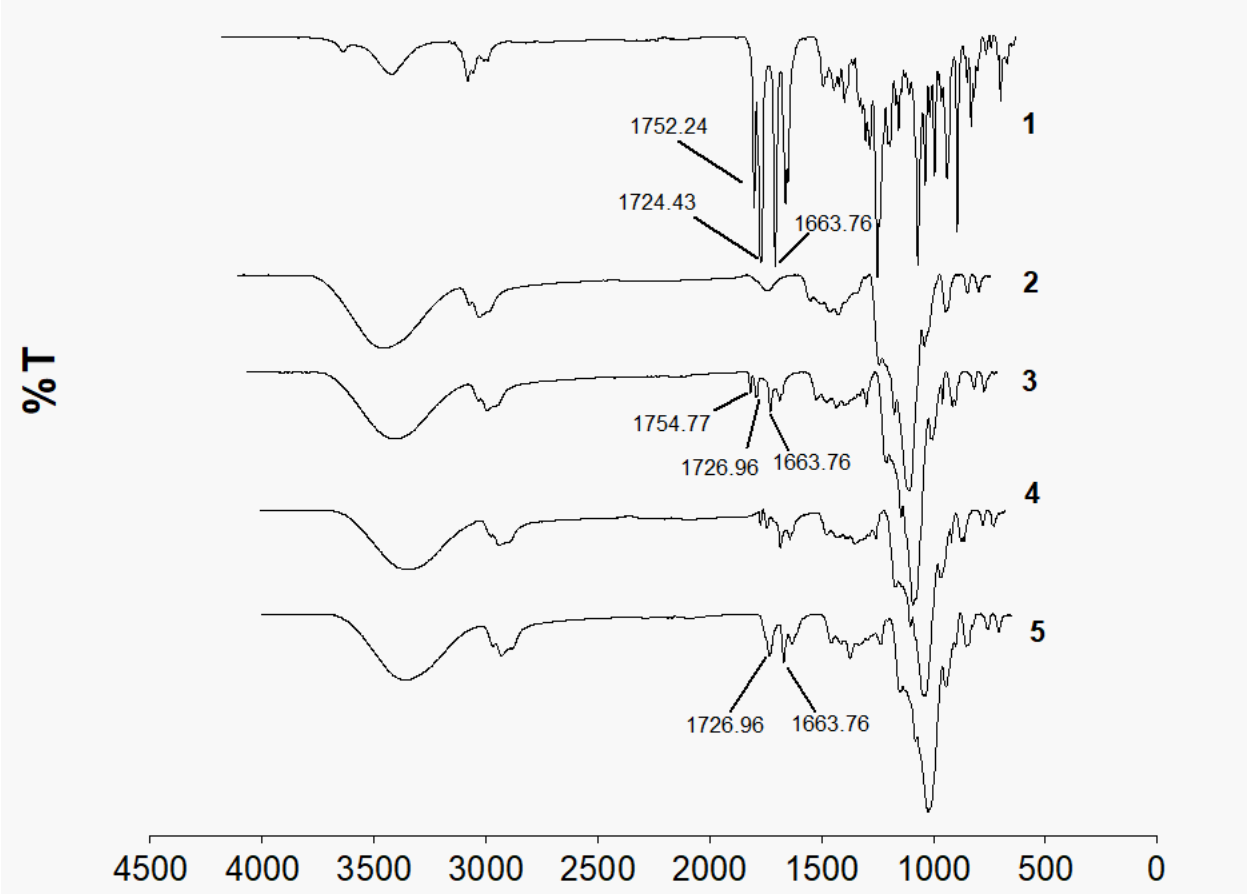

Figure 5.5: FT-IR data of various difluprednate-HPBCD mixtures to confirm the inclusion complex formation in the solid state. (1, Nepafenac; 2, HPBCD; 3, Dry mix; 4, Kneaded Mix; 5, Rotovap mix)

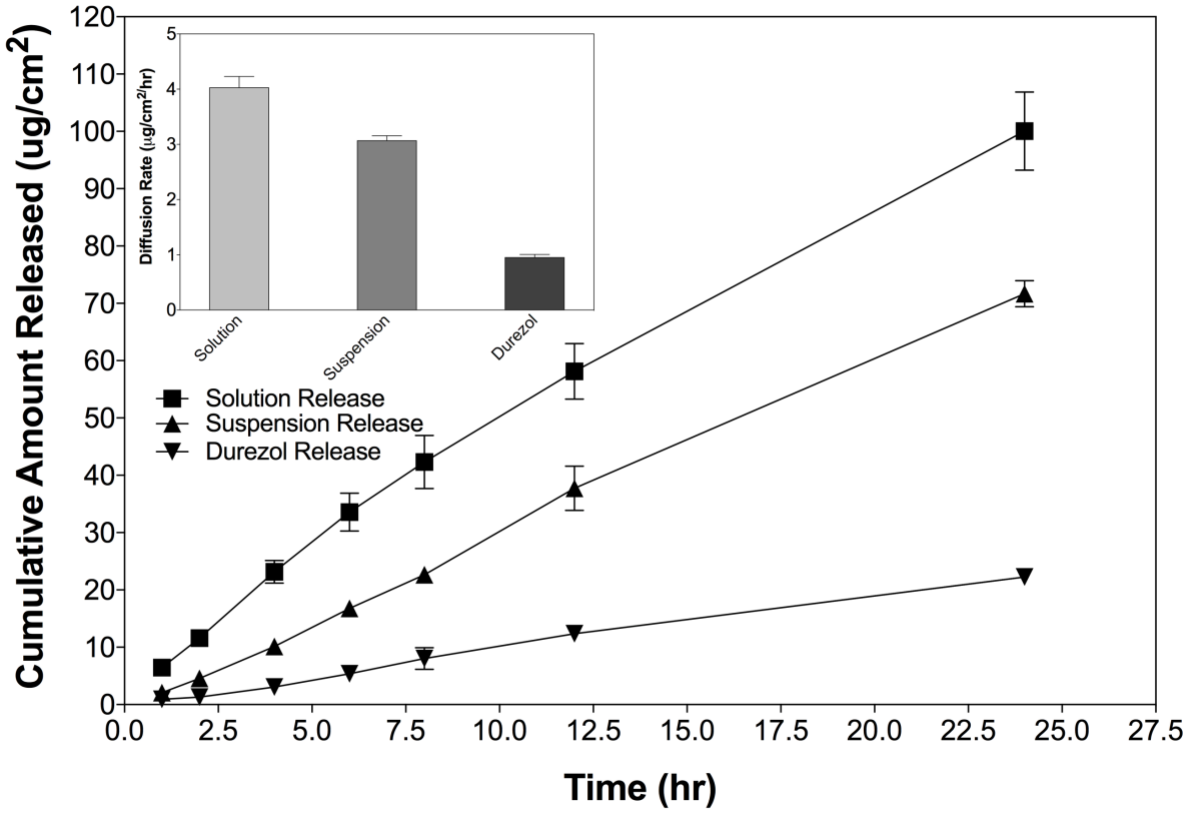

Figure 5.6: Difluprednate system release studies across dialysis membranes; Inset: diffusion rate. Error bars represent standard error mean (SEM). Error bars represent standard error mean (SEM).

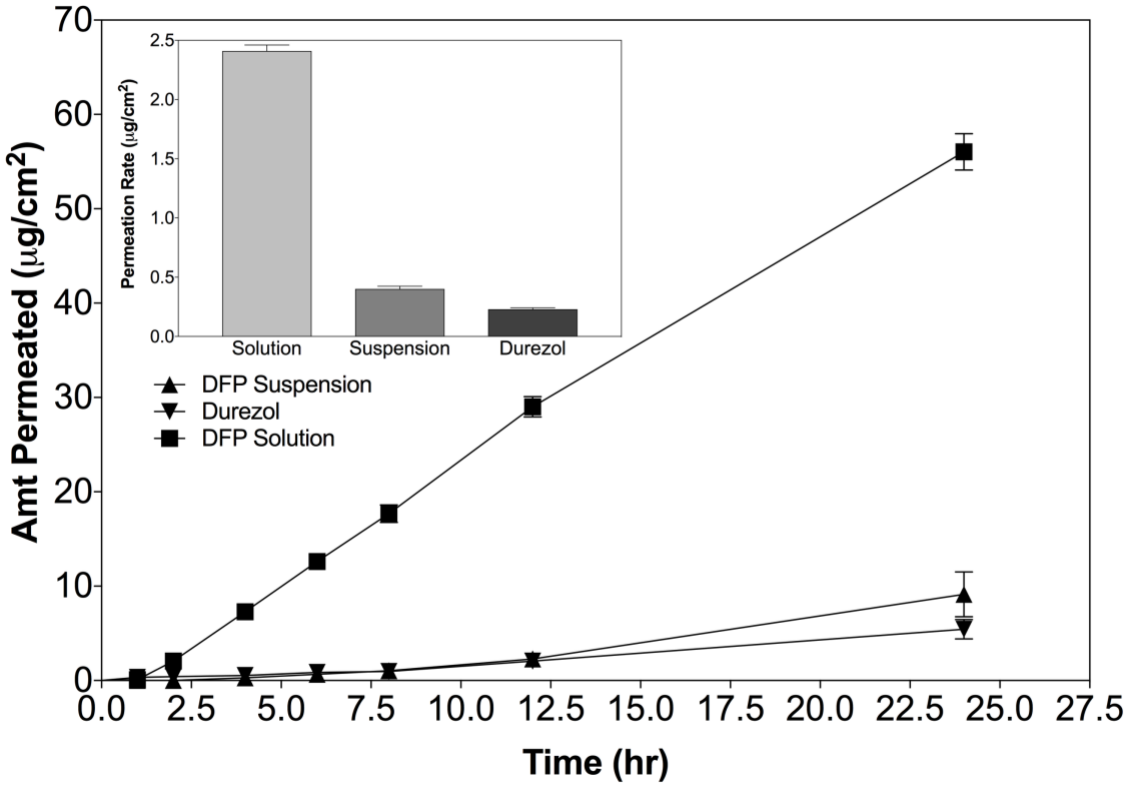

Figure 5.7: Permeation of difluprednate formulations across porcine cornea; Inset: Permeation rate (steady state flux). Error bars represent standard error mean (SEM).

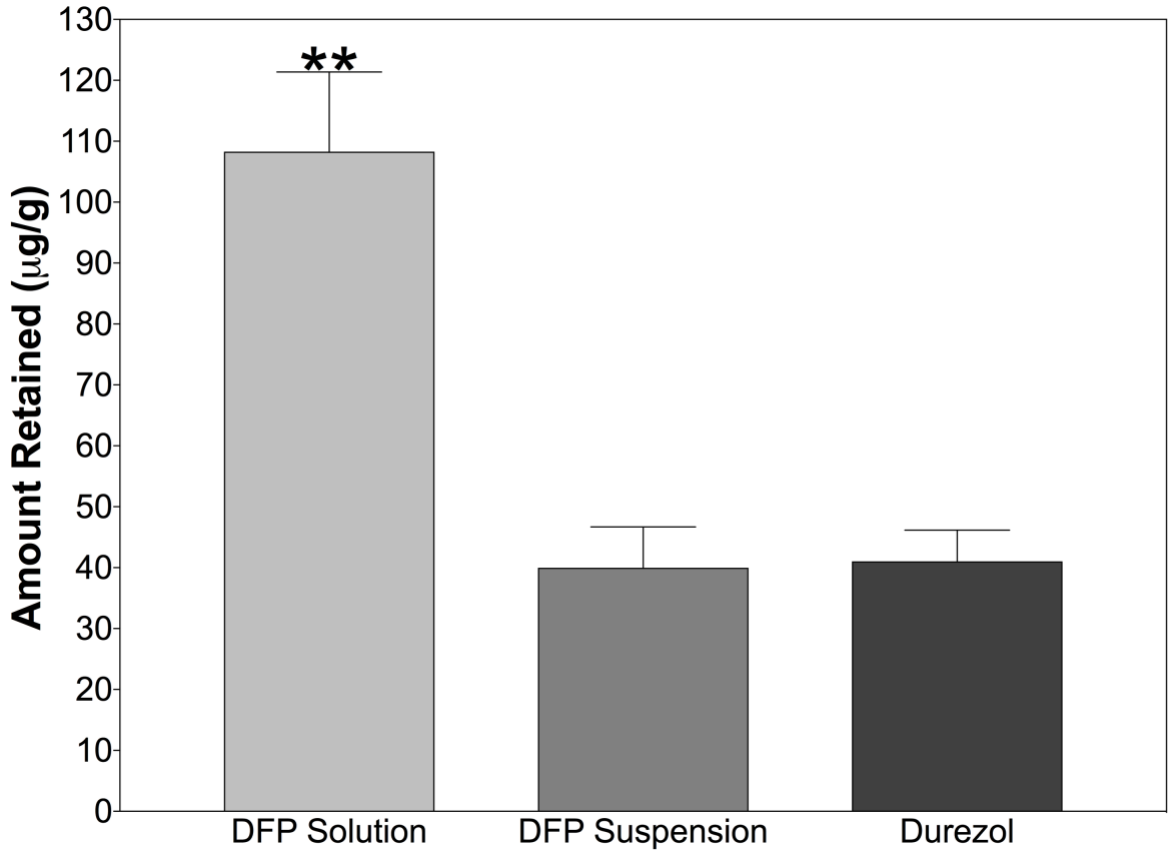

Figure 5.8: Corneal retention of difluprednate following permeation studies. Error bars represent standard error mean (SEM).

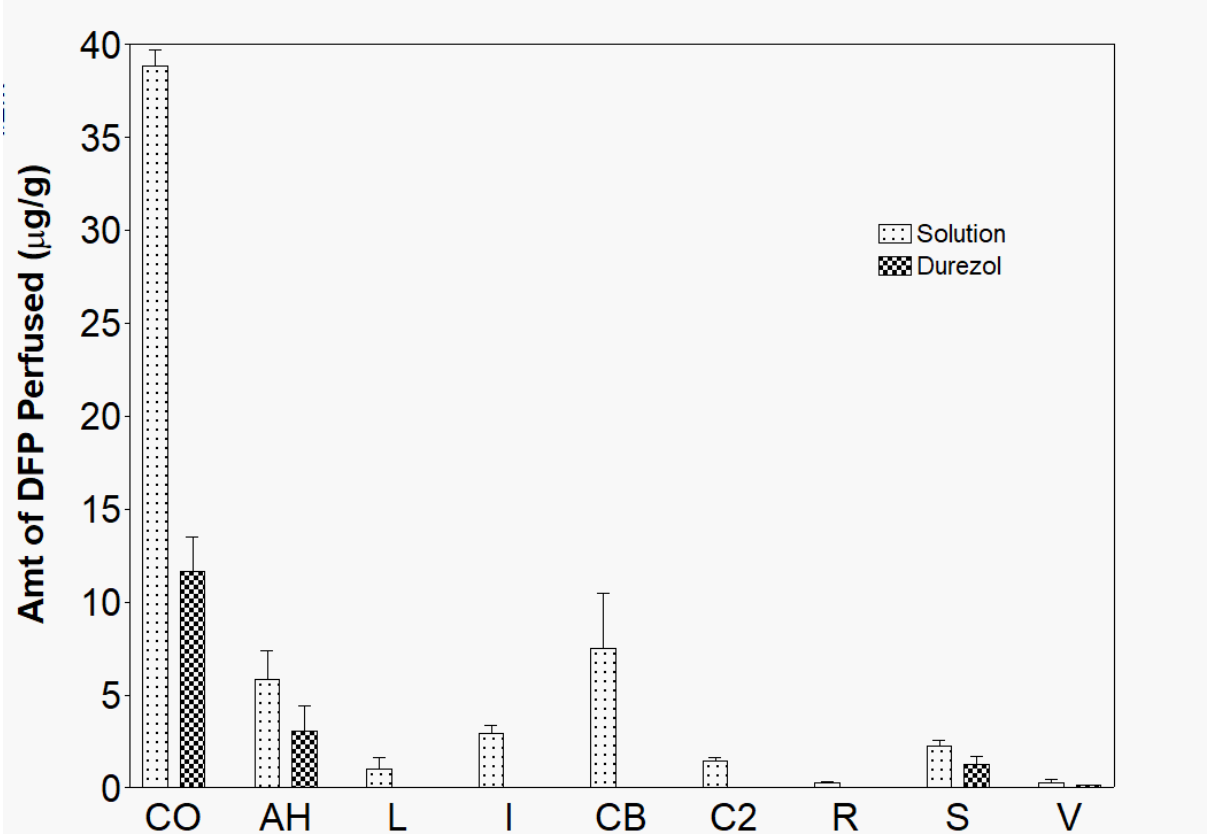

Figure 5.9: Ocular distribution of difluprednate in isolated porcine eyes in a continuous perfusion model. The experiments were terminated after 2 hours. Various ocular tissues were collected, and nepafenac in the tissues was quantified. [CO, Cornea; AH, Aqueous Humour; L, Lens; I, Iris; CB, Ciliary Body; C2, Choroid; R, Retina; S, Sclera; V, Vitreous humor] Error bars represent standard error mean (SEM).

Chapter 6. Drug Delivery to the Posterior Segment via Biodegradable Microneedles

6.1 Abstract

Difluprednate is a corticosteroid approved for treatment of anterior uveitis; however, recent studies have shown that difluprednate can treat posterior segment conditions. Difluprednate is currently only available as a topical emulsion, Durezol®. Topical formulations limit the amount of drug capable of penetrating to the posterior segment due to permeation barriers, lacrimation and lymphatic clearance. Contrarily, biodegradable microneedles patches can be used to bypass the tear film and sclera, improving the amount of drug delivered to the posterior segment. Biodegradable PLGA/PAA microneedle patches were fabricated using PAA for the rapid dissolvable backing and difluprednate as the active pharmaceutical ingredient. The patches were characterized by SEM and failure force analysis. Release studies across dialysis membranes and porcine scleral permeation studies were also performed. Failure force of the microneedles increased with molecular weight of the polymer. Release studies proved a slow steady release over the 7-day study was achieved. Scleral permeation studies revealed that the amount of drug retained in the sclera was inversely related to the failure force of each array. The difluprednate microneedles patches were strong, sharp and uniform, providing drug release for days.

6.2 Introduction

Topically administered ocular drug delivery systems (solutions, suspensions, ointments) lack long residence time, meaning patients have to administer the product multiple times a day (1). This is inconvenient for the patient and often leads to patient noncompliance, especially for chronic use. Additionally, topical formulations are only useful for delivery of drugs to the anterior segment of the eye (iris, ciliary body, cornea, lens) and cannot reach the posterior segment of the eye (choroid, vitreous body, retina) (2). Intravitreal injections, injections into the vitreous humor, are a common treatment for the posterior segment conditions due to enhanced localized delivery. However, intravitreal injections are not patient-friendly as they can result in pain, cataract formation, trauma and endophthalmitis (3). Furthermore, repeat injection is necessary. Thus, there is a strong need for noninvasive drug delivery to the posterior segment of the eye that includes the benefits of both topical delivery and intravitreal injections (2).

Difluprednate is a corticosteroid currently marketed to treat pain and inflammation in the anterior segment of the eye, currently available as a topical emulsion, Durezol® (4). However, research has shown that Durezol® was able to control symptoms of posterior segment conditions such as retinal vasculitis (5), ocular manifestations of Harada disease (6, 7), pars planitis (8) and macular edema (9, 10). Additionally, ocular distribution studies in rabbits revealed enhanced penetration to the choroid/retina using Durezol® (11). Furthermore, difluprednate is shown to have a large potency due to the high affinity between the glucocorticosteroid and the difluprednate active metabolite (12). Finally, only one reformulation of difluprednate has been achieved to date (13); therefore, difluprednate is ideal for the formulation of a noninvasive sustained-release drug delivery system with enhanced distribution to the posterior segment.

Biodegradable polymeric microneedles offer a noninvasive patient-friendly alternative to intravitreal injections while providing easy painless administration as they do not cause pain like traditional hypodermic needles. The microneedles can last for a specified duration, leading to a decrease in repeat administration and improved residence time. The microneedles can be made long enough to penetrate the sclera, which poses an ocular barrier for drug delivery to the posterior segment (14). To date, a variety of microneedle mechanisms have been attempted for ocular delivery such as solid coated microneedles (15, 16) and hollow microneedles (17-19). Fabrication of solid or hollow silicon microneedles are brittle and pose the risk of breaking off into the ocular tissue (20). Additionally, silicon and glass-based microneedles are complex, expensive to manufacture and complicated for patients to administer themselves. There has been one instance of rapidly dissolving ocular microneedles using polyvinylpyrrolidone (PVP) polymer (20), which is desirable for rapid drug release. However, a literature search revealed only one paper discussing sustained-release biodegradable PLA microneedles as a means for prolonged delivery of methotrexate (21). These biodegradable microneedle arrays are less complex for patient use and last for 8 weeks; therefore, further research should be conducted to formulate a sustained-release patient-friendly microneedle product.

PLGA or poly(lactic-co-glycolic acid) is a FDA-approved copolymer used in a plethora of biological applications such as nanoparticles and controlled drug delivery devices (22, 23). The degradation time of PLGA is based on the ratio of lactide to glycolide. As the lactide concentration increases, the water solubility of the polymer decreases leading to an increase in degradation time. However, the ratio of 50:50 lactide:glycolide has been shown to exhibit the fastest degradation time compared to all other ratios (24). The mechanical strength of PLGA is dependent on the crystallinity of the polymers which is directly related to the molecular weight. Furthermore, increased molecular weight generally results in slower degradation time. Therefore, biodegradable polymeric microneedles can be modified to degrade at a specific time by varying

the molecular weight and concentration of lactide. While many studies have been conducted using biodegradable microneedles for the transdermal applications (25-27), only one published work has been performed using sustained release ocular biodegradable microneedles (21, 28).

The objective of this work was to develop strong biodegradable microneedles for the sustained-released delivery of difluprednate to the suprachoiroidal space (SCS), for treatment of posterior segment conditions. Targeting the SCS allows for enhanced delivery to the retina and choroid with higher bioavailability compared to topical formulations and intravitreal injections (29, 30). Polymers with varying molecular weights and lactide concentrations will be tested to compare the mechanical strength and release profiles of each microneedle formulation. Furthermore, the microneedle patch will contain a Poly(acrylic acid) (PAA) backing that will undergo rapid dissolution upon instillation into the eye, leaving a thin malleable PLGA sheet with the microneedles imbedded in the sclera (25).

6.3 Experimental Methods

6.3.1 Materials

Difluprednate was procured from Chemieliva Pharmaceutical CO., LTD., Chongqing China. PAA 35% (w/w) solution in water, Resomer® R 202 S, Poly(D,L-lactide), Resomer® RG 503, Poly(D,L-lactide-co-glycolide), and Resomer® RG 756 S, Poly(D,L-lactide-co-glycolide) were purchased from Sigma Aldrich, St. Louis, MO. Room temperature vulcanizing (RTV) polydimethylsiloxane (PDMS) silicone microneedle molds were purchased from Micropoint Technologies PTE LTD, Singapore. All solvents used for high performance liquid chromatography (HPLC) were of analytical or HPLC grade.

6.3.2. Fabrication of PLGA Biodegradable Microneedles

To formulate the microneedles, 5mg of difluprednate was dissolved in acetonitrile and 50mg of desired polymer was added and sonicated for 30 minutes. 50µL of the mixture was pipetted into each RTV PDMS silicone microneedle mold and centrifuged for 30 minutes at 3300rpm using a Beckman Coulter Allegra™ 6R (Indiananapolis, IN) benchtop cell culture centrifuge. Following centrifugation, 60mg of 35% Poly(acrylic acid) (PAA) solution was placed into the microneedle molds using a dropper, to serve as the dissolving backing. The microneedle arrays were then left at ambient temperature overnight to dry.

6.3.3 High Performance Liquid Chromatography (HPLC) Analysis

An Alliance Waters e2695 Separations Module and a Waters 2998 Photodiode Array Detector, Singapore, was used for the difluprednate analysis. A Luna C18(2) 5µm, 150mm x 4.60mm reversed-phase HPLC column was employed for difluprednate analysis. The mobile phase consisted of 60:40 acetonitrile: phosphate buffer (10mM, pH=6). Samples were eluted at a flow rate of 1mL/min at ambient temperature. The absorbance wavelength was set at 254nm, with an injection volume of 10 µL.

6.3.4 Characterization of Microneedle Patches Containing Difluprednate

6.3.4.1 Scanning Electron Microscopy (SEM)

The microneedles were analyzed to determine microneedle structure and uniformity using a Jeol 7000f Scanning Electron Microscope, USA. Prior to analysis, each microneedle array was coated with a 20-22nm gold coating.

6.3.4.2 Microneedle PAA Backing Dissolution Study

The PAA backing dissolution test was performed by submerging the microneedle arrays in 5mL of PBS (pH=7.4) in a 6-well plate in a water bath (37°C). The backing was visually inspected at

15, 30 and 40min by removing the microneedle with a pair of tweezers and analyzing the backing thickness. The microneedles were removed once the backing was completely dissolved.

6.3.4.3 Microneedle Failure Force

The strength of the microneedle patches was determined by analyzing their failure force (27, 31). Stress-strain curves were produced using a displacement-force test station: TA-HDi Texture Analyzer, Texture Technologies Corp, Hamilton, MA. An individual microneedle array was pressed against a stainless-steel surface at a rate of 1mm/s until a preset distance was reached (1mm). Failure force was indicated by a sudden drop in applied force.

6.3.4.4 Microneedle Array Release Study

To measure the release rate of each microneedle patch, an individual array was glued to the bottom of a single well in a 24-well plate and submerged in 2mL of the dissolution media. The dissolution media was 80:20 PBS (pH=7.4): ethanol (200-proof), preheated to 37°C. The well-plate was placed in the water bath at 37°C. The full volume (2mL) of each well was removed at the following time points: 4, 8, 12, 24, 48, 72, 96, 120 and 168 hours, and replenished with the aforementioned dissolution media. All samples were analyzed via HPLC.

The drug release from each microneedle array was modeled using the Higuchi equation for matrix systems, which describes Fickian diffusion (32, 33):

$$\frac{M_t}{M_0} = 6\sqrt{\frac{D\tau}{r^2\pi}} \qquad \text{Eq. 1}$$

In this expression τ is time, r is the radius of the microneedle tip (10μm), D is the diffusion coefficient, M_t is the cumulative drug released at a specific time and M_0 is the total drug loaded in the microneedle patch, which was determined to be ~1mg by dissolving a microneedle patch in

100% acetonitrile. The diffusion coefficient is the only unknown and is calculated by fitting the experimental data to the aforementioned equation.

6.3.5 Ex-vivo Scleral Permeation Experiments

6.3.5.1 Scleral Excision

Porcine eyes were obtained from Auburn University Lambert-Powell Meats Laboratory (Auburn University, Auburn AL) and stored in 4°C until needed for the experiment. The animals were euthanized according to the Institutional Animal Care and Use Committee (IACUC) approved protocol (SOP 2015-2727). The excess tissue was first cut from the globe and the scleras were excised from the globe using a 3.0mm slit eagle blade to create an insertion point between the iris and the cornea. Corneal scissors were used to excise the sclera and the scleras were rinsed with saline to remove excess humour and then placed in phosphate buffered saline (PBS) at pH=7.4 until used in the permeation studies. The permeation studies began within 2 hours of scleral excision.

6.3.5.2 Scleral Permeation Studies

Franz Diffusion Cell apparatus was assembled to hold the sclera in position during the permeation experiments. All microneedle patches were tested in three replicate permeation experiments. The receptor cell was filled with 5 mL PBS buffer (pH 7.4) containing 20% ethanol, to maintain sink conditions. The scleras were placed on the receptor cell with the outer surface of the sclera facing up, the microneedle patch was then pressed into the sclera using tweezers and the donor cell was placed on top of the sclera and both cells were clamped together. 50µL of simulated tear fluid (STF) was then pipetted around the microneedle patch, and the donor cell was covered with Parafilm®. The receptor cell was sampled (1 mL) at 2, 4, 8, 12, and 24 h, and replenished with

fresh PBS buffer (pH 7.4) containing 20% ethanol. The samples were assayed by HPLC method as described earlier.

6.3.5.3 Extraction of Difluprednate from Scleras

At both the 12-hour and 24-hour time point, select microneedle patches were removed from the scleras, and the scleras were subsequently removed and cleaned with PBS buffer (pH 7.4) containing 20% ethanol using cotton swabs. The active diffusion area of the sclera was cut, weighed, minced and placed in individual vials with 2mL of the HPLC mobile phase (10mM phosphate buffer (pH=6):Acetonitrile 40:60). The vials were then sonicated for 30 minutes and stored for 24 hours at 4^{o}C to extract any drug retained in the sclera. Following the 24-hour extraction period, the vials were sonicated again for 30 minutes and the supernatant was filtered through 0.45µm Nylon membrane filter and assayed by HPLC. The microneedles were reserved for SEM analysis at both time points.

6.3.6 Statistical Analysis

All results are presented as mean ± standard error of mean (SEM). The calibration curve for difluprednate was tested over the following concentration range: 20-400 µg/mL (slope: y=18005x; R=0.9998). The cumulative amount of drug permeated through unit area of sclera was plotted as a function of time. *In vitro* steady-state flux was calculated from the slope of the linear portion of the plot. The amount of drug (mg) retained in the cornea was normalized to 1 gram of cornea. Analysis of variance was performed to determine the level of significance between the means. Mean differences with $P < 0.05$ were significant.

6.4 Results & Discussion

6.4.1 Fabrication of Biodegradable Microneedles

Polymer-based biodegradable microneedles arrays (8mm x 8mm) were fabricated using RGV silicone molds. PLGA and PLA were the polymer of choice due to the long degradation timescale, lasting for months, compared to other polymers(L. Lu, Garcia, & Mikos, 1999; MainilVarlet, Rahm, & Gogolewski, 1997; J. H. Park et al., 2006; Thakur et al., 2016). The microneedle array size was 8x8 for a total of 64 individual microneedles, with a microneedle length of 800µm and base height of 200µm. The 800µm length microneedles were chosen because they can easily be inserted into the sclera to target drug release into the suprachoiroidal space (SCS), space between choroid and sclera, without piercing the chorioretina (Kim, Edelhauser, & Prausnitz, 2014; Patel et al., 2012; Patel et al., 2011). Targeting delivery to the CSC yields enhanced bioavailability to the choroid/retina when compared intravitreal injections or topical formulations (Patel et al., 2011). The microneedle tips were 20µm in diameter and the needle pitch, distance between each needle tip, was 680µm. The final weight of the microneedles was approximately 35mg and each array contained 1mg of difluprednate. The compositions of each microneedle array can be found in Table 6.1.

6.4.2 Characterization of Microneedle Patches Containing Difluprednate

6.4.2.1 Scanning Electron Microscopy (SEM)

SEM analysis of the microneedles revealed that the arrays were uniform, and all microneedles appeared sharp without the presence of any cracks, fractures or broken tips (Figure 6.1).

6.4.2.2 Microneedle PAA Backing Dissolution Study

The PAA microneedle backing dissolved completely within 30-40 minutes after being submerged in 100% PBS. After the first inspection, the PAA backing began to transition into a gel and at each remaining time point the backing had continued to thin, meaning there is a slow

dissolution of the PAA backing. Finally, at the 40-minute time point, the backing was completely dissolved. Images before and after the dissolution of PAA can be seen in Figure 6.2.

6.4.2.3 Microneedle Failure Force

The failure force, or force required to break the microneedles, is evident by the sharp decrease in applied force in Figure 6.3 (Davis et al., 2004). The x-axis corresponds to the distance displaced by the upper stage after initial contact with the microneedle tips, the stage is then lowered until a preset distance of 1mm is reached. After the microneedles are fractured, the applied force dips and then begins to increase again as it continues pressing against the microneedle backing until the preset distance is reached (data shown ends after microneedle failure). The microneedle strength of each formulation is in the following order: C>B>A; which increases with the molecular weight of the polymer(s) used (Makadia & Siegel, 2011). Furthermore, the lowest molecular weight array, A, broke at a shorter distance compared to the higher molecular weight patches, B & C. Needle breakage was confirmed using microscopy following texture analysis.

6.4.2.4 Microneedle Array Release Study

To determine the release profile of the drug over a 7-day period, microneedle patches were submerged in 80:20 PBS (pH=7.4):Ethanol in individual cells of a 24-well plate, the plate was kept in a water bath at 37 ^{o}C. At designated time points, the full volume was removed, and the cells were replenished with the aforementioned medium. All samples were analyzed using HPLC. After the 7-day period, the overall drug release from the microneedle patches was between 20-25% of the initial drug concentration (Figure 6.4). The plot of the linear portion (48-168hr) was used to determine the release rate. Array B had significantly higher release compared to Array A and C, this observation was expected as it was previously reported that PLGA with a 50:50 ratio of lactide to glycolide has the fastest release compared to all other ratios ($P<0.05$) (Makadia & Siegel, 2011). Furthermore, there was no significant difference in the release rates for the microneedle

patches A (lowest MW) and C (highest MW), meaning the molecular weight does not have a significant effect on the release rate as much as the mechanical strength. The patches all contained at least 50% lactide content which would yield a slower degradation profile in the hydrophilic medium, compared to patches containing significantly more glycolide content (>50%). This is due to the fact that higher concentrations of glycolide will degrade more rapidly in a hydrophilic environment, while the inverse is true for lactide(Makadia & Siegel, 2011). This was evident in our experiment as Array B had the lowest lactide content and the highest release. The release kinetics were modelled using GraphPad Prism for Windows, GraphPad Software, La Jolla California USA.

All of the patches displayed a sustained-release profile, without the occurrence of a burst effect. The kinetic profiles are indicative of diffusion controlled drug release as the difluprednate release is proportional to the square root of time (Figure 6.5). By fitting the experimental data to the Higuchi equation (Eq. 1) the apparent diffusion coefficient, D, was determined for Arrays A-C: 9.164E-09 cm^2/s, 9.13E-09 cm^2/s, and 6.22E-09 cm^2/s, respectively. The corresponding correlation coefficients were 0.92, 0.96, and 0.86. PLGA was not expected to display release kinetics related to degradation and subsequent dissolution since significant degradation would not have occurred in a matter of hours to days (Faisant, Siepmann, & Benoit, 2002; J. H. Park et al., 2006). Based on the release trends we anticipate the microneedles to last for 3-4 weeks.

6.4.3 Ex-vivo Scleral Permeation Experiments

6.4.3.1 Scleral Permeation Studies

There was not a significant difference in the permeation rate among the three microneedle patches (Figure 6.6). This observation was expected since PLGA is known to degrade slowly (weeks-months), and our application is intended for much longer than 24 hours. Array C did not have any release until the 4-hour timepoint, due to the high molecular weight. In contrast, we

observed significant differences in the amount of drug retained in the scleral tissue meaning a larger difference may have been observed in the permeation rates if the study time had been extended, allowing the drug to fully permeate through the sclera. Furthermore, the scleral studies were not performed past 24-hours as the integrity of the tissues would most likely decrease. Viability studies conducted on the sclera reveal it to be viable for 4-hours, but no studies have evaluated the viability past 4 hours (Missel et al., 2010). We chose to study the permeation past 4 hours because very little difluprednate would be released at 4 hours due to the slow degradation timescale of PLGA.

6.4.3.2 Extraction of Difluprednate from Scleras

The amount of difluprednate retained in the scleras appears to increase inversely according to the molecular weight of the polymer: A>B>C (Figure 6.7). These results are opposite to the microneedle failure force, meaning the softer needles have a higher drug retention. Furthermore, the weaker microneedle tips could have broken off following removal of the patches, leaving the needles embedded in the tissue to continue degrading/releasing drug following the conclusion of the studies. Array A had a significantly higher retention after 24 hours compared to all other formulations ($P<0.05$). This observation is explained by the fact that the microneedles had the lowest molecular weight, failure force and the highest lactide content (100%). The lactide content increased the hydrophobicity of the patch, leading to faster degradation after being embedded in the hydrophobic scleral tissue. Furthermore, array A was the only array to have a significantly higher release after 24 hours compared to the 12-hour timepoint. Array B exhibited a significantly higher difluprednate retention in the sclera compared to the array C, due to the lower molecular weight of the Resomer RG 503 polymer. These significant differences were not observed in the permeation rate results, as the drug did not have sufficient time to permeate the sclera due to the short duration of the study. The SEM inspection of the C microneedle arrays at 0, 12 and 24

hours is shown in Figure 6.8. A visual difference can be seen among the three images, where the 24 hour image shows minimal erosion of the microneedles. This observation is expected as significant degradation should not be observed on such a small time scale since PLGA is known to degrade over a period of months (L. Lu et al., 1999).

6.5 Conclusions

Difluprednate was successfully loaded into biodegradable microneedles for sustained-release drug delivery. Three types of patches were formulated with PLGA of varying molecular weights. Poly(acrylic acid) was used to produce a backing that dissolved within 30-40 minutes upon interaction with tear secretions. Failure force analysis revealed that the needle fracture force increased with the molecular weight of the polymer used. Release studies in 80:20 PBS (pH=7.4): ethanol revealed diffusion-controlled release of difluprednate over 7 days, without the occurrence of a burst effect. Array B, which contained the lowest amount of lactide, had the highest release rate due to the higher hydrophilic nature of the microneedle array. Permeation studies using porcine scleras revealed no significant difference in permeation rate; however, the amount of drug retained in the sclera increased according to the molecular weight: A>B>C. These observations suggest that the molecular weight of the polymers affects the microneedle strength, while the lactide content directly affects the release rate, scleral permeation and retention of difluprednate. Thus, PLGA-based biodegradable microneedles have a future as a drug delivery system for the sustained-release of difluprednate for posterior segment conditions.

6.6 Acknowledgements

Authors acknowledge FMC Biopolymer and Auburn University Lambert-Powell Meats Laboratory for their generosity. Authors also acknowledge the financial support provided by the intramural grant program of the Auburn University.

6.7 References

Abarca, E. M., Salmon, J. H., & Gilger, B. C. (2013). Effect of Choroidal Perfusion on Ocular Tissue Distribution After Intravitreal or Suprachoroidal Injection in an Arterially Perfused Ex Vivo Pig Eye Model. *Journal of Ocular Pharmacology and Therapeutics, 29*(8), 715-722. doi:10.1089/jop.2013.0063

Chiang, B., Venugopal, N., Edelhauser, H. F., & Prausnitz, M. R. (2016). Distribution of particles, small molecules and polymeric formulation excipients in the suprachoroidal space after microneedle injection. *Experimental Eye Research, 153*, 101-109. doi:10.1016/j.exer.2016.10.011

Danhier, F., Ansorena, E., Silva, J. M., Coco, R., Le Breton, A., & Preat, V. (2012). PLGA-based nanoparticles: An overview of biomedical applications. *Journal of Controlled Release, 161*(2), 505-522. doi:10.1016/j.jconrel.2012.01.043

Davis, S. P., Landis, B. J., Adams, Z. H., Allen, M. G., & Prausnitz, M. R. (2004). Insertion of microneedles into skin: measurement and prediction of insertion force and needle fracture force. *Journal of Biomechanics, 37*(8), 1155-1163. doi:10.1016/j.jbiomech.2003.12.010

del Amo, E. M., & Urtti, A. (2008). Current and future ophthalmic drug delivery systems. A shift to the posterior segment. *Drug Discovery Today, 13*(3-4), 135-143. doi:10.1016/j.drudis.2007.11.002

DeMuth, P. C., Garcia-Beltran, W. F., Ai-Ling, M. L., Hammond, P. T., & Irvine, D. J. (2013). Composite Dissolving Microneedles for Coordinated Control of Antigen and Adjuvant Delivery Kinetics in Transcutaneous Vaccination. *Advanced Functional Materials, 23*(2), 161-172. doi:10.1002/adfm.201201512

Donnenfeld, E. D. (2011). Difluprednate for the prevention of ocular inflammation postsurgery: an update. *Clin Ophthalmol, 5*, 811-816. doi:10.2147/OPTH.S6541

Faisant, N., Siepmann, J., & Benoit, J. P. (2002). PLGA-based microparticles: elucidation of mechanisms and a new, simple mathematical model quantifying drug release. *European Journal of Pharmaceutical Sciences, 15*(4), 355-366. doi:Pii S0928-0987(02)00023-4

Doi 10.1016/S0928-0987(02)00023-4

Goto, S. N., Yamamoto, T., Kirii, E., Abe, S., & Yamashita, H. (2012). Treatment of diffuse diabetic macular oedema using steroid eye drops. *Acta Ophthalmologica, 90*(7), 628-632. doi:10.1111/j.1755-3768.2010.02066.x

Hines, D. J., & Kaplan, D. L. (2013). Poly(lactic-co-glycolic) Acid-Controlled-Release Systems: Experimental and Modeling Insights. *Critical Reviews in Therapeutic Drug Carrier Systems, 30*(3), 257-276. doi:DOI 10.1615/CritRevTherDrugCarrierSyst.2013006475

Hutton, A. R. J., Quinn, H. L., McCague, P. J., Jarrahian, C., Rein-Weston, A., Coffey, P. S., . . . Donnelly, R. F. (2018). Transdermal delivery of vitamin K using dissolving microneedles for the prevention of vitamin K deficiency bleeding. *International Journal of Pharmaceutics, 541*(1-2), 56-63. doi:10.1016/j.ijpharm.2018.02.031

Jager, R. D., Aiello, L. P., Patel, S. C., & Cunningham, E. T. (2004). Risks of intravitreous injection: A comprehensive review. *Retina-the Journal of Retinal and Vitreous Diseases, 24*(5), 676-698. doi:Doi 10.1097/00006982-200410000-00002

Jiang, J., Gill, H. S., Ghate, D., McCarey, B. E., Patel, S. R., Edelhauser, H. F., & Prausnitz, M. R. (2007). Coated microneedles for drug delivery to the eye. *Investigative Ophthalmology & Visual Science, 48*(9), 4038-4043. doi:10.1167/iovs.07-0066

Jiang, J., Moore, J. S., Edelhauser, H. F., & Prausnitz, M. R. (2009). Intrascleral Drug Delivery to the Eye Using Hollow Microneedles. *Pharmaceutical Research, 26*(2), 395-403. doi:10.1007/s11095-008-9756-3

Jorge, L. L., Feres, C. C., & Teles, V. E. (2010). Topical preparations for pain relief: efficacy and patient adherence. *J Pain Res, 4*, 11-24. doi:10.2147/JPR.S9492

Khopade, A. J. H., Arindam; Shah, Ankit Shaileshkumar. (2017). India Patent No. PCT Int. Appl. .

Kim, Y. C., Edelhauser, H. F., & Prausnitz, M. R. (2014). Targeted Delivery of Antiglaucoma Drugs to the Supraciliary Space Using Microneedles. *Investigative Ophthalmology & Visual Science, 55*(11), 7387-7397. doi:10.1167/iovs.14-14651

Kim, Y. C., Grossniklaus, H. E., Edelhauser, H. F., & Prausnitz, M. R. (2014). Intrastromal Delivery of Bevacizumab Using Microneedles to Treat Corneal Neovascularization. *Investigative Ophthalmology & Visual Science, 55*(11), 7376-7386. doi:10.1167/iovs.14-15257

Kurz, P. A., Chheda, L. V., & Kurz, D. E. (2011). Effects of twice-daily topical difluprednate 0.05% emulsion in a child with pars planitis. *Ocul Immunol Inflamm, 19*(1), 84-85. doi:10.3109/09273948.2010.512993

Lu, L., Garcia, C. A., & Mikos, A. G. (1999). In vitro degradation of thin poly(DL-lactic-co-glycolic acid) films. *Journal of Biomedical Materials Research, 46*(2), 236-244. doi:Doi 10.1002/(Sici)1097-4636(199908)46:2<236::Aid-Jbm13>3.0.Co;2-F

Lu, S., & Taban, M. (2016). Topical difluprednate for treatment of serous retinal detachment and panuveitis associated with Vogt-Koyanagi-Harada disease. *Digit J Ophthalmol, 22*(2), 54-57. doi:10.5693/djo.02.2015.05.004

MainilVarlet, P., Rahm, R., & Gogolewski, S. (1997). Long-term in vivo degradation and bone reaction to various polylactides .1. One-year results. *Biomaterials, 18*(3), 257-266. doi:Doi 10.1016/S0142-9612(96)00126-3

Makadia, H. K., & Siegel, S. J. (2011). Poly Lactic-co-Glycolic Acid (PLGA) as Biodegradable Controlled Drug Delivery Carrier. *Polymers, 3*(3), 1377-1397. doi:10.3390/polym3031377

Missel, P., Chastain, J., Mitra, A., Kompella, U., Kansara, V., Duvvuri, S., . . . Cheruvu, N. (2010). In vitro transport and partitioning of AL-4940, active metabolite of angiostatic agent

anecortave acetate, in ocular tissues of the posterior segment. *J Ocul Pharmacol Ther, 26*(2), 137-146. doi:10.1089/jop.2009.0132

Nakano, S., Yamamoto, T., Kirii, E., Abe, S., & Yamashita, H. (2010). Steroid eye drop treatment (difluprednate ophthalmic emulsion) is effective in reducing refractory diabetic macular edema. *Graefes Archive for Clinical and Experimental Ophthalmology, 248*(6), 805-810. doi:10.1007/s00417-010-1316-y

Onishi, S. M., Asahi, M. G., Chou, C., & Gallemore, R. P. (2015). Topical difluprednate for the treatment of Harada's disease. *Clin Ophthalmol, 9*, 157-167. doi:10.2147/OPTH.S72955

Palakurthi, N. K., Correa, Z. M., Augsburger, J. J., & Banerjee, R. K. (2011). Toxicity of a Biodegradable Microneedle Implant Loaded with Methotrexate as a Sustained Release Device in Normal Rabbit Eye: A Pilot Study. *Journal of Ocular Pharmacology and Therapeutics, 27*(2), 151-156. doi:10.1089/jop.2010.0037

Park, J. (2007). *Treatment of intraocular lymphoma using biodegradable microneedle implant*. Univ. of Cincinnati.

Park, J. H., Allen, M. G., & Prausnitz, M. R. (2005). Biodegradable polymer microneedles: Fabrication, mechanics and transdermal drug delivery. *Journal of Controlled Release, 104*(1), 51-66. doi:10.1016/j.jconrel.2005.02.002

Park, J. H., Allen, M. G., & Prausnitz, M. R. (2006). Polymer microneedles for controlled-release drug delivery. *Pharmaceutical Research, 23*(5), 1008-1019. doi:10.1007/s11095-006-0028-9

Patel, S. R., Berezovsky, D. E., McCarey, B. E., Zarnitsyn, V., Edelhauser, H. F., & Prausnitz, M. R. (2012). Targeted Administration into the Suprachoroidal Space Using a Microneedle for Drug Delivery to the Posterior Segment of the Eye. *Investigative Ophthalmology & Visual Science, 53*(8), 4433-4441. doi:10.1167/iovs.12-9872

Patel, S. R., Lin, A. S. P., Edelhauser, H. F., & Prausnitz, M. R. (2011). Suprachoroidal Drug Delivery to the Back of the Eye Using Hollow Microneedles. *Pharmaceutical Research, 28*(1), 166-176. doi:10.1007/s11095-010-0271-y

Prausnitz, M. R., & Noonan, J. S. (1998). Permeability of cornea, sclera, and conjunctiva: A literature analysis for drug delivery to the eye. *Journal of Pharmaceutical Sciences, 87*(12), 1479-1488. doi:DOI 10.1021/js9802594

Tajika, T., Isowaki, A., & Sakaki, H. (2011). Ocular distribution of difluprednate ophthalmic emulsion 0.05% in rabbits. *J Ocul Pharmacol Ther, 27*(1), 43-49. doi:10.1089/jop.2010.0093

Tajika, T., Waki, M., Tsuzuki, M., Kida, T., & Sakaki, H. (2011). Pharmacokinetic Features of Difluprednate Ophthalmic Emulsion in Rabbits as Determined by Glucocorticoid Receptor-Binding Bioassay. *Journal of Ocular Pharmacology and Therapeutics, 27*(1), 29-34. doi:10.1089/jop.2010.0106

Thakur, R. R. S., Tekko, I. A., Al-Shammari, F., Ali, A. A., McCarthy, H., & Donnelly, R. F. (2016). Rapidly dissolving polymeric microneedles for minimally invasive intraocular drug delivery. *Drug Delivery and Translational Research, 6*(6), 800-815. doi:10.1007/s13346-016-0332-9

Wang, J. C., Burkholder, B. M., & Butler, N. J. (2016). Topical difluprednate for the treatment of retinal vasculitis associated with birdshot chorioretinitis. *Am J Ophthalmol Case Rep, 3*, 22-24. doi:10.1016/j.ajoc.2016.04.009

Y.W. Chien, B. E. C., Stanley E. Mares. (1991). *Novel Drug Delivery Systems: Fundamentals, Developmental Concepts, Biomedical Assessments*. New York: Marcel Decker.

Table 6.1: Composition of each microneedle array.

Array Name	Resomer ® R 202 S MW: 10,000-18,000 Polylactide (100% lactide)	Resomer ® RG 503 MW: 24,000-38,000 Lactide:glycolide (50:50)	Resomer ® RG 756 S MW: 76,000-115,000 Lactide:glycolide (75:25)
A (L:G = 87.5:12.5)	50%	--	50%
B (L:G = 50:50)	--	100%	--
C (L:G = 75:25)	--	--	100%

* L:G = lactide:glycolide; MW= molecular weight

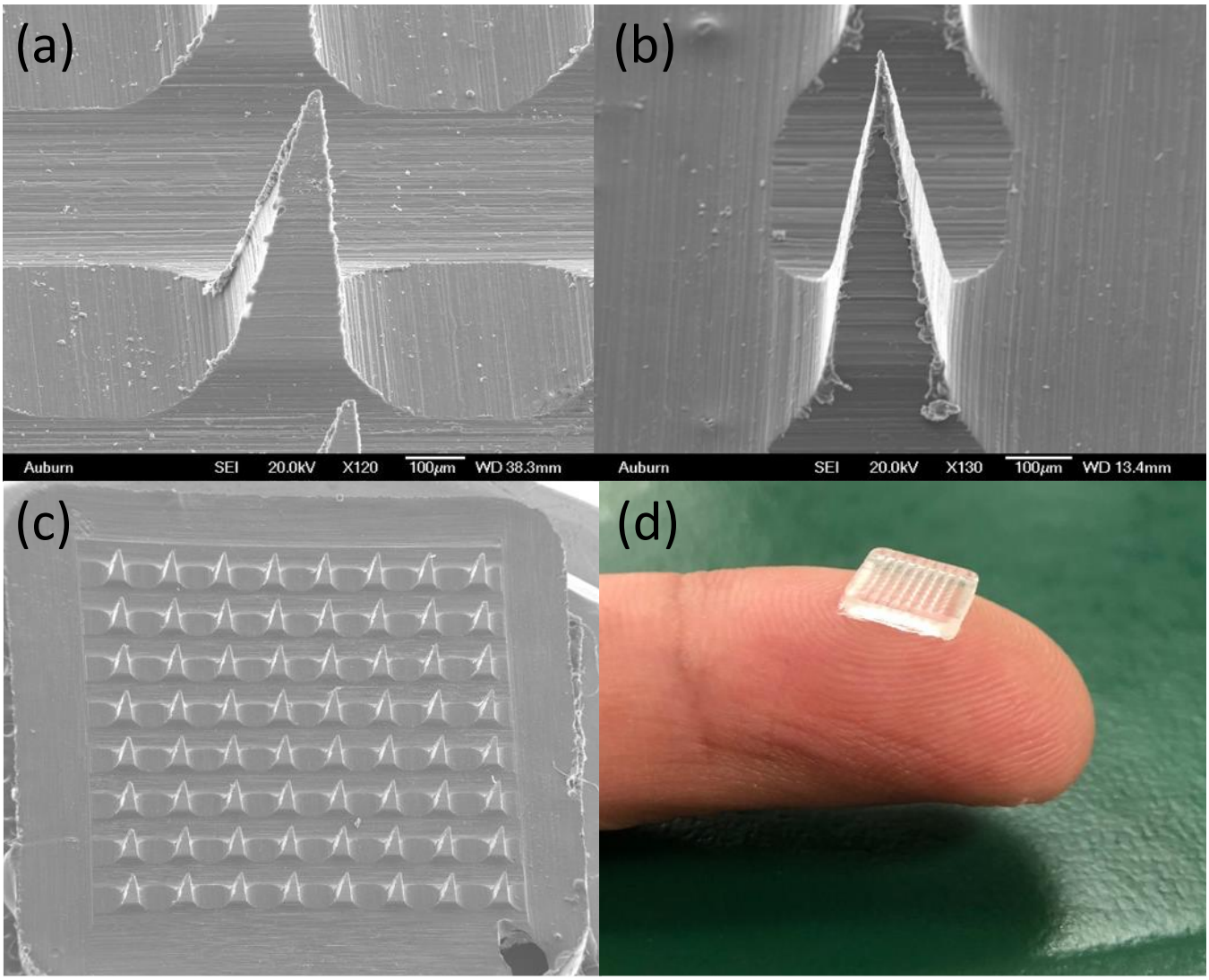

Figure 6.1: SEM images revealing structure and uniformity of microneedles: (a) front-view of the microneedle, (b) side-view of the microneedle, (c) full microneedle array, (d) microneedle relative to a fingertip.

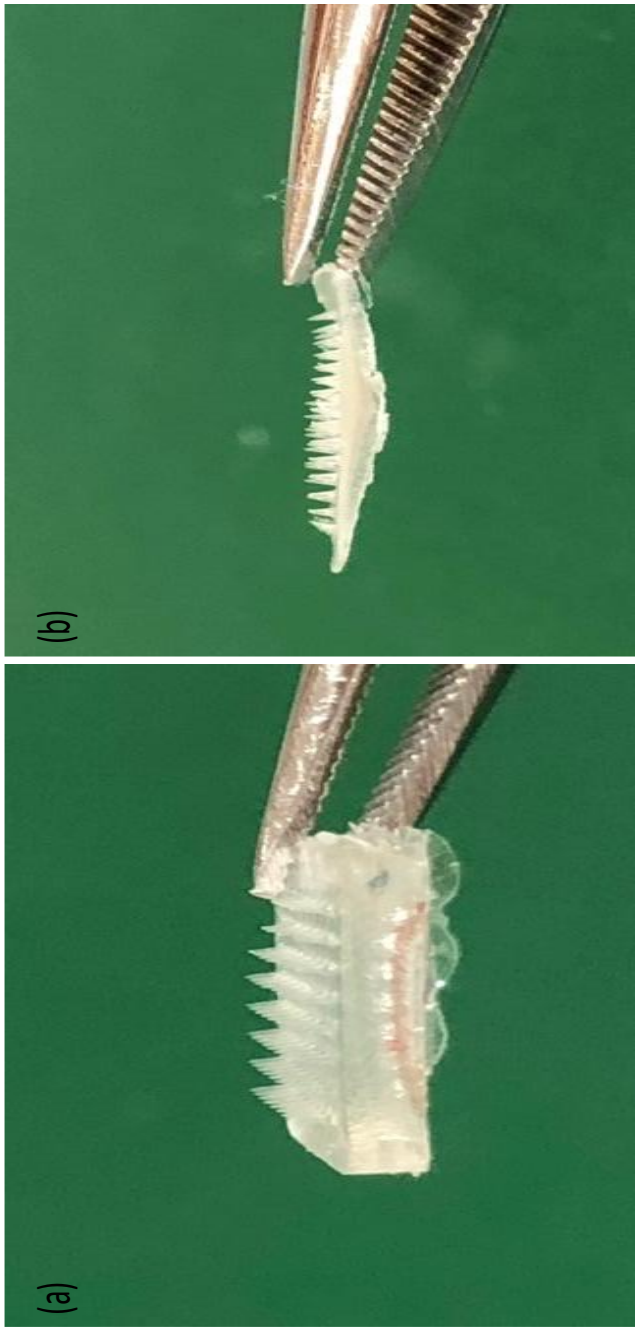

Figure 6.2: PLGA microneedle patch before dissolution of PAA backing (a) and after full dissolution in PBS (pH=7.4) (b)

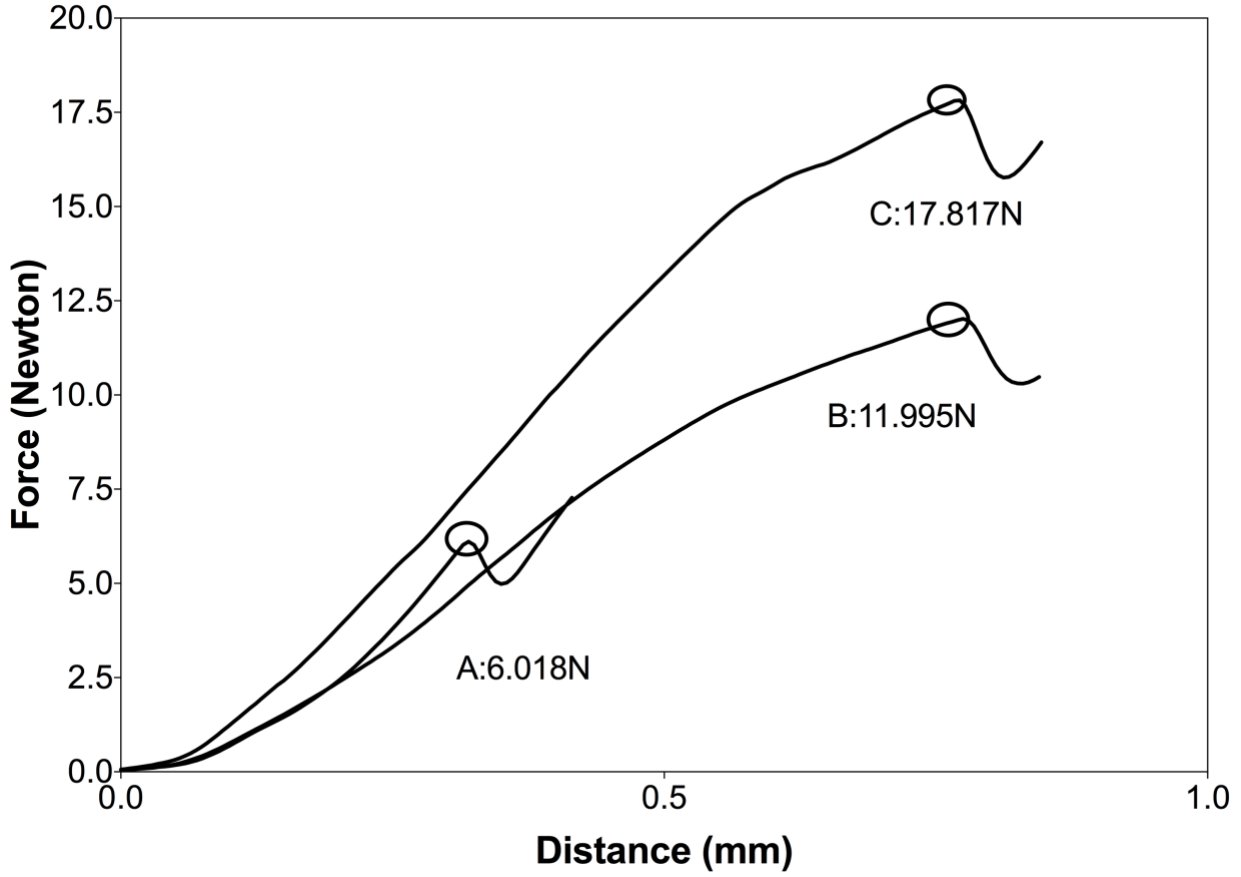

Figure 6.3: Stress-strain curves resulting from Texture Analyzer analysis. Plot shows data until microneedle failure point (dip in curve).

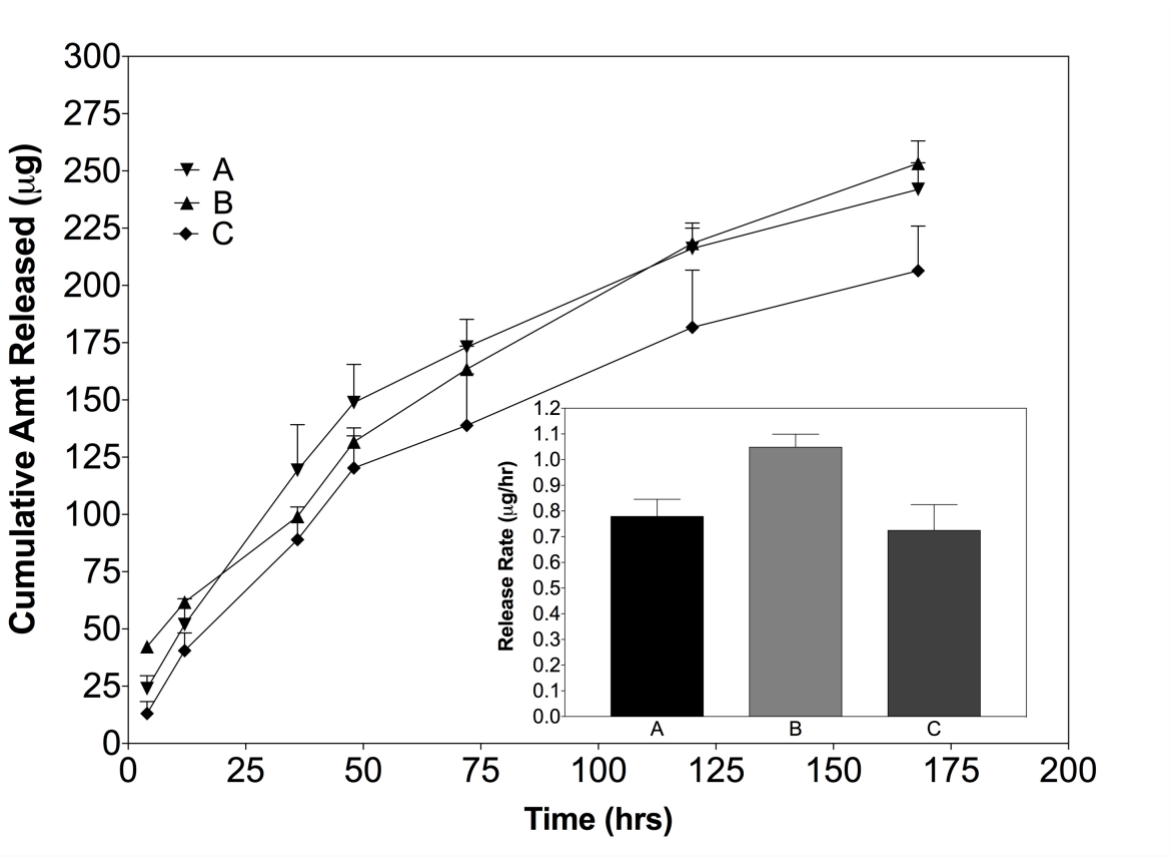

Figure 6.4: Sustained release of difluprednate from microneedle patches over a 7-day period. Error bars represent standard error mean (SEM).

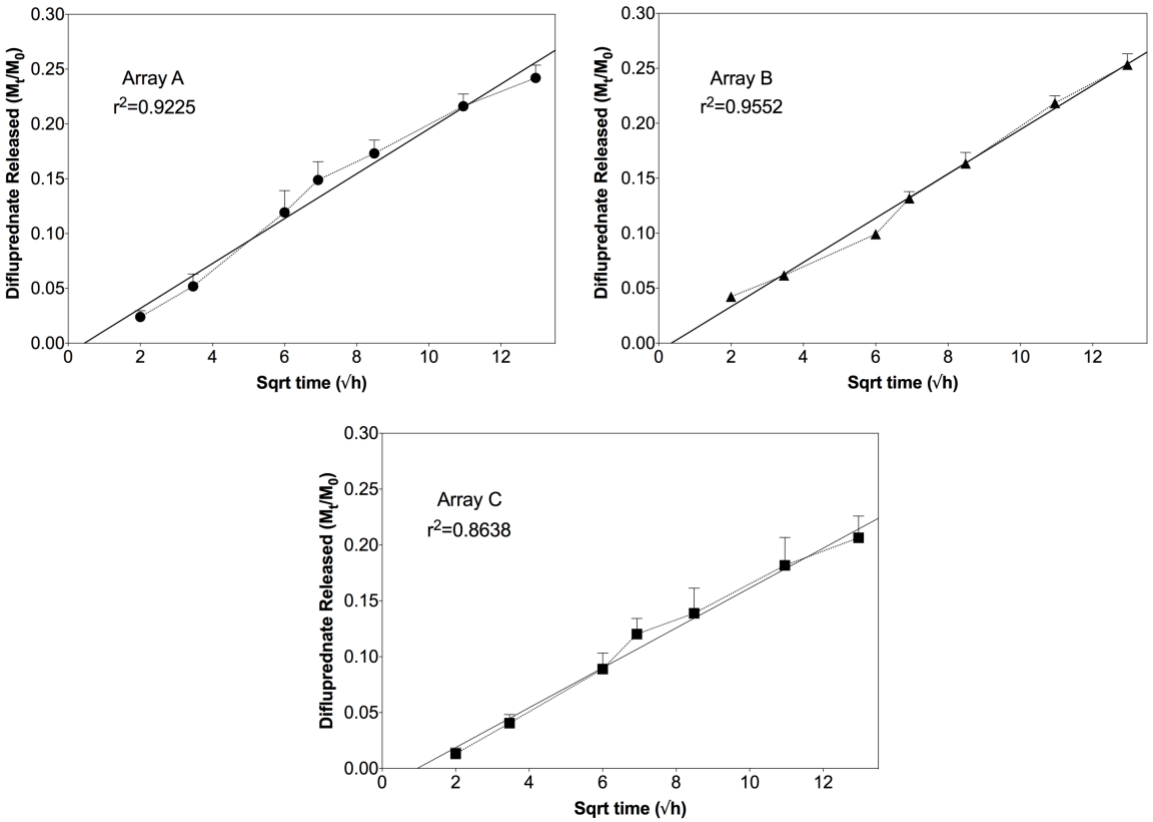

Figure 6.5: Experimental data modelled to the Higuchi equation (Eq. 1) as shown by the solid line. The data were plotted as a function of the square root of time to display the linear relationship of release to time, as described by the Higuchi equation. Early time points were eliminated to remove release due to the initial burst effect. Error bars represent standard error mean (SEM).

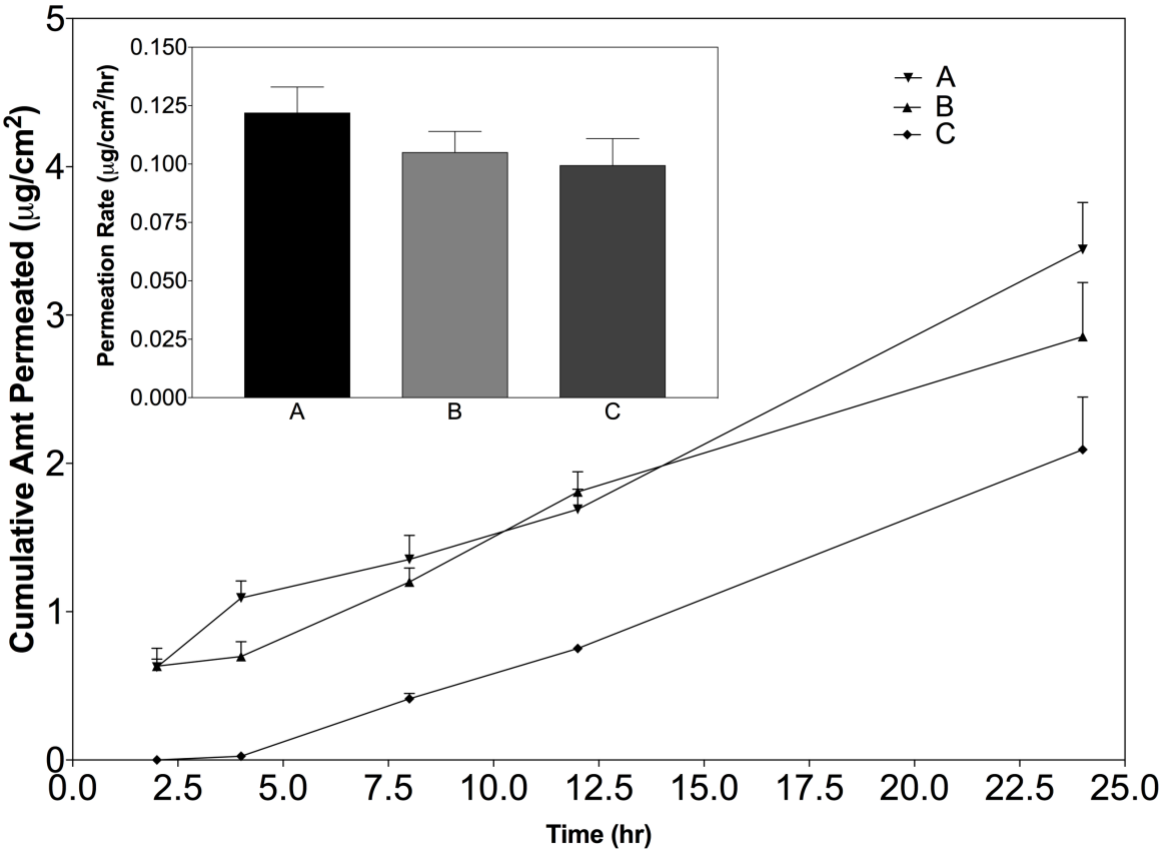

Figure 6.6: Permeation of difluprednate across porcine sclera; Inset: Permeation rate (steady state flux). Error bars represent standard error mean (SEM).

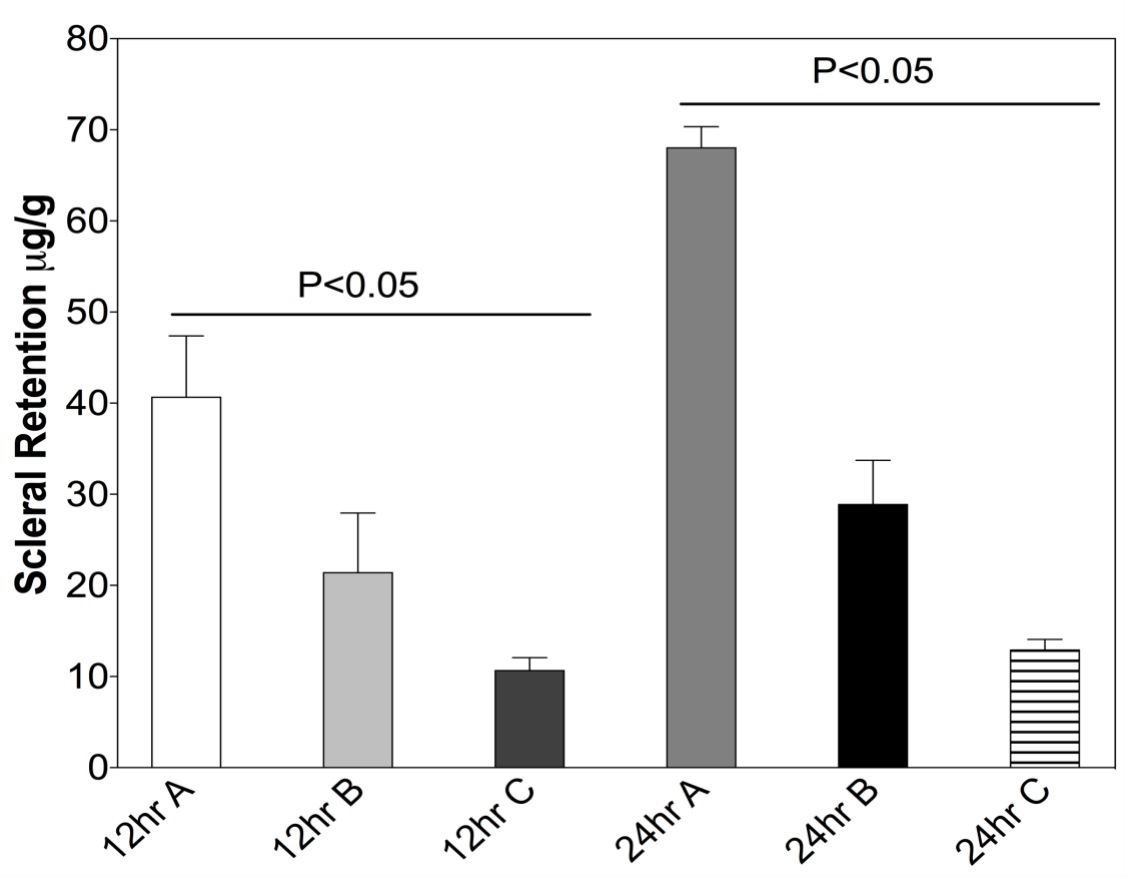

Figure 6.7: Retention of difluprednate in porcine sclera following 12 and 24 hour removal of microneedles. Error bars represent standard error mean (SEM).

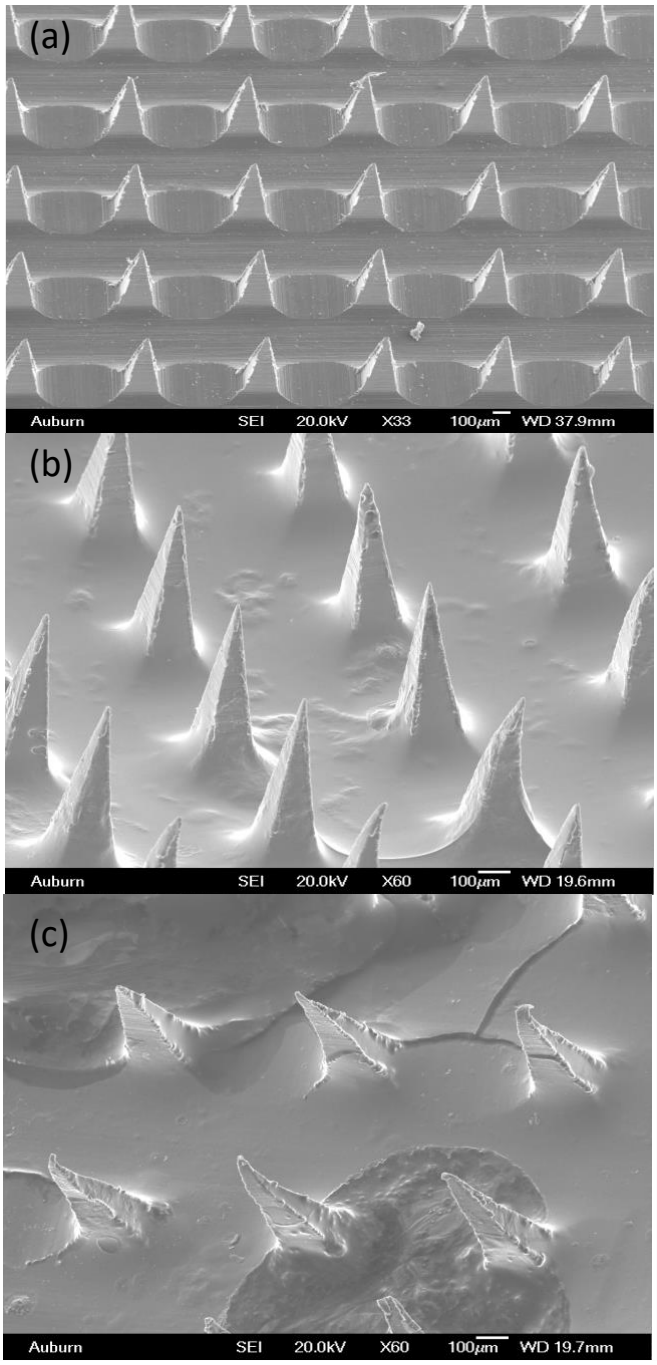

Figure 6.8: SEM images of microneedles at zero hours (a), removal from sclera after 12 hours (b), and 24 hours (c).

Chapter 7. Summary and Future Directions

This dissertation focused on different techniques used for solubilizing and delivering poorly soluble drugs to the eye, including the implementation of cyclodextrins and biodegradable microneedles. The applications of cyclodextrins in drug-delivery systems is limitless. Recently, they have become more common in a variety of pharmaceutical applications such as: drug delivery, gene delivery, cancer therapy, and biosensing. This means that cyclodextrins could very well become the next traditional excipient. Cyclodextrins have unique characteristics allowing molecules to be solubilized and stabilized for enhanced targetability and drug loading. The first chapter of this dissertation reviewed the uses of cyclodextrins in polymer, metallic, mesoporous, and lipid nanoparticles; whereas Chapters 3-5 discussed the use of cyclodextrins in improving the delivery of poorly soluble drugs to the eye.

Nepafenac was solubilized using HPBCD to form a 0.1% solution, which was subsequently used to compare to the commercial suspension, Nevanac®. The phase solubility studies revealed that there was a 1:1 interaction between HPBCD and nepafenac, meaning one cyclodextrin molecule is needed to solubilize one nepafenac molecule. The complex was confirmed using DSC, XRD, FT-IR and proton NMR. Molecular docking predicted that HPBCD interacts with the left side of the molecule, which is the more nonpolar region, this interaction was confirmed via NMR. Trans-corneal permeation studies using excised porcine corneas proved that the nepafenac solution achieved enhanced permeation (18 times) compared to the commercial. Additionally, the nepafenac retention in the cornea was 11 times higher than Nevanac®. Perfusion studies were

performed using whole porcine eyes to determine the drug distribution in the individual ocular tissues. Our solution formulation was capable of permeating into all ocular tissues, while the commercial product was not. These observations are a result of solubilization of the drug by HPBCD, allowing the drug to permeate the cornea more readily; therefore, a solution formulation was formulated for nepafenac that allows higher trans corneal permeation.

The aforementioned nepafenac:HPBCD complex was used to formulate an *in-situ* gel system for sustained release to the cornea. Traditional suspensions, such as Nevanac® lack long residence time in the eye; therefore, sodium alginate was added to our nepafenac solution to produce an ion-activated drug release system. By adding sodium alginate to the solubilized nepafenac complex, a formulation with both long residence time and enhanced permeation can be produced. Once the *in-situ* gel is instilled in the eye, the system interacts with the calcium ions in the tears. This interaction causes the sodium alginate to swell, yielding a gel-matrix for the sustained release of nepafenac. Rheology studies were conducted to determine the increase in viscosity after the addition of STF. The formulation containing 0.3% sodium alginate (F16) was determined to be the best formulation, as it had the largest increase in viscosity after interaction with STF and the lowest initial viscosity, which is ideal for easy patient administration. Permeation and release studies with varying concentrations of sodium alginate were performed and compared to the commercial formulation. All formulations were modelled using Peppas-Sahlin equation, which describes a dual-release mechanism via Fickian diffusion and a relaxational mechanism of the polymer. All *in-situ* gel systems display approximately 10 times higher permeation compared to Nevanac ®. Furthermore, perfusion studies were performed using F16. The *in-situ* gel system attained a higher retention of drug on the sclera compared to the commercial, due to the sodium alginate gel activation following STF interaction. Thus, an ion-activated *in-situ* gel system was formulated for the sustained release of nepafenac.

HPBCD was implemented to solubilize the recently approved corticosteroid, difluprednate. Phase solubility studies revealed that the relationship between difluprednate and HPBCD was a positive-type relationship, described by a second order polynomial line. This means that more than one HPBCD is needed to solubilize a single difluprednate molecule. The solid-state complex was confirmed via DSC, XRD and FT-IR. However, the FT-IR suggested that the more nonpolar right side of the molecule (ester side) was complexed while the left side of the molecule was left uncomplexed. Contrarily, molecular docking predicted that the difluprednate molecule was completely encapsulated, which does not agree with the FT-IR findings. This could be due to the fact that a stronger complex is formed with the right side, while the left side has a weaker less frequent complexation. A difluprednate 0.05% solution was prepared for comparison to the commercial emulsion Durezol®. The permeation rate of the solution across the porcine cornea was 12 times higher than the commercial product. Additionally, the corneal retention was 3 times higher than the commercial. Perfusion studies revealed that the solution was able to penetrate all of the ocular tissues due to the inclusion of HPBCD, whereas Durezol® was only able to permeate the cornea, aqueous humor, sclera and vitreous humor. Therefore, the difluprednate solution provided enhanced corneal permeation and retention compared to Durezol.

Research has shown that difluprednate can be used to treat posterior segment issues such as retinal vasculitis, pars planitis, macular edema, and ocular manifestations resulting from Harada's disease. However, topical treatments are not desirable for posterior segment treatment due to permeation barriers posed by the tear film layers and scleral tissue. Biodegradable polymeric microneedles provide a patient friendly alternative to intravitreal injections and poorly permeable topical formulations, while still providing the benefits of both delivery mechanisms. Difluprendate was loaded into PLGA-based microneedles for the sustained release to the posterior segment of the eye. PAA was used as the backing layer, because after instillation in the eye the PAA will interact with the tear fluid causing it dissolve within 30-40 minutes. PLGA of varying molecular

weights and lactide contents were used to formulate a variety of microneedle patches. These patches were tested and compared in force failure analysis and it was determined that the highest molecular weight patch had the strongest needles. Furthermore, release studies over a 7-day period, revealed that the patch with the lowest amount of lactide had the highest release rate. Permeation rates were not significant different across all of the patches, due to the short study duration. Contrarily, Array A had the largest scleral retention due to the higher concentration of lactide having an affinity for the hydrophobic sclera. The aforementioned observations suggest that the molecular weight affects the microneedle strength, while the lactide content affects the release, permeation and scleral retention. Thus, difluprednate loaded PLGA microneedle arrays were formulated for sustained delivery to the posterior segment of the eye.

In order for any of the aforementioned formulations to gain potential as marketable products, in-vivo studies using rabbits must be conducted. This will allow us to determine the irritation of the products as well as the in-vivo drug distribution and residence time in the eye. Furthermore, in-vivo studies comparing our formulations to the commercial formulations will provide valuable information. In the case of the biodegradable microneedles, additional work needs to be performed using different polymers, such as polyvinyl alcohol (PVA), polyvinylpyrrolidone (PVP) or PLGA with a higher glycolide content. Studying a variety of polymers will allow us to modify the difluprednate release rate and determine the best polymer for sustained drug delivery to the posterior segment. Finally, it would be ideal if the PAA backing dissolved within 5-10 minutes; therefore, a different dissolvable backing could be implemented to provide a more rapid dissolution after instillation in the ocular cul-de-sac.

Appendix: Publications and Conference Presentations

Publications

1. **H. Shelley**, R. Jayachandra Babu; (2018) Role of Cyclodextrins in Nanoparticle Based Drug Delivery Systems. Journal of Pharmaceutical Sciences, *In Press* (Epub ahead of print)

2. **H. Shelley**, R. Jayachandra Babu, Forrest T. Smith, Eva M. Abarca; Characterization of nepafenac/hydroxypropyl-β-cyclodextrin complex for improved ocular delivery. (Accepted to AAPS PharmSciTech).

3. **H. Shelley**, R. Jayachandra Babu; In-situ gel of nepafenac/hydroxypropyl-β-cyclodextrin complex for the sustained release to the cornea. (Submitted to JPharmSci)

4. **H. Shelley,** R. Jayachandra Babu; Physical characterization of difluprednate-hydroxypropyl-beta-cyclodextrin inclusion complex for ocular delivery. (In Preparation)

5. **H. Shelley,** R. Jayachandra Babu, Makenzie Grant; Biodegradable Difluprednate Biodegradable Microneedles For Delivery Into The Posterior Segment Of The Eye. (In Preparation)

6. Makenzie Grant, Charlotte Stewart, Sateesh Satigari, Gurkishan Chadha, Kasturi Pawar, Daniel Parsons, **H. Shelley** and R. Jayachandra Babu; Zero-order delivery from matrix tablets of Metoprolol or Diclofenac, (In preparation)

7. Roxanne Galarza, **H. Shelley**, Sue Duran, R. Jayachandra Babu, Eva Abarca; Species variability in the trans-corneal absorption of nepafenac eye drops.

Presentations

Podiums

1. **H. Shelley** Delivery to the Posterior Segment of the Eye Using Biodegradable Microneedles. *Auburn University's This is Research: Student Symposium, Auburn, AL, March 26, 2018.*

2. **H. Shelley** Microneedles for Delivery to the Posterior Segment of the Eye. *American Association of Pharmaceutical Scientist at Auburn University's Rapid Research Review, Auburn, AL, February 06, 2018.*

3. **H. Shelley** Research Update. *Auburn University: Department of Drug Discovery and Development, Auburn, AL, February 06, 2018.*

4. **H. Porter** Improved Retention of nepafenac on the ocular surface for sustained drug delivery. *Auburn University's This is Research: Student Symposium, Auburn, AL, April 13, 2017.*

5. **H. Porter** Cyclodextrins in Ophthalmic Drug Delivery. *Graduate Research Association of Students in Pharmacy (GRASP) Conference, Florida A&M University, Tallahassee, FL, July 23, 2016.*

6. **H. Porter** Improving Bioavailability of Nepafenac Using Hydroxypropyl-Beta-Cyclodextrin Complexes. *Three Minute Thesis Competition, Auburn University, Auburn, AL, October 26, 2016.*

7. **H. Porter** The Application of Cyclodextrin Derivatives in Drug Delivery. *Auburn University's This is Research: Student Symposium, Auburn, AL, April 8, 2016.*

8. **H. Porter** Research Update. *Auburn University: Department of Drug Discovery and Development, Auburn, AL, February 23, 2016.*

Posters

1. **H. Shelley,** R. Jayachandra Babu; Comparison of Nepafenac Drug Delivery Between Nevanac® and In Situ Gel in Perfused Porcine Eye Model; *International American Association of Pharmaceutical Scientists Annual Meeting ,San Diego, CA, November 12-16, 2017.*

2. **H. Shelley**, R. Jayachandra Babu; Ion-activated in-situ gel for prolonged release and enhanced retention in the porcine cornea; *Annual NanoBio Summit, Mobile, Al, November 9-10, 2017.* Poster# T6025

3. **H.Porter**,R.JayachandraBabu,ForrestT.Smith;PhysicochemicalCharacterizationofNepafenac by Hydroxypropyl-Beta-Cyclodextrin Complex for Ocular Delivery; *Annual Harrison School of Pharmacy Research Symposium in Auburn, Al, April 8, 2016.* ***Received first place award overall**

4. **H.Porter**,R.JayachandraBabu,ForrestT.Smith;PhysicochemicalCharacterizationofNepafenac by Hydroxypropyl-Beta-Cyclodextrin Complex for Ocular Delivery; *International American Association of Pharmaceutical Scientists Annual Meeting, Denver, CO, November 13-17, 2016.* ***Top 10 Most Viewed, 7th Most Shared (out of 2000 posters)**

5. **H.Porter**,R.JayachandraBabu,ForrestT.Smith;EvaluationofNepafenacIn-SituGelFormulation for Ocular Delivery; *International American Association of Pharmaceutical Scientist Annual Meeting, Denver, Colorado, November 13-17, 2016.*

6. **H. Porter,** R. Jayachandra Babu, Forrest T. Smith; Perfusion Studies of Ophthalmic In-Situ Nepafenac Gel on Porcine Eyes; *Annual NanoBio Summit, Auburn, Al, October 13-14, 2016.*

7. **H. Porter,** Forrest T. Smith, R. Jayachandra Babu; Ion-Activated Ocular In-situ Gel for Improved Residence Time in the Eye; *Graduate Research Association of Students in Pharmacy (GRASP) Conference, Florida A&M University, Tallahassee, FL, July 23, 2016.*

8. **H. Porter**, Forrest T. Smith, R. Jayachandra Babu; Solubilization of Lipophilic Drug Molecules via Complexation with Cyclodextrins; *Auburn University Golden Eagles Reunion in Auburn, Al, May 19, 2016.*

9. **H. Porter**, Forrest T. Smith, R. Jayachandra Babu; Ex-Vivo Permeation Studies of Cyclodextrin- Complexed NSAID using Porcine Corneas; *Annual NanoBio Summit, Birmingham, Al, October15- 16, 2015.*

10. **H. Porter**, Li Chen, S. Kurapati, V. Mulabagal, R. Jayachandra Babu; Stability and Degradation Profiles of Betamethasone Dipropionate in Topical Nanoparticle Formulation; *International American Association of Pharmaceutical Scientists Annual Meeting ,San Diego, CA, November 2- 6, 2014.*